



ELSEVIER

Available online at [www.sciencedirect.com](http://www.sciencedirect.com)

SCIENCE @ DIRECT®

Earth-Science Reviews xx (2004) xxx–xxx

[www.elsevier.com/locate/earscirev](http://www.elsevier.com/locate/earscirev)

1

## 2 Quaternary fault kinematics and stress tensors along the southern 3 Caribbean from fault-slip data and focal mechanism solutions

4 Franck A. Audemard\*, Gloria Romero, Herbert Rendon, Victor Cano

5 *Funvisis, Apdo. Postal 76.880, Caracas 1070-A, Venezuela*

6 Received 20 May 2003; accepted 17 August 2004

7

### 8 Abstract

9 Deformation along the southern Caribbean coast, as confirmed by the compilation of stress tensors derived from fault-plane  
10 kinematic indicators (microtectonics) and further supported by focal mechanism solutions herein presented, results from a  
11 compressive strike-slip (transpressional *senso lato*) regime characterized by a NNW–SSE maximum horizontal stress ( $\zeta_H = \zeta_1$ )  
12 and/or an ENE–WSW minimum ( $\zeta_h = \zeta_3$  or  $\zeta_2$ ) horizontal stress, which is responsible for present activity and kinematics of six  
13 sets of brittle features: east–west right-lateral faults, NW–SE right-lateral faults—synthetic Riedel shears, ENE–WSW to east–  
14 west dextral faults—P shears, NNW–SSE normal faults, almost north–south left-lateral faults—antithetic Riedel shears, and  
15 ENE–WSW reverse faults—sub-parallel to fold axes and mostly in the subsurface; the latter ones being associated to ENE–  
16 WSW trending folding. In this particular region, the brittle deformation obeys the simple shear model, although not all the  
17 deformation can be accounted for it since partitioning is also taking place (regional folding and thrusting is essentially due to the  
18 normal-to-structure component of the partitioned maximum horizontal stress). Conversely, the maximum horizontal stress on  
19 the Maracaibo block and south of the Oca–Ancón fault progressively turns counter-clockwise to become more east–west  
20 oriented, allowing left- and right-lateral slip along the north–south striking and NE–SW striking faults, respectively. The  
21 orientation and space variation of this regional stress field in western Venezuela results from the superposition of the two major  
22 neighboring interplate maximum horizontal stress orientations ( $\zeta_H$ ): roughly east–west trending stress across the Nazca–South  
23 America type-B subduction along the pacific coast of Colombia and NNW–SSE oriented one across the southern Caribbean  
24 boundary zone.

25 © 2004 Published by Elsevier B.V.

26 *Keywords:* Quaternary tectonics; Geodynamics; Stress tensor; Focal mechanism solution; Caribbean; Venezuela

27

### 1. Introduction

28

29 Northern Venezuela essentially lies in the inter-  
30 action zone between the South America and Carib-  
31 bean plates, whereas western Venezuela and northern  
32 Colombia show a more complex geodynamic setting

\* Corresponding author. Fax: +58 2 257 9977.

*E-mail addresses:* [faudemard@funvisis.org.ve](mailto:faudemard@funvisis.org.ve)  
(F.A. Audemard), [gromero@funvisis.org.ve](mailto:gromero@funvisis.org.ve) (G. Romero),  
[hrendon@funvisis.org.ve](mailto:hrendon@funvisis.org.ve) (H. Rendon), [vcano@funvisis.org.ve](mailto:vcano@funvisis.org.ve)  
(V. Cano).

33 involving a number of tectonic blocks or microplates  
 34 (Fig. 1). A wide consensus establishes that the  
 35 Caribbean plate moves eastward relatively to South  
 36 America (Bell, 1972; Malfait and Dinkelman, 1972;  
 37 Jordan, 1975; Pindell and Dewey, 1982; Sykes et al.,  
 38 1982; Wadge and Burke, 1983; among others), this  
 39 being strongly supported by recent GPS results lately  
 40 (Freymueller et al., 1993; Kaniuth et al., 1999; Weber  
 41 et al., 2001a,b, Pérez et al., 2001; Trenkamp et al.,  
 42 2002). But this Caribbean–South America plate  
 43 boundary—which drives and defines active tectonics  
 44 along northern Venezuela (from Colombia to Trini-  
 45 dad)—is not of the simple dextral type (Soulas, 1986;  
 46 Beltrán, 1994) since it is an over 100 km wide active  
 47 transpressional zone (Audemard, 1993; Singer and  
 48 Audemard, 1997; Audemard, 1998; Ysaccis et al.,  
 49 2000), partly occurring offshore and onshore northern  
 50 Venezuela. Very important positive relieves within the

51 onshore portion of the plate boundary zone, such as  
 52 the Coastal and Interior ranges (I, J and Q in Fig. 2),  
 53 are along the northern and eastern Venezuelan coast.  
 54 This would seem inconsistent with the Caribbean  
 55 motion vector in a direction  $086^{\circ}\rho 2^{\circ}$  with respect to  
 56 the Central range of Trinidad predicted by Weber et al.  
 57 (2001a,b), and  $N084^{\circ}\rho 2^{\circ}E$  with respect to South  
 58 America (Canoa site) by Pérez et al. (2001) from GPS  
 59 data, which attest for almost pure wrenching along the  
 60 plate boundary zone and would instead support slight  
 61 transtension in eastern Venezuela. This issue shall be  
 62 discussed in more detail later in this paper. This wide  
 63 transpressional boundary (in its widest definition,  
 64 meaning coexistence of strike-slip and compression  
 65 but not necessarily accommodated jointly on one  
 66 single structure) extends southwestward into the  
 67 Mérida Andes (MA in Fig. 1). The plate boundary  
 68 in western Venezuela is eventually up to 600 km wide

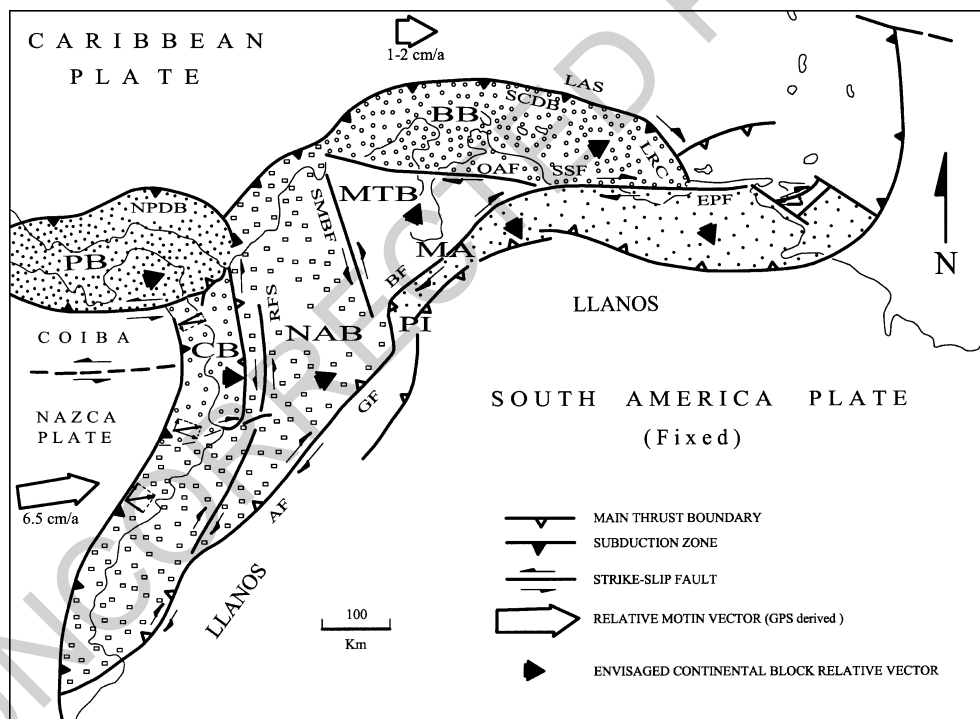


Fig. 1. Simplified general geodynamic setting of the southern Caribbean (modified from Audemard, 2002). Region is subject to a complex block tectonics. Vector decomposition of the convergence vector at the Nazca subduction may explain the along-strike slip change of the Romeral fault system. Equivalence of used acronyms is as follows: Bonaire (BB), Chocó (CB), Maracaibo (MTB), North Andean (NAB) and Panamá (PB) blocks; Mérida Andes (MA) and Pamplona indenter (PI). Some major faults are also reported: Algeciras (AF), Boconó (BF), El Pilar (EPF), Guaicaramo (GF), Romeral (RFS), Santa Marta–Bucaramanga (SMBF), San Sebastián (SSF) and Oca–Ancón (OAF); and other features as well: Leeward Antilles subduction (LAS), Los Roques Canyon (LRC), North Panamá deformation belt (NPDB), and Southern Caribbean deformation belt (SCDB).

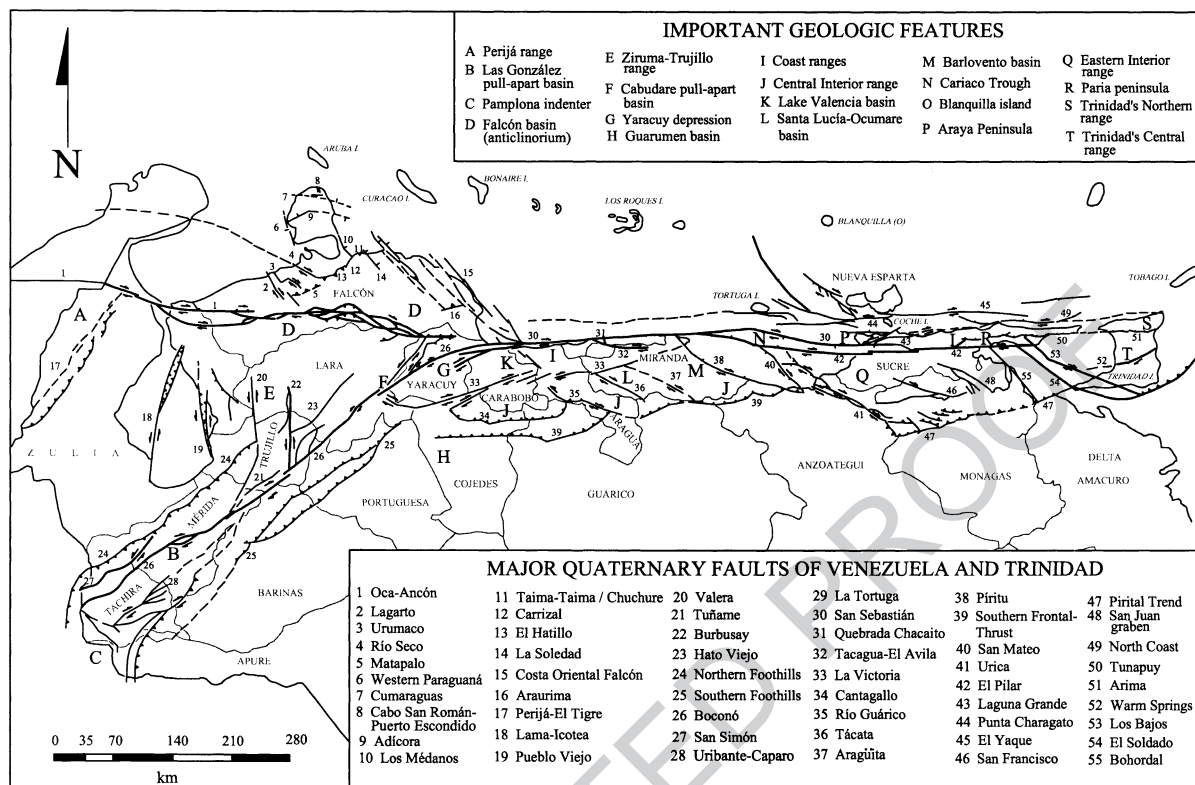


Fig. 2. Schematic map of Quaternary faults of Venezuela (simplified from Audemard et al., 2000). Faults and toponyms used throughout this contribution are identified. Very few localities are only reported in Fig. 3.

69 and comprises a set of discrete tectonic blocks or  
 70 microplates (Fig. 1), independently moving among the  
 71 surrounding larger plates (Caribbean, South America  
 72 and Nazca), among which Maracaibo block stands out  
 73 for its perfect triangular shape (MTB in Fig. 1). This  
 74 independent block is bounded by the left-lateral  
 75 strike-slip Santa Marta–Bucaramanga fault (SMBF)  
 76 in Colombia and right-lateral strike-slip Boconó fault  
 77 (BF) in Venezuela and separated on the north from the  
 78 Bonaire block (BB in Fig. 1) by the right-lateral  
 79 strike-slip Oca–Ancón fault (OAF). Besides, both  
 80 Maracaibo and Bonaire blocks are roughly being  
 81 extruded northward—while the Bonaire block also  
 82 moves slightly east—and are overriding the Caribbean  
 83 plate north of the Leeward Antilles islands, where a  
 84 young south-dipping, amagmatic, flat subduction  
 85 (LAS) has been forming in recent times (mainly in  
 86 the last 5 ma). Extrusion of these blocks is induced by  
 87 the collision of the Panamá arc (PB in Fig. 1) against  
 88 the Pacific side of northern South America and its

89 later suturing (Audemard, 1993, 1998). Recent results  
 90 from GPS plate motion studies (Freymueller et al.,  
 91 1993; Kellogg and Vega, 1995; Kaniuth et al., 1999;  
 92 Trenkamp et al., 2002), such as the CASA project,  
 93 confirm this northeastward escape of both blocks,  
 94 which override the Caribbean plate and generate the  
 95 Southern Caribbean Deformation Belt (SCDB) north  
 96 of the Netherlands Leeward Antilles.

97 The present Caribbean–South American geody-  
 98 namic configuration results from a transpressive  
 99 evolution that has occurred throughout the Tertiary  
 100 and Quaternary, initiated as an oblique type-B  
 101 subduction (NW-dipping, South American-attached  
 102 oceanic lithosphere under Caribbean plate island arc).  
 103 This plate boundary zone later evolved into a long-  
 104 lasting east-younging oblique-collision (SSE-vergent  
 105 Caribbean-affinity nappes overriding destroyed-pas-  
 106 sive-margin-affinity nappes, all overthrust onto  
 107 undeformed South America passive margin) and in  
 108 turn has shifted to a partitioned transpression when

109 and where collision became unsustainable (for more  
110 details refer to Audemard, 1993, 1998). Its latest  
111 evolutionary stage is still active in Eastern Venezuela  
112 and Trinidad, which recreates the shift from oblique  
113 subduction to partitioned oblique collision at present-  
114 day of this east-younging oblique convergent margin  
115 that has acted diachronically throughout the evolution  
116 of this entire northern portion of the plate boundary  
117 (Audemard, 2000b). This clearly indicates that,  
118 through time, the plate boundary zone has become  
119 more of the wrenching type and progressively less  
120 compressional, with a major shift in that sense that  
121 started at around 17–15 Ma in northwestern Venezuela  
122 (Audemard, 1993, 1998). This tectonically complex  
123 region in the southeastern Caribbean is undergoing  
124 two major geodynamic processes: (a) strain partition-  
125 ing characterized by NNW–SSE-trending shortening  
126 across the entire region from north of La Blanquilla  
127 island (O in Fig. 2) to the southernmost active thrust  
128 front of the Interior range and right-lateral strike-slip  
129 along the main east–west striking El Pilar and NW–  
130 SE striking Los Bajos–El Soldado faults, as well as  
131 along other minor parallel and/or synthetic Riedel  
132 shear faults (Fig. 2); and (b) slab detachment  
133 associated with an incipient type-A subduction (e.g.,  
134 Russo and Speed, 1992; Russo, 1999; responsible for  
135 the largest onshore negative Bouguer anomaly of the  
136 world, located south of the southern edge of the  
137 Interior range). These processes concur with a plate  
138 boundary geometry such as the present one, where the  
139 El Pilar fault transfers its slip eastward to one of its  
140 synthetic Riedel shears (Los Bajos and El Soldado  
141 faults), which is acting as a “lithospheric tear fault”,  
142 thus separating the transpressional boundary on the  
143 west from the conventional type-B Lesser Antilles  
144 subduction zone on the east. These two distinct  
145 seismic domains were originally identified by Pérez  
146 and Aggarwal (1981). These different seismicity  
147 patterns support contrasting geodynamic contexts  
148 (oblique collision and oblique subduction west and  
149 east of the Los Bajos–El Soldado fault system,  
150 respectively). Recent GPS findings by Weber et al.  
151 (2001a,b) indicate that most of the strike-slip motion  
152 of the El Pilar fault is transferred onto the Warm  
153 Springs fault system of the Central Range of Trinidad  
154 rather than onto a fault south off Trinidad (Fig. 2).  
155 This would imply that the Paria gulf is functioning at  
156 present as a pull-apart basin bounded by the El Pilar

and Warm Springs faults on the north and south, 157  
respectively, at a releasing stepover. Both faults 158  
exhibit a similar slip rate, in the order of 8–10 mm/ 159  
year (compare Audemard et al., 2000; Saleh et al., 160  
under review). The Warm Spring fault accounts for 161  
half of the dextral motion occurring across Trinidad 162  
(Saleh et al., under review). So does the El Pilar fault 163  
(Audemard et al., 2000), if the relative Caribbean– 164  
South America motion is in the order of 20 mm/year 165  
in eastern Venezuela, as published by Pérez et al. 166  
(2001) and Weber et al. (2001a,b). However, this 167  
crustal deformation does not exclude that a major 168  
plate boundary is underlying this region, as portrayed 169  
by the instrumental seismicity; conclusion originally 170  
drawn by Pérez and Aggarwal (1981) and later 171  
confirmed by Sobiesiak et al. (2002). 172

As in eastern Venezuela, strain partitioning is also 173  
a common feature along the rest of the transpressional 174  
boundary zone. In the Mérida Andes, strain is nicely 175  
partitioned between the right-lateral strike-slip 176  
Boconó fault (BF) running slightly oblique along 177  
the axis of the chain and thrust faults bounding the 178  
chain on both flanks (Audemard and Audemard, 179  
2002). The north-central coastal ranges also exhibit 180  
strain partitioning, where dextral slip in the range core 181  
is accommodated by both the San Sebastián and La 182  
Victoria faults and other minor synthetic Riedel 183  
shears, whereas transverse shortening is mainly taken 184  
by the relief growth and the frontal thrust faults 185  
bounding the chain along its southern edge, such as in 186  
the Guarumen basin (Cojedes state; Audemard, 187  
1999b). A mirror thrust fault system may exist on 188  
the north but it is under water at present, although the 189  
easternmost portion of the Southern Caribbean 190  
Deformation Belt and its related type-B subduction 191  
(LAS in Fig. 1) should account for some shortening 192  
farther north. This configuration both in the Andes 193  
and in the eastern Interior range was described by 194  
Rod in 1956b and some others, much before the 195  
concept of “partitioning” was even formally applied in 196  
the mid-1990s. 197

A large portion of the dextral slip along this 198  
complex boundary seems to be presently accommo- 199  
dated by the major right-lateral strike-slip Boconó– 200  
San Sebastián–El Pilar–Los Bajos fault system or 201  
segments of it (Molnar and Sykes, 1969; Minster and 202  
Jordan, 1978; Pérez and Aggarwal, 1981; Stephan, 203  
1982; Schubert, 1980a,b, 1982; Aggarwal, 1983; 204

205 Schubert, 1984; Soulas, 1986; Beltrán and Giraldo,  
 206 1989; Singer and Audemard, 1997, Audemard et al.,  
 207 2000; Weber et al., 2001a,b; Pérez et al., 2001). This  
 208 slip is now known being transferred farther east onto  
 209 the Warm Springs fault system of central Trinidad  
 210 (after Weber et al., 2001a,b's results). It is still matter  
 211 of debate whether this is either a transcurrent or  
 212 transform system, depending on the authors and the  
 213 proposed geodynamic models. Most authors accept or  
 214 postulate this major right-lateral strike-slip fault  
 215 system as the plate boundary (e.g., Hess and Maxwell,  
 216 1953; Schubert, 1979; Aggarwal, 1983; among many  
 217 others), whereas few others propose different plate  
 218 boundary models along this right-lateral strike-slip  
 219 plate boundary zone: (a) orogenic float type for the  
 220 Andes (Audemard, 1991a; Jácome, 1994; Audemard  
 221 and Audemard, 2002) or eastern Venezuela (Ysaccis  
 222 et al., 2000), thus being flanked by both an A- and B-  
 223 type subductions; and (b) SE-directed A-subduction  
 224 or underthrusting under the Mérida Andes (Kellogg  
 225 and Bonini, 1982; De Toni and Kellogg, 1993;  
 226 Colletta et al., 1996, 1997). However, the incorpo-  
 227 ration of the Boconó fault into this major right-lateral  
 228 strike-slip fault system is a rather recent event, that  
 229 relates to the northward extrusion of the Maracaibo  
 230 block, because the former transcurrent boundary used  
 231 to comprise the east–west-striking Oca–Ancón fault  
 232 system (OAF) located farther north in northwestern  
 233 Venezuela (Audemard, 1993, 1998). Therefore, the  
 234 Oca–Ancón fault system belonged to this major right-  
 235 lateral strike-slip plate boundary zone along the  
 236 southern Caribbean from when transpression started  
 237 at around 17–15 Ma to when essentially ceased or  
 238 considerably slowed down at around 5–3 Ma.  
 239 Although the Caribbean with respect to South  
 240 America is moving at rates between 12 mm/year on  
 241 the west (geologic slip rate from Nuvel 1-A model)  
 242 and  $18 \pm 2$  mm/year on the east (GPS-derived slip rate  
 243 by Weber et al., 2001a,b), the present major strike-slip  
 244 (Boconó–San Sebastián–El Pilar–Warm Spring faults)  
 245 boundary slips at  $\sim 1$  cm/year (Pérez and Aggarwal,  
 246 1981; Soulas, 1986; Freymueller et al., 1993; Aude-  
 247 mard et al., 2000; Pérez et al., 2001; Weber et al.,  
 248 2001a,b; Trenkamp et al., 2002), whereas secondary  
 249 faults at least slip one order of magnitude less faster;  
 250 as a matter of fact, most of them exhibit slip rates  
 251 under 0.5 mm/year, except for: Oca–Ancón (2 mm/  
 252 year, estimated from a paleoseismic assessment

performed by Audemard, 1996), Burbusay ( $\delta 3$  mm/  
 year), Valera and La Victoria ( $\delta 1$  mm/year) faults (for  
 more details, refer to Audemard et al., 2000, and to  
 Fig. 2 for relative location).

We believe that recent GPS results from Pérez et al.  
 (2001) support ongoing transpression in this Carib-  
 bean southeastern corner. From these authors' Figs. 1  
 and 3, four determinant issues can be deduced as to  
 this: (a) the elastic strain across this plate boundary  
 zone affects a region at least 110 km wide; (b) 68% of  
 the 20.5 mm/year right-lateral slip motion measured  
 across most of the plate boundary zone (almost 14  
 mm/year) is elastically taken by a 30-km-wide fault  
 zone, which includes the El Pilar fault and other  
 subparallel faults located north of it; (c) although  
 subordinate to the right-lateral strike-slip motion,  
 compression is taking place along the plate boundary  
 zone as attested by those vectors located south of the  
 main wrenching system in their Fig. 1, which  
 confirms and supports the earlier collected geologic  
 data through several decades, and compiled to some  
 extent by Audemard et al. (2000); and (d) these slip  
 vectors do not exclude the occurrence of strain  
 partitioning.

This paper presents an updated compilation of  
 stress tensors derived from fault-plane kinematic  
 indicators measured essentially in sedimentary rocks  
 of Plio-Quaternary age along northern continental  
 South America, as well as a few published stress  
 tensors derived from wellbore breakouts, comple-  
 mented with a compilation of focal mechanism  
 solutions for most important Venezuelan earthquakes  
 of the second half of the past century and beginning  
 of the present one (1957–2003). These datasets are  
 discussed in terms of their interrelation with the  
 regional Quaternary tectonics and their significance  
 with respect to the interactions among the Car-  
 ibbean, South America and Nazca plates and other  
 involved minor continental blocks of northwestern  
 South America.

## 2. Quaternary tectonics of Venezuela

Active tectonics in Venezuela at present is driven  
 by tectonic plate and microplate interactions, as  
 explained above. This is the common scenario world-  
 wide. Knowledge about this southern Caribbean plate

298 boundary zone has much evolved from the original  
299 ideas of Hess and Maxwell (1953), when a rather  
300 simple dextral wrenching system had been proposed.  
301 Over 20 years of neotectonic analysis—which com-  
302 prises studies in the disciplines of surface geology,  
303 geomorphology, microtectonics, seismotectonics and  
304 paleoseismology, combined with data from conven-  
305 tional geologic studies and seismic reflection survey-  
306 ing both onshore and offshore, now give us a more  
307 precise view of the complex active geologic setting in  
308 Venezuela and surrounds.

309 Neotectonics for Venezuela, as for everywhere else  
310 in the world, is defined as the tectonics resulting from  
311 the last and still active stress field. Then, Venezuelan  
312 neotectonics refers to the tectonics that takes place in  
313 Quaternary times (after Soulas, 1986), implying that  
314 tectonic features that either show no evidence of  
315 activity during that timeframe or have an orientation  
316 not susceptible to be reactivated during the near future  
317 under the present stress tensor, are not included in this  
318 compilation. The latest version of the neotectonic  
319 (Quaternary fault) map depicted in Fig. 3 is the third  
320 version of this type of maps (Audemard et al., 2000),  
321 after the first version made by Soulas in 1985, and  
322 published in 1986 (Soulas, 1986), which was later  
323 updated by Beltrán (1993). It differs from previous  
324 ones in: (a) new incorporations corresponding to  
325 onshore areas studied from the neotectonic viewpoint  
326 by Funvisis between 1993 and 1999: the southern  
327 frontal thrusts of the Interior range in eastern  
328 Venezuela, the southern foothills of the Mérida Andes  
329 and a preliminary assessment of the inner active  
330 deformation of the triangular block defined by the  
331 Oca–Ancón, Boconó and Valera faults; (b) the San  
332 Sebastián–El Pilar relay at the Cariaco trough has  
333 been reinterpreted, more like the interpretation of  
334 Blanco and Giraldo (1992); and (c) although the map  
335 is simpler in terms of number of faults (imposed by  
336 the aim of the ILP-II-2 project), like near the  
337 Colombia–Venezuela border (known as the Pamplona  
338 indenter–PI), faults on the map exhibit both their  
339 Quaternary kinematics and are discriminated both by  
340 age of latest activity and slip rate, which allows easy  
341 and quick identification of the major active features.  
342 This latest version also includes a report that contains  
343 relevant information about each fault and/or fault  
344 section (length, attitude, age, sense of slip, slip rate,  
345 geomorphic expression, latest activity from geologic

data, and so on) and its seismogenic potential 346  
(maximum credible earthquake and its recurrence). 347  
For more details on these issues, the reader is asked to 348  
refer to the accompanying report to the map that is 349  
available from the USGS web page. 350

351 As mentioned earlier, most of northern and western  
352 Venezuela sits on a complex plate boundary zone.  
353 Due to this complexity, it is beyond the scope of this  
354 paper to discuss all aspects of the Venezuelan  
355 neotectonics but to simply portray the main features  
356 in order to provide a general outline of the Quaternary  
357 tectonics. All names of the active tectonic features  
358 used throughout this paper are provided in Fig. 2.  
359 Later, the seismotectonics of the region shall be  
360 discussed on the basis of focal mechanism solutions  
361 and stress tensors derived from fault-slip data.

362 As imaged in Fig. 3 by Audemard et al. (2000), the  
363 following general issues about Venezuela Quaternary  
364 tectonics can be put forward.

365 (1) The Quaternary deformation is not all over the  
366 country but strain concentrates along localized stripes  
367 or belts (Singer and Audemard, 1997); all of them  
368 located in western and northern Venezuela. Most of  
369 these mobile belts exhibit high positive relief. So, an  
370 important amount of shortening is implicit along this  
371 plate boundary, but it does not exclude that some belts  
372 show negative relief. The latter features are of more  
373 local extent.

374 (2) The most conspicuous mobile belt is at least  
375 100 km wide and runs over 1200 km in length from  
376 the Colombian border near San Cristobal in the  
377 southwest into Trinidad in the east. This major  
378 belt—which seems to be prolonging from the Eastern  
379 Cordillera of Colombia—corresponds to an alignment  
380 of mountain chains that comprises from southwest to  
381 east: the NE–SW-trending Mérida Andes and the E–  
382 W-oriented Coast and Interior ranges both in north-  
383 central and northeastern Venezuela. This belt exhibits  
384 a first-order dextral fault system that mostly runs  
385 along the chain backbone. This system of over 1200  
386 km in length comprises the NE–SW-trending Boconó  
387 fault in the Andes section (VE-06 in Fig. 3), and both  
388 E–W-striking San Sebastián fault (VE-16 in Fig. 3) in  
389 central Venezuela and El Pilar fault (VE-13 in Fig. 3)  
390 in eastern Venezuela (Singer and Audemard, 1997).  
391 Most of the dextral slip between the Caribbean and  
392 South America plates is essentially accommodated by  
393 this fault system. In fact, this fault system moves at



Fig. 3. Map of Quaternary faults of Venezuela (after Audemard et al., 2000). Also accessible as a pdf file from the USGS web page in open file reports (ofr-00-0018). Line thickness is proportional to fault slip rate: the thickest indicates  $>5$  mm/year and the thinnest  $<1$  mm/year. Faults with historical or contemporary activity from geologic criteria are in red while Holocene active faults are in yellow. Shown faults, regardless of line color and thickness, have proven Quaternary activity.

394 about 1 cm/year when most of other faults show slip  
395 rates below 1 mm/year (Audemard et al., 2000).  
396 Combination of this rather fast slip rate and the  
397 significant length of the Boconó–San Sebastián–El  
398 Pilar fault system translate into an associated seis-  
399 micity of moderate frequency and magnitude. This  
400 system has been claimed responsible for most large  
401 (>7) historical earthquakes that have struck the  
402 country since the first ever reported event in 1530;  
403 more precisely accounted to some particular segments  
404 of this plate boundary (e.g., Rod, 1956a; Cluff and  
405 Hansen, 1969; Aggarwal, 1983; Audemard, 1997a,b,  
406 1999c, 2002; Pérez et al., 1997b).

407 (3) Some secondary mobile zones branch off from  
408 the major one. Four of these minor mobile zones are:  
409 the E–W-striking dextral Oca–Ancón fault system  
410 (VE-01 in Fig. 2) in northwestern Venezuela and three  
411 NW–SE trending normal–dextral fault systems  
412 respectively located from west to east in eastern  
413 Falcón, along the submarine canyon of Los Roques  
414 and in the gulf of Paria. The three latter ones exhibit  
415 much of negative relief due to the significant normal  
416 component involved. Another deformation belt per-  
417 fectly matches with the NNE–SSW trending Perijá  
418 range in westernmost Venezuela, whose crestline  
419 defines the border with Colombia.

420 (4) The major Boconó–San Sebastián–El Pilar fault  
421 system displays several structural complexities of  
422 kilometric to several-kilometre scale, either in trans-  
423 tension (pull-apart basins such as those of San Juan de  
424 Lagunillas—south of Mérida, Cabudare, Cariaco  
425 trough, gulf of Paria; among others; refer to Fig. 2  
426 for relative location), or in transpression (Caigüire  
427 hills at Cumaná, and Las Manos and Guarapiche—  
428 west and east of the 1997 epicentre, respectively, in  
429 Fig. 3; all in Sucre state, in eastern Venezuela and  
430 related to the El Pilar fault), but has no complication  
431 of regional scale, except for both ends (Singer and  
432 Audemard, 1997). On one end, at the Colombia–  
433 Venezuela border, the Boconó fault is taken into the  
434 Pamplona indenter (as defined by Boinet, 1985).  
435 Here, the Boconó fault sharply bends to connect with  
436 the N–S-striking Chitagá fault, which shows a strong  
437 reverse slip when joining the Boconó fault, but  
438 progressively becomes a dominant left-lateral fault  
439 towards the south. Farther south, slip is transferred to  
440 the NE–SW-trending sinistral Pamplona–Chucarima–  
441 Morro Negro fault system (CO-37 in Fig. 3). On the

442 other end, at the Paria gulf and Trinidad, the major  
443 right-lateral strike-slip fault system also bends rather  
444 sharply, 45° clockwise this time. The fault system  
445 splays into several NW–SE-striking offshore faults—  
446 among which are the Los Bajos (VE-15 in Fig. 3), El  
447 Soldado and Bohordal faults (in Fig. 2)—that exhibit  
448 both normal and dextral components. Los Bajos–El  
449 Soldado fault system is claimed to link the major  
450 transcurrent fault system to the southern tip of the  
451 type-B Lesser Antilles subduction; hypothesis that is  
452 not necessarily shared by Weber et al. (2001a,b), who  
453 postulate that slip transfer takes place along the Warm  
454 Springs fault of the Central Range of Trinidad from  
455 repeated GPS measurements. At this eastern tip, the El  
456 Pilar fault also shows a splay in the north compart-  
457 ment that branches off towards ENE. This splay,  
458 named the Tunapuy fault, exhibits a dominant reverse  
459 component with minor dextral slip. Beltrán (1998)  
460 proposes that the reverse Tunapuy fault in the Paria  
461 peninsula prolongs into the reverse Arima fault of  
462 northern Trinidad that bounds the southern foothills of  
463 the Northern range of Trinidad (Fig. 2). Weber et al.  
464 (2001b) have demonstrated that the Arima fault, based  
465 on calcite and quartz geothermometry applied to  
466 south-dipping shear bands and cataclastic zones  
467 studied along the southern border of the Northern  
468 range in Trinidad, is a south-dipping range-bounding  
469 normal fault, whose activity as such could not be  
470 better resolved than between 12 and 1 Ma. Instead,  
471 Saleh et al.'s (under review) results, based on geodetic  
472 data (triangulation and GPS data merging), argue for a  
473 reverse slip along the Arima fault. So, GPS data seem  
474 to confirm the Arima fault slip determined from  
475 aerial-photo interpretation based on landforms of  
476 Quaternary activity carried out by Beltrán (1998).

477 (5) Several second-order faults of considerable  
478 length diverge obliquely from the major right-lateral  
479 strike-slip fault system. Many of them are simply  
480 large synthetic Riedel shear faults to the main feature  
481 along the direct Caribbean–South America plate  
482 interaction in north-central and northeastern Vene-  
483 zuela, such as: Río Guárico (VE-09 in Fig. 3),  
484 Tacagua-El Avila (VE-10 in Fig. 3), Tácata (VE-11  
485 in Fig. 3), Píritu (VE-12 in Fig. 3), San Mateo (Jose;  
486 VE-14 in Fig. 3), Urica and San Francisco, among  
487 several others. In the Andes, the Boconó fault does  
488 not image this configuration, although many faults  
489 also branch off. Among them deserve mentioning the

490 north–south-striking sinistral Valera (VE-04 in Fig. 3)  
491 and Burbusay faults and the subparallel dextral  
492 Caparo fault (SE of San Cristobal; Fig. 2). But this  
493 configuration is also present in the Falcón range in  
494 association to the Oca–Ancón fault system.

495 (6) Other fault slips different from the main right-  
496 lateral strike-slip fault system—which is also accom-  
497 modated by synthetic Riedel shears (as mentioned  
498 before) and faults sub-parallel to it (e.g., San Simón  
499 and Caparo in the Andes, La Victoria in north-central  
500 Venezuela and North Coast in eastern Venezuela)—  
501 are also present in the mobile belts. Left-lateral strike-  
502 slip faults usually trend almost north–south, like the  
503 Quebrada Chacaito fault does, but slightly oblique  
504 faults to the main dextral system in northeastern  
505 Venezuela also exhibit sinistral motion: Punta Char-  
506 agato fault in the Cubagua island and Laguna Grande  
507 fault in the Araya peninsula. Special attention needs to  
508 be devoted to these Left-lateral strike-slip faults, since  
509 their orientation and slip seem atypical with respect to  
510 their tectonic setting in northeastern Venezuela. These  
511 ENE–WSW striking faults, in combination with the  
512 east–west striking dextral faults, bound wedge-shaped  
513 tectonic blocks, whose acute angle points to between  
514 ENE and east. Some blocks in this region show a slip  
515 vector that slightly diverges to ENE ( $N084^{\circ}\rho2^{\circ}E$  after  
516 Pérez et al., 2001), which matches rather well with the  
517 orientation of the bisecting line between both fault  
518 trends. This could argue for the occurrence of block  
519 expulsions to some extent in this complex south-  
520 eastern corner of the Caribbean in order to reduce  
521 mass excess. This would give a satisfactory explan-  
522 ation to the apparent transtension postulated by other  
523 authors from GPS vectors (e.g., Weber et al.,  
524 2001a,b), when transpression is actually the operating  
525 mechanism at plate-boundary scale.

526 (7) Active thrust faults are present along most  
527 chain fronts, although they may be blind or hidden  
528 behind triangular zones or intracutaneous wedges.  
529 They have been detected onshore along the northern  
530 edge of the presently inverted Falcón basin (south of  
531 Coro), along both Mérida Andes foothills and along  
532 the southern front of the Interior range both in central  
533 (e.g., Cantagallo overthrust) and eastern (e.g., Pirital  
534 and sub-parallel thrusts) Venezuela (Figs. 2 and 3).  
535 However, compression is explicitly recorded by chain  
536 uplift and build-up, and occasionally by intense  
537 folding in sedimentary sequences like in the Falcón

basin (“D” in Fig. 2), the eastern Interior range (“Q” in  
Fig. 2), the Andes foothills, and even in the Neogene–  
Quaternary foreland sequence of the central Interior  
range.

542 (8) Normal faults are also common and widespread  
543 within the deformation belts. Tuñame in the Mérida  
544 Andes (VE-05 in Fig. 3), Los Médanos (north of Coro),  
545 Cabo San Román and Puerto Escondido (north tip of  
546 the Paraguaná peninsula in northwestern Venezuela)  
547 and Río San Juan graben (in eastern Venezuela) faults  
548 are some examples of normal faulting (refer to Fig. 2  
549 for location). Except for the Tuñame fault located in the  
550 Andes (Figs. 2 and 3), all other normal faults—which  
551 are located in northern Venezuela—strike NNW–SSE.  
552 Instead, the normal slip of the Tuñame fault—that  
553 roughly strikes ENE–WSW and is located at the  
554 convergence of the Valera and Boconó faults—is a  
555 consequence of a void effect induced by a bookshelf  
556 rotation mechanism produced by simple shear between  
557 the Oca–Ancón and Boconó faults.

558 (9) In western Venezuela, the mobile belt is much  
559 wider than in northern Venezuela, reaching up to 600  
560 km in width, and comprises the entire Maracaibo  
561 block (MTB) that covers also part of northern  
562 Colombia (Audemard, 2000b; Audemard et al.,  
563 2000). This block is bounded by the sinistral  
564 Bucaramanga fault (SMBF in Fig. 1) on the southwest  
565 and the dextral Boconó and Oca–Ancón faults. For  
566 other authors, the block is defined on the north by the  
567 contact with the flat subduction (LAS in Fig. 1),  
568 responsible for the Southern Caribbean Deformation  
569 Belt (SCDB) established from seismic tomographic  
570 studies by Van der Hilst (1990), rather than by the  
571 Oca–Ancón fault system (OAF in Fig. 1). In  
572 Venezuelan territory, this block contains two deforma-  
573 tion belts with positive relief: the Perijá range and  
574 the western part of the Mérida Andes, between which  
575 the Maracaibo basin is being squeezed and shortened  
576 in NW–SE direction. The Perijá range happens to be  
577 the least studied area in terms of active tectonics  
578 because of accessibility and personal security.

579 (10) The triangular Maracaibo block (MTB) shows  
580 an intense internal fragmentation where blocks are  
581 individualized by north–south to NE–SW trending  
582 faults. Most of these faults are essentially left-lateral  
583 in slip, with a minor thrust component in many cases,  
584 such as from west to east: Icotea, Pueblo Viejo,  
585 Valera, Burbusay, among others. This structural and

586 geometrical configuration may result from a bookshelf  
587 rotation mechanism induced by simple shear gener-  
588 ated between the dextral Boconó and Oca–Ancón  
589 faults (Audemard et al., 1999). But the two faults are  
590 not parallel and are at an angle of 45°, which is an  
591 atypical configuration that must result in particular  
592 complex deformations, as well as switching sense of  
593 slip along faults through time.

594 (11) Fault and fold spatial configuration at regional  
595 scale and their kinematics, both deduced from the  
596 neotectonic mapping solely, points out that the  
597 Northern Falcón basin (northwestern Venezuela) is  
598 undergoing a stress tensor characterized by a NNW–  
599 SSE to N–S maximum horizontal stress and an ENE–  
600 WSW minimum (or intermediate) horizontal stress  
601 (Audemard, 1993, 1997b, 2001), thus meaning that  
602 the simple shear model associated with strike-slip  
603 faulting proposed by Wilcox et al. (1973) applies;  
604 although regional folding does not simply result from  
605 wrenching, but also from regional compression. Both  
606 folding due to wrenching in close association with the  
607 Oca–Ancón fault system (transpression s.s.) and to  
608 regional compression occur together (transpression  
609 s.l.). The neotectonic mapping in this region also  
610 allows gathering the active brittle structures in five  
611 distinguishable families based on their orientation and  
612 kinematics (Audemard, 1993, 1997b; Audemard and  
613 Singer, 1996; Figs. 2 and 3): (1) East–West right-  
614 lateral faults (Oca–Ancón Fault System—VE-01,  
615 Adícora Fault); (2) NW–SE right-lateral faults,  
616 synthetic to the east–west faults (Urumaco—VE-02,  
617 Río Seco—VE-03, and La Soledad faults); (3) NNW–  
618 SSE normal faults (Western Paraguaná, Cabo San  
619 Román, Puerto Escondido and Los Médanos faults,  
620 all fault-bounding the Paraguaná peninsula); (4)  
621 North–South to NNE–SSW left-lateral faults, anti-  
622 thetic to the east–west faults (Carrizal, El Hatillo and  
623 other minor faults); and (5) ENE–WSW reverse  
624 faults, parallel to folding axis (Araurima, Taima-  
625 Taima/Chuchure and Matapalo faults). In terms of slip  
626 rate, most Quaternary tectonic features in Northern  
627 Falcón are rather slow, showing slip rates generally  
628 below 0.4 mm/year, with the exception of the major  
629 east–west trending right-lateral strike-slip Oca–Ancón  
630 fault system whose maximum rate in Venezuela is  
631 close to 2 mm/year.

632 (12) The Coast and Interior ranges of central and  
633 eastern Venezuela is the only portion of the plate

634 boundary zone to result from rather simple direct  
635 interaction between the Caribbean and South America  
636 plates. So does northwestern Venezuela (essentially  
637 recorded in the Falcón basin, or applicable at larger  
638 scale to the Bonaire block bounded between the  
639 Leeward Antilles subduction and the Oca–Ancón fault  
640 system). Therefore, this region also complies with the  
641 Wilcox et al. (1973)'s simple shear model, at least for  
642 the brittle tectonics; and partitioning also takes places  
643 along this plate boundary segment. Within the  
644 Mesozoic metamorphic-dominated SSE-overthrust  
645 nappes of central Venezuela, six families of active  
646 tectonic features are distinguishable from their ori-  
647 entation and present kinematics (Figs. 2 and 3): (1)  
648 East–West right-lateral faults (San Sebastián, La  
649 Tortuga and El Avila faults); (2) NW–SE right-lateral  
650 faults, synthetic to the east–west faults (Río Guá-  
651 rico—VE-09, Tácata—VE-11 and Aragüita faults); (3)  
652 NW–SE to NNW–SSE normal–dextral to dextral-  
653 normal faults (Píritu—VE-12 and Tacagua—VE-10  
654 faults); (4) North–South to NNE–SSW left-lateral  
655 faults, antithetic to the east–west faults (Quebrada  
656 Chacaito faults); (5) ENE–WSW reverse faults,  
657 parallel to folding axis (Nappe fronts, among which  
658 the Cantagallo overthrust); and (6) ENE–WSW to E-  
659 W dextral faults—P shears (La Victoria fault—VE-  
660 08). This is actually the only case of active *P* faulting  
661 recognized in the plate boundary zone.

662 (13) For eastern Venezuela, the configuration of the  
663 active structures is as follows (Figs. 2 and 3): (1) East-  
664 West right-lateral faults (El Pilar—VE-13, El Yaque  
665 and North Coast faults); (2) NW–SE right-lateral faults,  
666 synthetic to the east–west faults (San Mateo—VE-14,  
667 Urica and San Francisco faults); (3) NW–SE to NNW-  
668 SSE normal–dextral to dextral–normal faults (San Juan  
669 Graben, Bohordal, Los Bajos and El Soldado—VE-  
670 15—faults); (4) ENE–WSW left-lateral faults, which  
671 do not obey the simple shear model (Laguna Grande  
672 and Punta Charagato faults; issue discussed earlier in  
673 this paper); and (5) ENE–WSW reverse faults, parallel  
674 to folding axis (frontal thrust of the Interior range,  
675 among which the Pirital thrust stands out).

676 (14) All present deformations along northern  
677 Venezuela are to be related to the present oblique  
678 convergence vector directed WNW–ESE of the  
679 Caribbean plate with respect to South America (e.g.,  
680 N75°W, after Minster and Jordan, 1978; later con-  
681 firmed by many others from GPS data, as indicated

682 earlier). Meanwhile, western Venezuela is undergoing  
683 a more complex scenario that shall be described later  
684 in this paper. This scenario is even affected by the  
685 convergence vector between the Nazca and South  
686 America plates that sits much farther south, in  
687 Colombian territory.

### 688 3. Instrumental seismicity

689 Seismicity in Venezuela clearly matches geograph-  
690 ically with the deformation belts (compare Figs. 3 and  
691 4), and consequently with areas of positive relief  
692 (Mérida Andes, Coast and Interior ranges and Perijá,  
693 Ziruma–Trujillo and Falcón ranges). Seismicity nation-  
694 wide is shallow and essentially lies in the first 20 km  
695 (Fig. 4A), with the rare exception of certain seismicity  
696 deeper than 40 km and mainly intermediate in depth  
697 that lies under the continental shelf off northern Falcón  
698 and the Zulia (Perijá), Falcón and Lara states, in  
699 northwestern Venezuela (Fig. 4B). This seismic activ-  
700 ity had been already reported by Van der Hilst (1990);  
701 and later seismologically studied in more detail by  
702 Malavé and Suárez (1995), Pérez et al. (1997a) and  
703 Jaimes et al. (1998). Besides, there are two other  
704 regions exhibiting seismicity deeper than 40 km but  
705 essentially outside Venezuela (Fig. 4B): (a) the south-  
706 ern tip of the Lesser Antilles subduction under Trinidad  
707 and Tobago, the Paria peninsula and the active island  
708 arc of the Lesser Antilles and (b) the Bucaramanga nest  
709 in Colombia, but near the border with Venezuela.  
710 Seismicity of the southern termination of the Antilles  
711 subduction has been studied to a certain extent (Pérez  
712 and Aggarwal, 1981; Russo et al., 1992; Choy et al.,  
713 1998; Sobiesiak et al., 2002, among many others).  
714 Those studies have led to establishing the existence of  
715 two very distinct seismotectonic provinces that are  
716 juxtaposed by the Los Bajos–El Soldado fault system  
717 within the Paria gulf. The first province—located SW  
718 of the fault system—is characterized by an intra-  
719 continental shallow seismicity, whereas the second  
720 one perfectly images the NW-sinking intermediate-dip  
721 slab of the southern termination of the Lesser Antilles  
722 oceanic subduction.

723 Seismicity in Venezuela, as clearly imaged by Fig.  
724 4, is diffuse and small to moderate in magnitude. This  
725 supports the fact that the plate boundary zone is rather  
726 wide and tectonic activity is distributed among many

active faults within mobile belts (Audemard and 727  
Romero, 1993). But this makes reliable seismotectonic 728  
associations almost an impossible task (Audemard and 729  
Singer, 1997). However, the instrumental seismicity 730  
distribution along the major wrenching boundary zone 731  
reveals some gaps (Audemard, 2002), from SW to 732  
east: (1) along the southwesternmost segment of the 733  
Boconó fault, astride Táchira and Mérida states; (2) 734  
along the Boconó and San Sebastián faults, between 735  
Barquisimeto and west of Choroní (sea town north of 736  
Maracay, Aragua state); and (3) along the San 737  
Sebastián and El Pilar faults, between north of the 738  
Guarenas–Guatire depression (about 20 km east of 739  
Caracas) and Cumaná (Sucre state). As verified by 740  
Audemard (2002), these present seismic gaps match 741  
rather well with the individual fault segments broken 742  
during some of the largest most recent historical 743  
earthquakes: 1894 in the southern Andes; 1812 in 744  
the Yaracuy depression and 1853 (El Pilar splay) and 745  
1900 (San Sebastián splay) along the Cariaco trough. 746

### 4. Stress tensors from microtectonic data 747

We present herein a first compilation and integration 748  
of stress tensors derived from geologic (microtectonic) 749  
data at national scale, which has been originally 750  
collected by Funvisis. In order to ascertain the 751  
characterization of the latest and still active tectonic 752  
phase, this compilation only integrates stress tensors 753  
derived from Plio-Quaternary sedimentary rocks. The 754  
data are presented in two different—but complemen- 755  
tary—ways: (1) stress tensors are characterized 756  
numerically in Table 1. Relevant issues such as location 757  
of the microtectonic analysis, performer of the analysis, 758  
quality of the data, size of the dataset, age of the 759  
deformation or of the disturbed sedimentary sequence 760  
are also given; and (2) stress tensors derived from 761  
microtectonic data, as well as wellbore data, are 762  
displayed in Fig. 5. This compilation map has been 763  
fractioned into three parts for a better quality, more 764  
legible display (western, central and eastern Venezuela, 765  
corresponding to Fig. 5a through c, respectively). 766  
These three fraction maps can be easily overlapped 767  
and merged in one, if needed. A few stress tensors 768  
derived from in-situ borehole data (from natural 769  
breakouts or hydraulic fracturing) are also incorporated 770  
herein. Scarcity of this type of data is directly related to 771

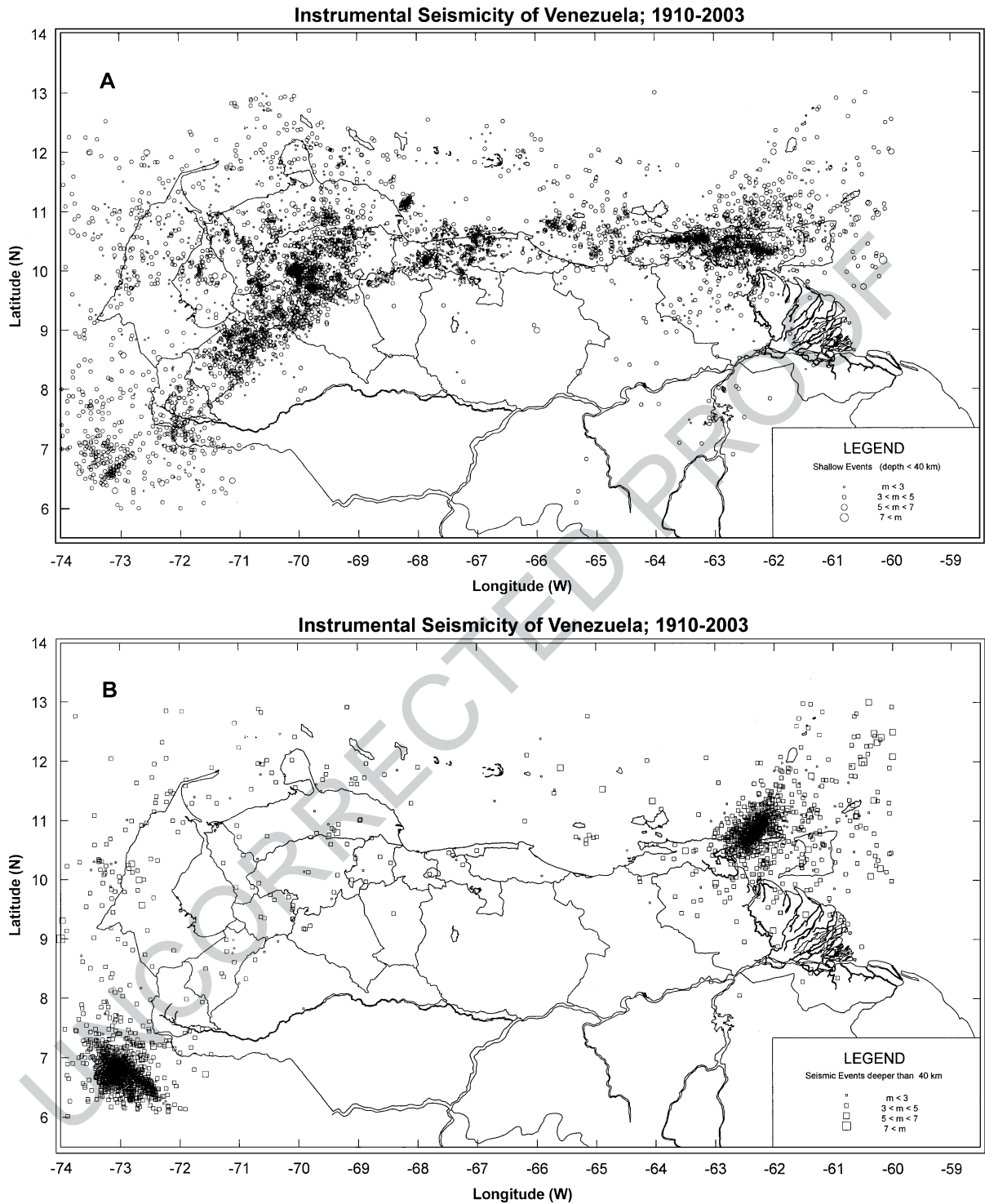


Fig. 4. Instrumental seismicity of Venezuela, between 1910 and 2003 (from Funvisis seismic catalog). Earthquakes are categorized by both magnitude and depth. (A) Events shallower than 40 km; (B) events deeper than 40 km.

t1.1 Table 1

t1.2 Compilation of Quaternary stress tensor data obtained by inversion methods relying on fault-plane kinematic indicators; and rarely on disposition of major active tectonic structures (updated and modified from Audemard et al., 1999)

## t1.3 Quaternary stress tensors

t1.4	Station	Locality	$\zeta_H$ (max)		$\zeta_h$ (min)		Age	Observations and interpretations	Reference
t1.5	no. ( $\xi$ )		Strike	Dip	Strike	Dip			
t1.6	1	Central-western Falcón	N 117°	Subhor.	N 027°	Subhor.	Pliocene	Determined from regional structure configuration.	Soulas et al., 1987
t1.7	2	Central-western Falcón	N 160°	Subhor.			Q	Determined from regional structure configuration.	Soulas et al., 1987
t1.8	3	Central-northern Falcón	N 170°	Subhor.			Q	Originally estimated by Total-CFP. Determined from spatial configuration of regional structures.	Audemard and De Mena, 1985
t1.9	4	Central-northern Falcón	N 130°–140°	Subhor.			Pliocene	Determined from fractures affecting sedimentary rocks of various ages.	Wozniak and Wozniak, 1979
t1.10	5	Central-northern Falcón	N 170°	Subhor.			Q	Established from structural analyses at different scales.	Wozniak and Wozniak, 1979
t1.11		Lat: +11.37°; Long: –69.47°							
t1.12	6	Oca Fault; Hato El Guayabal; (western Falcón)	N 137°	Subhor. (1°N)	N 054°	Subhor. (4°S)	Holocene	Compressive transcurrent regime.	Audemard, 1993
t1.13		Lat: +10.90°; Long: –71°						Data from paleoseismic trench.	
t1.14								Few measures.	
t1.15	7	Río Seco Fault; near pipelines	N 170°	Subhor. (10°N)	N 077°	Subhor. (16°S)	Q	Excellent microtectonic station.	Audemard, 1993, 1997b
t1.16		Lat: +11.37°; Long: –70.13°						Compressive transcurrent regime.	Audemard, 2000a; Audemard et al., 1992
t1.17	8	Falla Río Seco; close to Mitare	N 158°	20°N	N 150°	71°S	Q	Good quality microtectonic dataset.	Audemard, 1993, 2000a; Audemard et al., 1992
t1.18		Lat: +11.30°; Long: –69.98°						Compressive regime.	
t1.19	9	Urumaco Fault; close to Mamón creek	N 151°E	Subhor. (12°N)	N 064°	Subhor. (12°N)	Q	Excellent microtectonic station.	Audemard, 1993, 1997b
t1.20		Lat: +11.25°; Long: –70.23°						Transcurrent regime.	Audemard, 2000a; Audemard et al., 1992
t1.21	10	Punta Sauca (Falcón state)	N 122°E	Subhor. (4°N)	N 024°	47°S	Pliocene (?)	Syn-sedimentary to Punta Gavilán fm. deposition.	Audemard, 1993; Audemard et al., 1992
t1.22		Lat: +11.47° Long: –68.87°						Stress tensor apparently tilted with sequence.	

t1.23	11	Caujarao (Falcón state) Lat: +11.40° Long: -69.63°	N 350°ρ21°	Subhor.	Subvertical	Q	Superimposed younger tectonic phase? Younger than Coro fm. deposition.	Audemard, 1993, 1997b Audemard, 2000a; Audemard et al., 1992
t1.24							Transcurrent compressive to compressive regime. Excellent microtectonic station. Shows the progressive northward tilting of the fanglomerate sequence.	
t1.25							Transcurrent compressive to compressive regime.	
t1.26	12	La Vela anticline, at Puente de Piedra (Falcón state) Lat: +11.52°; Long: -69.42°	N 166°	Subhor. (17°N)	N 022°	69°S	Q	Audemard, 1993, 2000a; Audemard et al., 1992; Gallardo, 1985
t1.27							Good quality microtectonic station, regardless of few measures.	
t1.28	13	Camare dam (Oca-Ancón fault system) Lat: +10.90°; Long: -70.13°	N 155°	Subhor.	N 075°	Subhor.	Q	In fault gouge material. Gallardo, 1985
t1.29							Good quality microtectonic station, regardless of few measures.	
t1.30	14	Ziruma-Trujillo range Estimates: Lat: +10.20°; Long: -70.75°	N 160 <sup>a</sup>	Subhor.			Post-Miocene	Acute angle between conjugate strike-slip faults: N140°-striking right-lateral, N180°-striking left-lateral Mathieu, 1989
t1.31								
t1.32	15	Guarumen basin	N 160°	Subhor.			Q	Established normal to thrust faults. Blin, 1989
t1.33	16	Yay (Lara state) Lat: +9.78°; Long: -69.63°					Pliocene	Sub-radial extension Giraldo, 1985a,b
t1.34								( $\zeta_H$ max $\zeta_1$ ). $\zeta_1$ =N 106° 62°W (after counter-tilting sequence, $\zeta_1$ becomes vertical)
t1.35	17	Quibor-Cubiro road (km 10) Lat: +9.85°; Long: -69.60°	N 110°	Subhor.	N 020°	Subhor.	Q	Transcurrent compressive regime. Giraldo, 1985a,b
t1.36								
t1.37	18	San Jerónimo (Lara state) Lat: +9.85°; Long: -69.52°	$\zeta_2$ : N 70°	Subhor.	N 160°	Subhor.	Q	Localized extension ( $\zeta_1$ vertical) in probable pull-apart basin at fault divergence between Boconó fault and one of its synthetic Riedel shears (*). Giraldo, 1985a,b
t1.38								$\zeta_2$ would be $\zeta_H$ max

(continued on next page)



t1.54	25	Villa de Cura (Aragua state)	N 145°E	Subhor.	N 055°	Subhor.	Q	Roadcut 2 km north of Villa de Cura, on road to Cagua. Good dataset in lower Pleistocene alluvial deposits.	Audemard et al., 1988
t1.55		Lat: +10.05° Long: -67.47°							
t1.56	26	La Puerta (Aragua state)	N 120°E	Subhor.	N 030°	Subhor.	Q?	In gouge of La Puerta fault, on Villa de Cura–San Juan de Los Morros road. Good microtectonic dataset.	Audemard et al., 1988
t1.57		Lat: +9.95°; Long: -67.37°							
t1.58	27	Hacienda La Morita (Aragua state)	N 160° ρ30°	Subhor.	N 070° ρ20°	Subhor.	Q	North of the Camatagua dam. Few microtectonic measures.	Audemard et al., 1988
t1.59		Lat: +9.93°; Long: -67.07°							
t1.60	28	North-central litoral	N 140°	Subhor.			Q?	Based on configuration of structures at regional scale.	Fanti et al., 1980
t1.61	29	Cantinas; Caracas–La Guaira old road (Federal District)	N 143°	Subhor. (23°S)	N 077°	43°S	Q	North of Cantinas oil tanks, associated to the Tacagua–El Avila fault. Stress tensor slightly tilted south; alike to rock foliation (*)	Acosta, 1995, 1997
t1.62		Lat: +10.53°; Long: -66.95°							
t1.63	30	Gallery in south abutment of first viaduct of Caracas–La Guaira highway (Federal District)	N 169°	33°S	N 069°	57°S	Q?	Stress tensor seems tilted south with respect to other tensors in the region. Good microtectonic dataset.	Audemard et al., 1993
t1.64		Lat: +10.53°; Long: -66.97°							
t1.65	31	Santa Lucia– Ocumare del Tuy graben (Miranda state)	NW–SE	Subhor.			Q	From disposition of structures at regional scale; partly confirmed by microtectonic analyses. Synsedimentary tectonic phase to Tuy Formation and younger.	Beck, 1979, 1986
t1.66	32	Urbanización Industrial Río Tuy (south of Charallave)	N 08° ρ07°	Subhor. or Subvert.	Sub-vertical		Q	Deformation in Tuy Formation of Plio–Q age. Good microtectonic dataset.	Audemard, 1984, 1985; Loyo, 1986
t1.67		Lat: +10.22°; Long: -66.87°							

(continued on next page)

Table 1 (continued)								
Quaternary stress tensors								
Station no. ( $\xi$ )	Locality	$\zeta_H$ (max)		$\zeta_h$ (min)		Age	Observations and interpretations	Reference
		Strike	Dip	Strike	Dip			
t1.68 t1.69 t1.70 t1.71	33 W of Cúa and SW of road junction leading to San Casimiro and Tácata (Miranda state)	N 06° $\rho$ 43°	variable	N 104° $\rho$ 37°	variable	Q	Next to metamorphic–sedimentary faulted contact (Tuy fm.). Very small microtectonic dataset.	Audemard, 1984, 1985; Loyo, 1986
t1.72 t1.73 t1.74	34 Santa Lucía sand pit; east of Sta. Lucía and on left bank of Guaire river (Miranda state) Lat: +10.17°; Long: –66.90°	~N–S	Subhor.	E–W	horizontal	Q	Within Tuy fm.(?), near metamorphic–sedimentary contact. calculated tensor: $\zeta_1$ : N024°E $\rho$ 12°; $\zeta_3$ : N114°E $\rho$ 12°; with intermediate dips both, before countertilting actual bedding attitude (N053°W 20°S). Few microtectonic measures.	Audemard, 1984, 1985; Loyo, 1986
t1.75	35 Puente Pichao–Caracas–Sta. Lucía road Lat: +10.37°; Long: –66.63°	N 174° $\rho$ 30°	Subhor.	N 056°	Subhor.	Q	In the basin-margin conglomerates of the Pichao member. The youngest tectonic phase is established from crosscutting relationship between different striation generations. Excellent microtectonic dataset.	Audemard, 1984, 1985; Loyo, 1986
t1.76 t1.77 t1.78	36 W of Cúa; south of Cúa–Tácata road (near poultry farm) Lat: +10.17°; Long: –66.90°	~N–S	variable	E–W		Q	In association with La Victoria fault. Close to (<250 m) metamorphic–sedimentary contact (in Tuy fm.). North tilted sequence. Very few microtectonic measures.	Audemard, 1984, 1985; Loyo, 1986
t1.79	37 Arichuna; La Peñita exchanger (NE of Charallave); zLat: +10.28; Long: –66.83	N 158° $\rho$ 07°	Subhor.	N 068° $\rho$ 07°	!56°N	Q	In Tuy Formation sedimentary rocks. Excellent microtectonic dataset.	Audemard, 1984, 1985; Loyo, 1986

t1.80	38	Sta. Lucía–Turgua road Lat: +10.35°; Long: –66.67°	N 135°ρ25°	Subhor.	N 045°ρ25°	Subhor.	Q	NNW of Santa Lucía, at metamorphic–sedimentary contact (in Siquire fm. sedimentary rocks). Few microtectonic measures.	Audemard, 2000a
t1.81	39	Santa Lucía–Ocumare del Tuy graben (Miranda state)			NE–SW	Subhor.	Pliocene–lower Pleist.	Extensional tectonic phase affecting the entire basin. 17 microtectonic stations spread over the basin support this phase, that predates the Q compressional phase.	Audemard, 1984, 1985; Loyo, 1986
t1.82	40	Caracas–La Guaira highway Lat: +10.60°; Long: –67°	N 160°	Subhor.	N 070°	Subhor.	Q?	In metamorphic rocks. Small dataset. Compressive transcurrent regime.	Funvisis, 1984
t1.84	41	Caracas–La Guaira highway	N 150°	Subhor.	N 060°	Subhor.	Q?	In metamorphic rocks. Extensional transcurrent regime. It is likely that $\zeta_H$ is more oriented N 170°E (*).	Funvisis, 1984
t1.85	42	Caracas–La Guaira highway; south bank of Tacagua river Lat: +10.57°; Long: –67.02°	N 150°	Subhor.	N 060°	Subhor.	Q	Near the Tacagua–El Avila fault. In metamorphic rocks. Estimated from acute angle between conjugate strike-slip faults.	Funvisis, 1984
t1.87	43	Boyacá highway, dirt track to Galipán (El Avila range), Caracas Lat: +10.53°; Long: –66.90°	N 140°	Subhor.	N 050°	Subhor.	Q	Derived from acute angle between conjugate strike-slip faults, in metamorphic rocks; and confirmed by meso-structural analyses. In association with the Tacagua–El Avila fault.	Funvisis, 1984
t1.88	44	Guarenas–Guatire highway (Guarenas–Guatire basin, Miranda state) Lat: +10.47°; Long: –66.52°	N 155°ρ20°	Subhor.	N 065°	Subhor.	Q	Good dataset of strike-slip faults, in Pliocene sedimentary fill of the Guarenas–Guatire basin.	Funvisis, 1984
t1.90	45	El Rodeo–Guatire (Miranda state) Lat: +10.45°; Long: –66.48°	N 175°ρ30°	Subhor.	N 085°	Subhor.	Q	Large population of conjugate strike-slip faults. In Pliocene fill of the Guarenas–Guatire basin.	Funvisis, 1984

(continued on next page)



t1.105	52	Tapipa, Barlovento basin, Miranda state Lat: +10.24°; Long: -66.35°	$\zeta_2$ : 174	Subhor. (10°)	N 265°	Subhor. (05°)	Q	Faulting in Caucagua formation. Transcurrent-extensional regime (R=0.95) of local significance, related to pull-apart basin at horse-tail splay of the La Victoria fault.	Hernández and Rojas, 2002
t1.106	53	Jose; Petrochemical Complex “José Antonio Anzoátegui” (Anzoátegui state) Lat: +10.06°; Long: -64.83°	N 144°	Subhor. (24°S)	N 020°	Subhor. (23°S)	Q	Large population of striated fault planes in alluvial ramps of Early Pleistocene age. Extensional trans current regime. In association to folds at southern tips of the Píritu and San Mateo (Jose) faults.	Audemard and Arzola, 1995
t1.107									
t1.108	54	El Yaque (Nueva Esparta state) Lat: +10.93°; Long: -63.95°	N-S	Subhor.	E-W	Subhor.	Q	Derived from tension gashes in Upper Pliocene hydro-thermal travertine deposits.	Beltrán and Giraldo, 1989; Giraldo and Beltrán, 1988
t1.109	55	Cerro El Diablo; east of Araya, Sucre state Lat: +10.63°; Long: -64.15°	~N-S	Subhor.	E-W	Subhor.	Q	Excellent microtectonic dataset in sediments of Cubagua fm. (Upper Miocene-Lower Pliocene).	Beltrán and Giraldo, 1989; Giraldo and Beltrán, 1988
t1.110									
t1.111	56	El Obispo; east of Araya, Sucre state Lat: +10.63°; Long: -64.00°	N 163° $\rho$ 11°	Subhor.	N080°		Q	Several measures in sedimentary rocks of Cubagua fm. (Upper Miocene-Lower Pliocene).	Beltrán and Giraldo, 1989; Giraldo and Beltrán, 1988
t1.112	57	Punta Amarilla; east of Manicuaire, Sucre state Lat: +10.58°; Long: -64.20°	N 030° $\rho$ 25°	Subhor.	N 120° $\rho$ 15°	Subhor.	Q	Near Laguna Grande fault. Few striated fault planes in Cubagua fm. rocks. Tensor may only have local significance due to proximity to the fault (*)	Beltrán and Giraldo, 1989; Giraldo and Beltrán, 1988
t1.113	58	Cumaná Brickyard (NE of International Airport; Cumaná, Sucre state) Lat: +10.47°; Long: -64.15°	N 165° $\rho$ 40°	Subhor.			Q	Near the El Pilar fault. From microfaults in Cubagua fm. rocks.	Beltrán and Giraldo, 1989; Giraldo and Beltrán, 1988
t1.114									

(continued on next page)

t1.115 Table 1 (continued)

## t1.116 Quaternary stress tensors

Station no. ( $\xi$ )	Locality	$\zeta_H$ (max)		$\zeta_h$ (min)		Age	Observations and interpretations	Reference
		Strike	Dip	Strike	Dip			
t1.117 t1.118 59	Marigüitar, southern coast of Cariaco gulf, Sucre state	N 150° $\rho$ 10°	Subhor.	N 60°E	Subhor.	Q	In Pleistocene fine-grained continental sediments.	Beltrán and Giraldo, 1989; Giraldo and Beltrán, 1988
t1.119 t1.120 60	Lat: +10.45°; Long: –63.95° Juan Sánchez village; south of Casanay, Sucre state	N 170°	Subhor.	N080°E	Subhor.	Q	Excellent microtectonic dataset in sedimentary rocks of Cubagua fm. (Upper Miocene–Lower Pliocene).	Beltrán and Giraldo, 1989; Giraldo and Beltrán, 1988
t1.121 t1.122 61	Lat: +10.48°; Long: –63.31° Northeastern Venezuela	NNW–SSE (NW–SE $\leftrightarrow$ N–S)	Subhor.	NE–SW	Subhor.	Q	Derived from spatial disposition of major structures (folds and faults) and fault kinematics	Beltrán and Giraldo, 1989; Giraldo and Beltrán, 1988
t1.123 t1.124 62	Campoma (heading to Chiguana) Edo. Sucre Lat: +10.51°; Long: –63.61°	N 160° $\rho$ 20°	Subhor.			Q	Derived from orientation of synsedimentary folding axis in Chiguana fm. sedimentary rocks of Pliocene–Lower Pleistocene age.	Mocquet, 1984
t1.125 63	Villa Frontado; in road to Blascoa, Sucre state Lat: +10.47°; Long: –63.65°	N 015° $\rho$ 30°	variable	N 105° $\rho$ 40°	variable	Q	Few measures in sediments of Villa Frontado fm (Pliocene–Lower Pleistocene). After revision, new $\sigma_H$ orientation becomes N160°E.	Mocquet, 1984

t1.126	64	Los Carneros Point; Caribbean coast of Araya Península; Sucre state Lat: +10.65°; Long: -63.71°	N 135°ρ20°	Subhor. to intern.	N 045°ρ20°	Subhor. to intern.	Q	In association with Laguna Grande fault	Mocquet, 1984
t1.127									
t1.128	65	1,5 km to the south of Cariaco; Sucre state Lat: +10.48°; Long: -63.53°	N 140°ρ40°	Subhor. to intern.			Q	Few measures in sediments of Villa Frontado fm (Pliocene–Lower Pleistocene). Close to El Pilar fault, which may disturb the stress field (*)	Mocquet, 1984
t1.129	66	Punta de Piedra; eastern Sucre state Lat: +10.54°; Long: -62.43°	ς <sub>2</sub> : 267	Subhor. (07°)	174°	22°	Q	Radial extension (R=0.08) of local significance, related to pull-apart basin at step-over between the El Pilar and Warm Springs faults. Microtectonic station of rather good quality. Faulting in Río Salado formation, at northern tip of the Los Bajos fault.	Audemard et al., 2003
t1.130									
t1.131	67	Río Arriba; eastern Sucre state Lat: +10.63°; Long: -62.40°	147°	11°	241°	19°	Q	Faulting in Río Salado formation. Transcurrent-extensional regime (R=0.70) of local significance, related to pull-apart basin at step-over between the El Pilar and Warm Springs faults. Microtectonic station of low quality due to very small dataset.	Audemard et al., 2003
t1.132									

t1.133 (ξ) The station no. corresponds to Fig. 4 labelling.

t1.134 (\*) Authors' own interpretation.

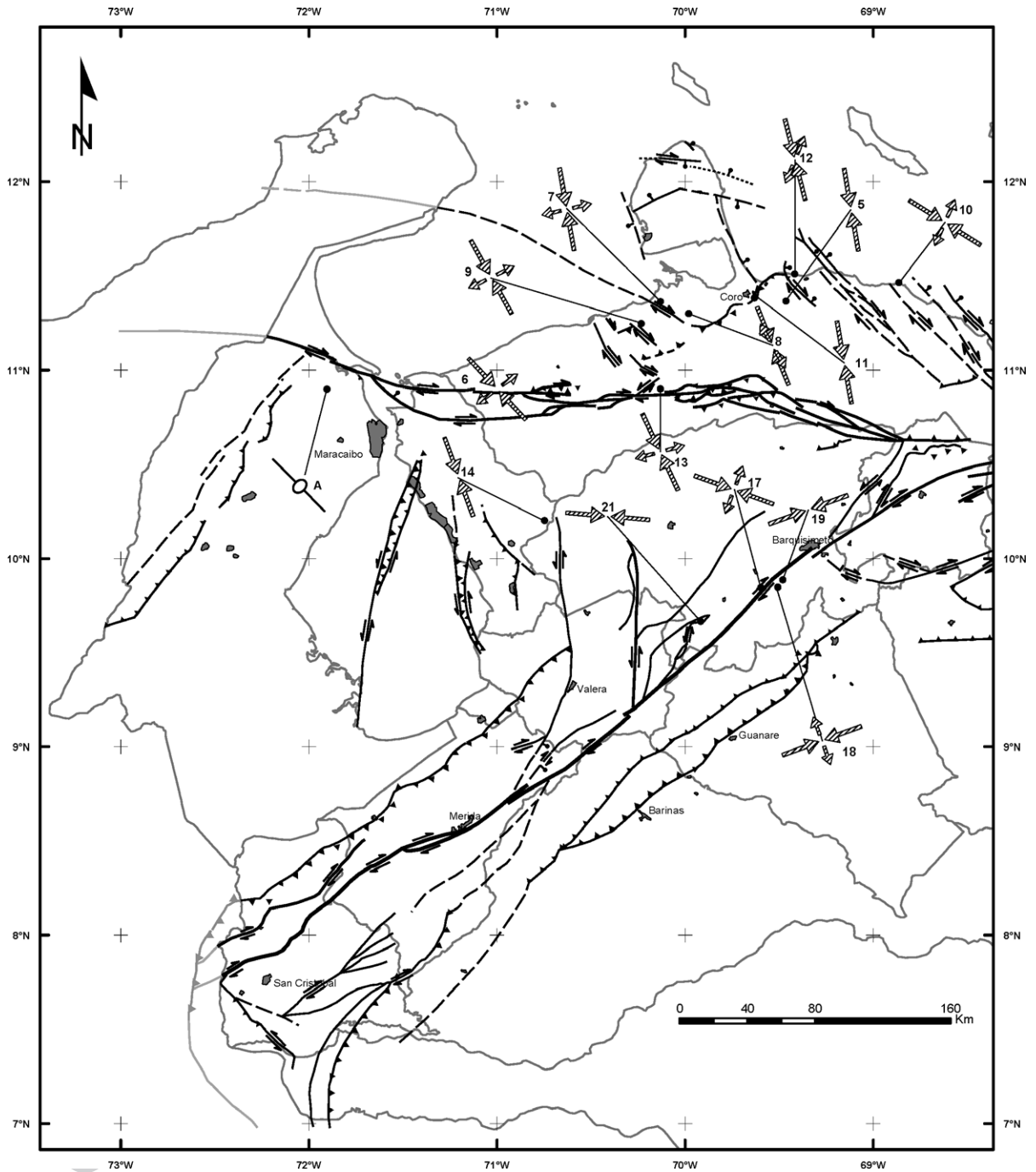


Fig. 5. Map of Plio-Quaternary stress tensors for Venezuela derived from fault-slip data (Table 1; updated and modified from Audemard et al., 1999) and wellbore data (Table 2). Note: non-orthogonal stress axes in plan-view imply that the stress tensor is off the vertical position. Wellbore data (A through D) are represented by either ellipses for breakouts, where  $\sigma_H$  is indicated by the axis, or an open fissure for hydraulic fracturing; or both representations. Stress tensor labelling corresponds to the numbers in Table 1. As to the wellbore data, datapoint A is from Sánchez et al. (1999), datapoints B and C are from Muñoz (2002) and D is from Willson et al. (1999). This map is fractionated regionally in three (a through c): western, central and eastern Venezuela. The tectonic base map corresponds to the one displayed in Figs. 2 and 3 (for toponyms, refer to those figures).

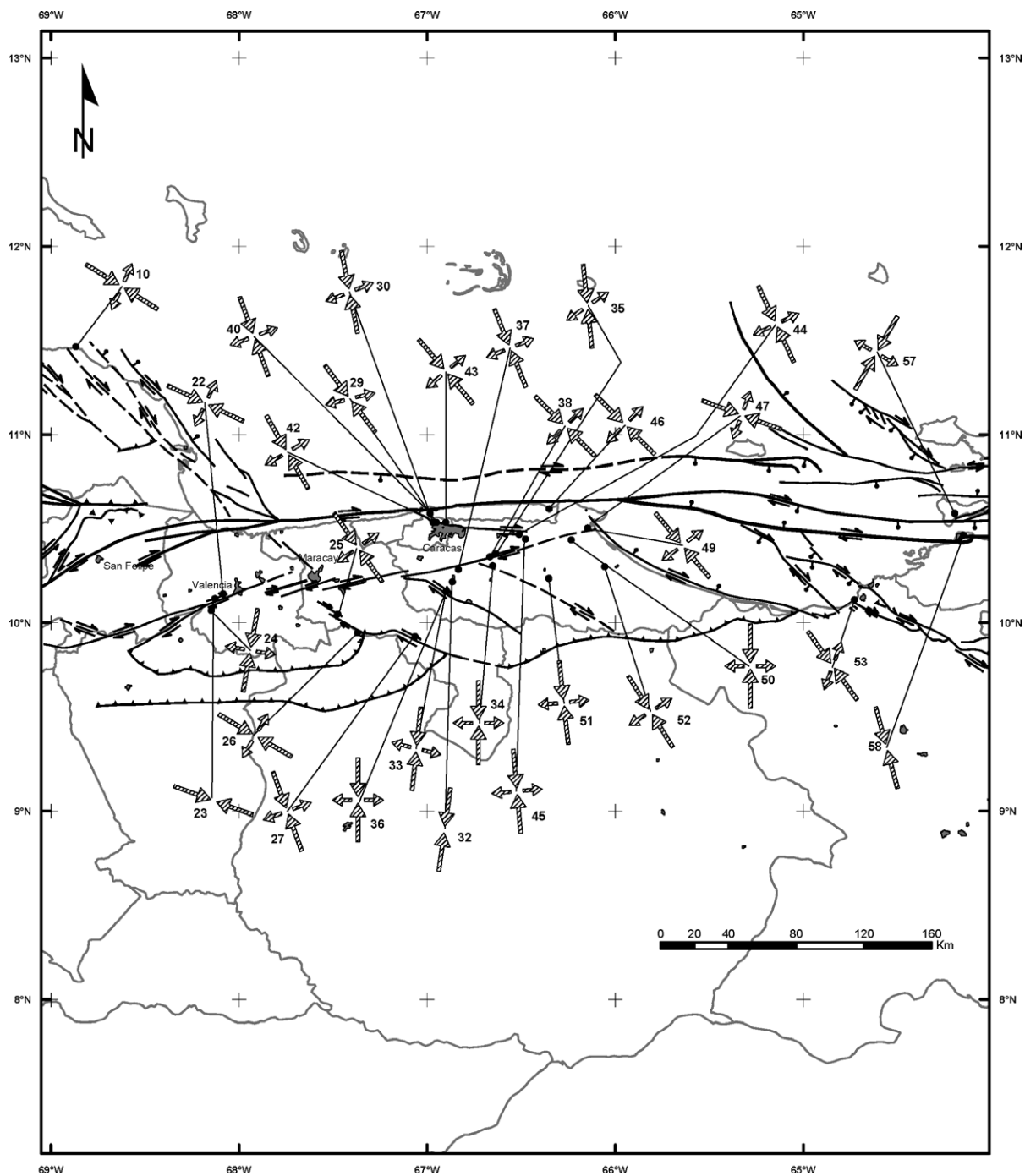


Fig. 5 (continued).

868 confidentiality imposed by the Venezuelan oil-indus-  
 869 try. In general, these data are rarely released; and  
 870 even more rarely published (e.g., Sánchez et al.,

1999; Willson et al., 1999; Muñoz, 2002). The same  
 table format as for the Quaternary stress tensors  
 derived from microtectonic data has been used for

871  
 872  
 873

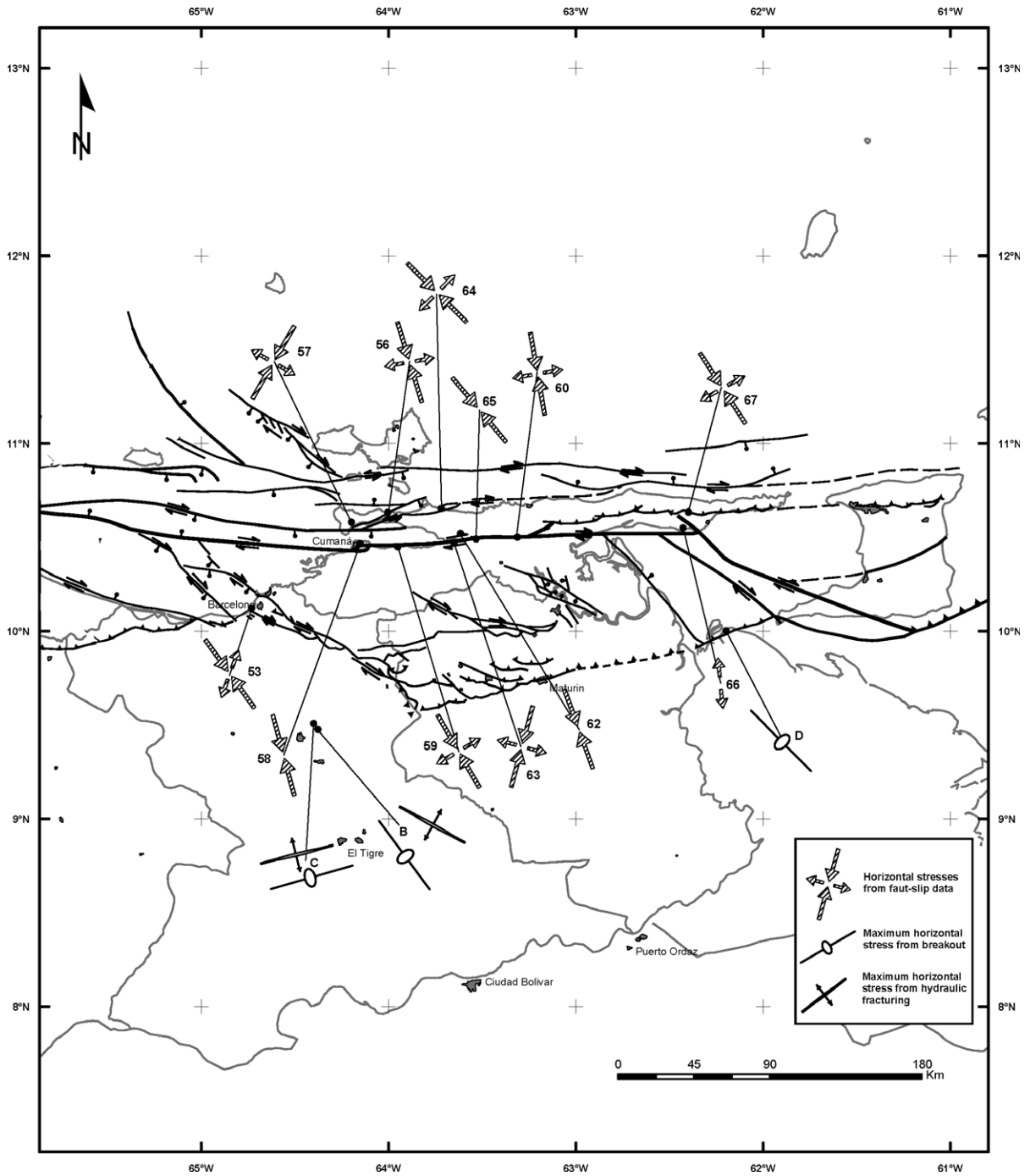


Fig. 5 (continued).

874 those from wellbore data, which are summarized in  
 875 Table 2. Table labels perfectly correspond to Fig. 5  
 876 labelling.

877 Previously to the present compilation and integra-  
 878 tion of stress tensors derived from geologic (micro-  
 879 tectonic) data at national scale, this type of attempt

t2.1 Table 2

t2.2 Compilation of available stress tensors derived from borehole data

t2.3 Stress tensors from wellbore data

t2.4	No.	Locality	$\zeta_H$ (max)	$\zeta_h$ (min)	Depth	Observations and interpretations	Reference
t2.5	1	Mara Oeste oil-field northwestern plain of Maracaibo lake, Zulia state	N 135°	N 045°			Sánchez et al., 1999
t2.6		Estimates: Lat: +10.90° Long: -71.90°					
t2.7	2	Santa Rosa Dome, Area Mayor de Oficina, 10 km NE of Anaco, Anzoátegui state.	N 135°	N 045°	6800'	Well RG231 located on dome crest In Oficina formation. Breakout orientations: N 045°	Muñoz, 2002
t2.8		Estimates: Lat: +9.483° Long: -64.383°					
t2.9	3	Santa Rosa Dome, Area Mayor de Oficina, 10 km NE of Anaco, Anzoátegui state.	N 140–150°	N 050–060°	9900'	Well RG231 located on dome crest In Merecure formation. Breakout orientations: N 050–060°	Muñoz, 2002
t2.10	4	Santa Rosa Dome, Area Mayor de Oficina, 10 km NE of Anaco, Anzoátegui state.	N 130–150° and N170°	N 040–060° and N080°	11,000'	Well RG231 located on dome crest In San Juan formation. Breakout orientations: N 040–060° and 080°	Muñoz, 2002
t2.11	5	Santa Rosa Dome, Area Mayor de Oficina, 10 km NE of Anaco, Anzoátegui state.	N 145–160°	N 055–070°	12,500'	Well RG231 located on dome crest In San Antonio formation. Breakout orientations: N 055–070°	Muñoz, 2002
t2.12	6	Santa Rosa Dome, Area Mayor de Oficina, 10 km NE of Anaco, Anzoátegui state.	N 120° N 145–160°	N 030° N 055–070° N088°	13,500'	Well RG231 located on dome crest In San Antonio formation, near main thrust fault plane. Breakout orientations: N 030°, N 055–070° and N088°	Muñoz, 2002
t2.13	7	Santa Rosa Dome, Area Mayor de Oficina, 10 km NE of Anaco, Anzoátegui state.	N 135° N 175° N 025°	N 045° N 085° N 115°	14,000' => 15,256'	Well RG231 located on dome crest In Oficina formation, right under the thrust. Breakout orientations: very variable but three predominant modes: N045°, N 085° and N 115°	Muñoz, 2002
t2.14	8	Santa Rosa Dome, Area Mayor de Oficina, 10 km NE of Anaco, Anzoátegui state.	N 120–130°	N 030–040°	Not indicated	Well RG231 located on dome crest Hydraulic fractures: N 120–130°	Muñoz, 2002
t2.15		Estimates: Lat: +9.483° Long: -64.383°					

(continued on next page)

t2.16 Table 2 (continued)

t2.17 Stress tensors from wellbore data

t2.18	No.	Locality	$\zeta_H$ (max)	$\zeta_h$ (min)	Depth	Observations and interpretations	Reference
t2.19	9	Santa Rosa Dome, Area Mayor de Oficina, 10 km NE of Anaco, Anzoátegui state. Estimates: Lat: +9.508° Long: -64.40°	N 070–080°(*)	N 160–170°	10,000'	Well RG229 located on gently dipping northern limb of the so-called dome (highly asymmetric SSE-verging anticline*) In Oficina formation Breakout orientations: N 160–170° (* This orientation seems atypical in this region. It may be related to moment bending normal faulting close to fold crest. In such a case, that orientation corresponds to $\zeta_h$	Muñoz, 2002
t2.20							
t2.21	10	Santa Rosa Dome, Area Mayor de Oficina, 10 km NE of Anaco, Anzoátegui state. Estimates: Lat: +9.508° Long: -64.40°	N 070–080°(*)	N 160–170°	Not indicated	Well RG229 located on gently dipping northern limb of the so-called dome Hydraulic fractures: N 070–080° (* That orientation may well correspond to $\zeta_h$ , if it is related to moment bending normal faulting	Muñoz, 2002
t2.22	11	Pedemales oil-field, mouth of the Mánamo river, eastern Venezuela. Estimates: Lat: +10.00° Long: -62.20°	N 135°±30°	N 045°±30°	–	Theoretical wellbore breakouts oriented N 045°±30°, since they were not actually measured, but are derived from reported instabilities during drilling operations in this field	Willson et al., 1999
t2.23							

880 was only carried out at regional scale. Giraldo and  
881 Beltrán (1988) for a CONICIT project, later published  
882 by Beltrán and Giraldo (1989), integrated this type of  
883 data for eastern Venezuela. In the following two sub-  
884 sections, more details are given by separate as to the  
885 applied methodology and the present stress regime  
886 that is actuating across Venezuela.

#### 887 4.1. Methodology

888 A logic sequence of analysis steps is needed to  
889 determine the ongoing stress regime from fault-slip  
890 (microtectonic) data in a given region. First, the active  
891 tectonic framework of the study region has to be  
892 known. To achieve this, the active tectonic features of  
893 a given region need to be identified and characterized  
894 using two complementary and interrelated activities:  
895 (1) aerial photo interpretation of landforms diagnostic  
896 of Quaternary faulting and folding, at scales ranging  
897 between 1:50,000 and 1:25,000. Several reference  
898 works—such as those of Vedder and Wallace (1970),

899 Wesson et al. (1975), Slemmons (1977) and Aude-  
900 mard, 1999b—can be used for this sort of landform  
901 analyses; and (2) field verification of the interpreted  
902 geomorphic evidence of either brittle or ductile  
903 tectonic activity, which then leads to the selection of  
904 favourable sites exposing Quaternary deformation,  
905 primarily of the brittle type. The detail evaluation of  
906 these deformed outcrops, usually named microtec-  
907 tonic analysis for simplification purposes, comprises:  
908 (a) detailed logging of the outcrop, through which  
909 mesoscopic geometric and/or chronologic relationship  
910 among tectonic structures—as well as with respect to  
911 sedimentary sequence—are established; (b) determi-  
912 nation of fault slip using fault-plane kinematic  
913 indicators (grouped here under microtectonic data),  
914 among which deserve mention: steps, Riedel shears,  
915 recrystallizations, stylolitic peaks, slickolites (oblique  
916 stylolites, combining slickensides with stylolites), tool  
917 marks and/or gypsum fibre growth in some cases,  
918 such as those described by Tjia (1971), Mattauer  
919 (1973), Proust et al. (1977), Petit et al. (1983),

920 Hancock and Barka (1987) and Angelier (1994); and  
921 (c) measuring of throws and offsets, generally using  
922 crosscutting relationships between tectonic structures  
923 and planar sedimentary features. Finally, in the case of  
924 evaluating the last tectonic regime, to properly apply  
925 this evaluation, age constraints on the onset of the  
926 present-day tectonic phase are only achieved when the  
927 Neogene–Quaternary litho- and chrono-stratigraphy  
928 of the study region are well known beforehand.

929 In Venezuela, Funvisis' personnel, for over 20  
930 years, have calculated all stress tensors derived from  
931 sets of striated fault planes, which have remained  
932 mostly unpublished. This approach relies on an  
933 inversion method, through which the stress tensor is  
934 derived from the measured strain. Therefore, the  
935 applied method and quality of the resulting tensors  
936 through time have been strongly conditioned by the  
937 evolution of the methods. In few words, the collected  
938 dataset quality is definitely uneven. In the 1980s, the  
939 right dihedral method proposed by Angelier and  
940 Mechler (1977) was practiced “by hand” using a  
941 lower hemisphere Wulff net. Then, differentiating  
942 superposed tectonic phases was a rather heavy and  
943 time-consuming task with that crude method. Several  
944 automated inverse methods were developed almost  
945 simultaneously, including the Angelier and Mechler's  
946 method which has also been applied later to focal  
947 mechanism populations in order to derive a common  
948 stress tensor for earthquake populations that spatially  
949 cluster (e.g., Choy et al., 1998; Palme et al., 2001).  
950 The large majority of these methods were then at an  
951 experimental stage and mainly available to university  
952 research staff. In the second half of the 1980s,  
953 Funvisis applied the method developed by Etchecopar  
954 et al. (1981) among many others (Carey, 1976;  
955 Fleischmann and Nemcok, 1991; Phan-Trong,  
956 1993), simply due to availability. This lack of  
957 availability did not refrain other researchers to  
958 propose stress tensors but only relying on the spatial  
959 configuration of major tectonic features, such as in the  
960 Falcón basin by Audemard and De Mena (1985).

961 The Etchecopar et al.'s (1981) method, like many  
962 others, is based on the Bott's principle (Bott, 1959),  
963 which determines the stress tensor by minimizing the  
964 deviation between the shear stress and the measured  
965 slip on fault surfaces. Consequently, this tensor  
966 calculation depends strongly on determining correctly  
967 the sense of slip on each fault of a population, which

968 is obtained from the joint observation of several fault  
969 plane kinematic indicators listed earlier in this section,  
970 that have to necessarily comply with persistency and  
971 consistency among them. For instance, Audemard  
972 (1993) collected some 400 measures of fault striations  
973 on either fault planes or cobble surfaces in northern  
974 Falcón to have a robust dataset (stations 6 through 12  
975 in Table 1). Limitations of this particular inversion  
976 method were dealt very thoroughly by Ritz (1991).

977 Since the neotectonic period in Venezuela, as  
978 indicated earlier, corresponds roughly to the Quater-  
979 nary after Soulas (1986), the microtectonic data  
980 collection was essentially performed in Plio-Quater-  
981 nary sedimentary rocks (Table 1), to ensure that the  
982 defined stress tensors do correspond to the ongoing  
983 tectonic regime. However, few tensors were excep-  
984 tionally measured in Mesozoic metamorphic rocks,  
985 such as in the Caracas surrounds (stations 29, 30 and  
986 40 through 43, in Table 1). Needless to say that these  
987 tensors were only included if in agreement with other  
988 tensors obtained in the same region from the adjacent  
989 Neogene–Quaternary sedimentary fills of the Santa  
990 Lucía–Ocumare del Tuy, Barlovento and lake Valen-  
991 cia depressions and along the northern coast of the  
992 central Coast range, near Cabo Codera (La Sabana–  
993 Chuspa region); all these localities being in the north-  
994 central region of Venezuela and less than 150 km  
995 away from Caracas (refer to Fig. 2 for relative  
996 location). Moreover, some of these microtectonic  
997 stations (locality where a population of several striated  
998 fault planes is measured, from which a stress tensor—  
999 or as many stress tensors as tectonic phases hap-  
1000 pened—is later derived by an inversion method) were  
1001 located near tectonic features of confirmed Quaternary  
1002 activity (for instance, in the Tacagua valley along the  
1003 Tacagua fault, located WNW of Caracas; Fig. 2).  
1004 Some tensors, those ones derived from spatial con-  
1005 figuration of major faults/folds, are also listed in Table  
1006 1 (Appendix 1) but not included in the compilation  
1007 shown in Fig. 5, because they were not calculated by  
1008 an inversion method. Except for those tensors  
1009 (stations 6 through 13, 16 through 21, 29, 30, 48  
1010 through 53, 66 and 67) calculated with the Etchecopar  
1011 et al.'s (1981) method (Giraldo, 1985a,b; Audemard et  
1012 al., 1992, 1993, 2003; Audemard, 1993; Acosta,  
1013 1995; Audemard and Arzola, 1995; Acosta, 1997;  
1014 Espínola and Ollarves, 2002; Hernández and Rojas,  
1015 2002), the rest have been calculated using the right

1016 dihedral method designed by Angelier and Mechler  
1017 (1977). This latter method is less accurate than that of  
1018 Etchecopar et al., which is also capable of establishing  
1019 the qualitative shape of the stress tensor ellipsoid  
1020 through the value of “ $R$ ”. This ratio  $R$  is defined as  
1021  $(\sigma_2 - \sigma_3) / (\sigma_1 - \sigma_3)$ . The principal stress in vertical  
1022 position indicates the dominant tectonic regime but  
1023  $R$  helps to better define it (refer to Ritz, 1991, for  
1024 more details).

1025 The stress tensor compilation herein presented  
1026 gathers 67 entries from microtectonic data and 6 from  
1027 wellbore data (4 from breakouts and 2 from hydraulic  
1028 fracturing; refer to Tables 1 and 2 and Fig. 5), of  
1029 which about only 59 tensors are reliable. Many  
1030 tensors have been discarded because (1) they result  
1031 from just a simplistic regional structural interpretation;  
1032 or (2) some tensors do not reflect the present-day  
1033 phase (stations 39 and 48 in Table 1), since a younger  
1034 tectonic phase is superimposed.

#### 1035 4.2. Stress inversion results

1036 Several main results can be drawn from this  
1037 compilation (Fig. 5a through c).

1038 (1) Northern Venezuela—covering the Falcón  
1039 basin and the central and eastern Coast and Interior  
1040 ranges from west to east—is characterized by a Plio-  
1041 Quaternary stress tensor of rather uniform and  
1042 constant orientation throughout. The prevailing ori-  
1043 entations of this tensor are NW–SE to NNW–SSE  
1044 ( $145^\circ$  to  $170^\circ$ ) and NE–SW to ENE–WSW for the  
1045 maximum horizontal stress ( $\sigma_H$ ) and/or minimum  
1046 horizontal stress ( $\sigma_h$ ), respectively. Therefore, there  
1047 is a good consistency among stress tensors at regional  
1048 scale. In addition, tensors derived from microtectonic  
1049 and wellbore data also agree well among them. This  
1050 geologically derived tensor mostly represents a trans-  
1051 current regime (intermediate stress in vertical posi-  
1052 tion). Where the Etchecopar et al.’s method was  
1053 applied, such as in the Falcón region (upper part of  
1054 Fig. 5a), the stress regime can be constrained better  
1055 and is of the compressive transcurent type (Aude-  
1056 mard, 1991b, 1993, 1997b, 2001). Some authors name  
1057 this tectonic regime as transpressive and refer to the  
1058 enlarged sense of the term and do not keep its use only  
1059 for the localized stress changes introduced by strike-  
1060 slip motion near the wrench fault. This stress tensor is  
1061 highly oblique to the general east–west trend of the

major wrench faults of northern Venezuela (Oca–  
Ancón, San Sebastián and El Pilar faults). This strong  
obliquity is responsible for, on one hand, the  
occurrence of partitioning (right-lateral strike-slip  
along east–west trending wrench faults and transverse  
shortening in NNW–SSE direction). Should partition-  
ing be occurring, is it then appropriate to define the  
tectonic regime as transpressional? On the other hand,  
it is also responsible for simultaneous left-lateral  
strike-slip motion on faults that are slightly oblique  
to the east–west trending dextral faults, as it is the case  
of the WSW–ENE-striking Punta Charagato and  
Laguna Grande faults in eastern Venezuela (Figs. 2  
and 5c). It is worth mentioning that many micro-  
tectonic stations, if not most of them, are located close  
to or on major active faults. Therefore, it could be  
thought that they might just have a local significance.  
However, their consistency throughout the entire  
boundary zone between the Caribbean and South  
America plates gives them a more regional meaning.

(2) Since the stress tensor along northern Ven-  
ezuela from west to east (from northwestern Colombia  
to Trinidad) is very constant in its orientation, local  
variations of the stress regime can be clearly  
identified. Most of these local stress changes coincide  
with known transtensional geometries, such as sta-  
tions 16 (Yay depression; Table 1), 18 (transtension at  
fault divergence; Fig. 5a), 20 (Cabudare pull-apart  
basin; relative location in Fig. 2), 51 and 52  
(Barlovento basin; Table 1 and Fig. 5b) and 67  
(transtensional horse-tail splay at northern tip of Los  
Bajos fault; Table 1 and Fig. 5c). Occasionally, local  
variations occur at transpressional geometries (such as  
station 6 on the Oca fault at Hato El Guayabal; Table  
1 and Fig. 5a); also in association with bending-  
moment faulting (normal faulting at anticline crests  
during buckling; e.g., stations 53 at Jose Petrochem-  
ical complex and 66 at Punta de Piedras near Güiría;  
Table 1 and Fig. 5c). These changes are easily  
identifiable because the stress tensor orientation  
remains essentially constant but their principal stress  
magnitudes vary (stress tensor permutation, where  
maximum and intermediate stresses may interchange  
positions).

(3) At an even more local scale, detail micro-  
tectonic studies and the subsequent stress tensor  
determination by an inverse method may allow to  
reveal, for instance, the occurrence of block rotation

1110 (i.e., between the two strands of the Río Seco fault in  
1111 northern Falcón; refer to Audemard, 2001) or pro-  
1112 gressive tectonic tilting (i.e., Guadalupe–Chuchure  
1113 thrust at the Coro Formation stratotype locality—  
1114 south of Coro, Falcón state; refer to Audemard, 2001).  
1115 However, some structures may not definitively be  
1116 related to the regional stress field and respond to local  
1117 perturbations of the stress field, such as the folding at  
1118 Punta Macolla, at the convergence of the Western  
1119 Paraguaná and Cumaraguas faults, in the Paraguaná  
1120 peninsula (Audemard, 1993). These particular cases  
1121 are dealt in detail in the cited references, but are  
1122 omitted from this compilation because of their very  
1123 local significance, which is not the aim of this current  
1124 compilation.

1125 (4) The stress tensor calculated by either the  
1126 Etchecopar et al.'s (1981) automated method or the  
1127 right dihedral method of Angelier and Mechler  
1128 (1977) well represents the stress field for the  
1129 present-day kinematics of seven major families of  
1130 active faults along northern Venezuela: (a) east–west  
1131 right-lateral faults; (b) NW–SE right-lateral faults,  
1132 synthetic to the east–west faults; (c) NNW–SSE  
1133 normal faults; (d) NW–SE to NNW–SSE normal–  
1134 dextral to dextral–normal faults; (e) North–South to  
1135 NNE–SSW left-lateral faults, antithetic to the east–  
1136 west faults; (f) ENE–WSW to east–west right-lateral  
1137 faults—P shears; and (g) ENE–WSW reverse faults,  
1138 paralleling folding axis, which is also active. Spatial  
1139 configuration of these brittle tectonic structures  
1140 indicates that the region is undergoing a transpres-  
1141 sional s.l. (compressive-transcurrent) regime that  
1142 complies with the simple shear model proposed by  
1143 Wilcox et al. (1973). Therefore, this regional  
1144 configuration is related to the slightly oblique  
1145 convergence between the Caribbean and South  
1146 America plate in the west—and almost perfect  
1147 wrenching in eastern Venezuela with some  
1148 “apparent” transtension (Pérez et al., 2001; Weber  
1149 et al., 2001a,b), that is directly responsible for east–  
1150 west trending dextral wrenching along northern  
1151 Venezuela. In northeastern Venezuela, the apparent  
1152 inconsistency between the GPS derived slip vectors  
1153 from both Pérez et al. (2001) and Weber et al.  
1154 (2001a,b), which would seem to support some  
1155 transtension north of the El Pilar fault, and the  
1156 stress tensors herein presented (stations 54 through  
1157 61 in Table 1), which seem to support a regionally

1158 coherent transpression, can be resolved if microblock  
1159 extrusions north of the El Pilar fault were occurring.  
1160 In addition, this would, not only explain the slip  
1161 vector direction of  $N84^{\circ}\rho2^{\circ}E$  calculated north of the  
1162 El Pilar fault, but also the sinistral motion along the  
1163 ENE–WSW-striking Punta Charagato and Laguna  
1164 Grande faults. On the other hand, in the particular  
1165 case of northwestern Venezuela, this process is  
1166 accentuated by the convergence between the Bonaire  
1167 block (BB) and the Caribbean plate along the rather  
1168 flat Southern Caribbean subduction located offshore  
1169 the Netherland Antilles islands (LAS), which is in  
1170 turn driven by the NNE-directed extrusion common  
1171 to the Maracaibo and Bonaire blocks. Consequently,  
1172 it can be stated that there is a good accordance  
1173 between stress tensors derived from microtectonic  
1174 data and large-scale neotectonic structures.

1175 (5)  $\sigma_H$  in the northern Mérida Andes (Lara state),  
1176 when nearing the Boconó fault, tends to become east–  
1177 west oriented, which allows the ongoing simultaneous  
1178 functioning of the NE–SW-striking dextral (e.g.,  
1179 Boconó, Caparo, San Simón) faults, the equally  
1180 trending thrust faults along both Mérida Andes  
1181 foothills and the north–south striking sinistral faults  
1182 (e.g., Valera and Burbusay, among several others;  
1183 Figs. 2 and 5a).

1184 (6) Therefore, the stress field on the Maracaibo  
1185 block (MTB) and south of the Oca–Ancón fault  
1186 progressively turns counterclockwise from a NNW–  
1187 SSE trend in the north (Beltrán and Giraldo, 1989;  
1188 Audemard, 2001; this paper) to east–west oriented to  
1189 the south (Audemard et al., 1999; Fig. 5a). The stress  
1190 field in this region then resembles like a folding fan  
1191 with vertex pointing to the SE (Audemard and  
1192 Audemard, 2002). The orientation of this regional  
1193 stress field in western Venezuela results from the  
1194 superposition of the two major neighbouring inter-  
1195 plate maximum horizontal stress orientations ( $\zeta_H$ ):  
1196 roughly east–west trending stress across the Nazca–  
1197 South America type-B subduction along the Pacific  
1198 coast of Colombia and NNW–SSE oriented one  
1199 across the Caribbean southern boundary (Audemard,  
1200 2000b; Fig. 1). Therefore, the Maracaibo block is  
1201 simultaneously being shortened along the NW–SE  
1202 direction (expressed by the vertical growth of the  
1203 Santa Marta block and Perijá and Mérida ranges) and  
1204 roughly extruded north to NNE (Audemard, 1993,  
1205 1998, 2000b; Audemard and Audemard, 2002).

## 12065. Focal mechanisms

1207 Previous focal mechanism solution compilations in  
 1208 Venezuela include local coverage (Giraldo and Bel-  
 1209 trán, 1988; Beltrán and Giraldo, 1989; Kozuch, 1995;  
 1210 Choy et al., 1998), and more regional or nationwide  
 1211 coverage (Molnar and Sykes, 1969; Dewey, 1972;  
 1212 Kafka and Weidner, 1981; Pennington, 1981; Cister-  
 1213 nas and Gaulon, 1984; Tovar, 1989; Romero, 1994).  
 1214 Most frequent are solutions for single earthquakes  
 1215 (e.g., Rial, 1978; Badell, 1981; Giraldo, 1985b;  
 1216 Suárez and Nabelek, 1990; Ramos and Mendoza,  
 1217 1993; Rodríguez, 1995; Acosta et al., 1996; Funvisis  
 1218 et al., 1997; Choy, 1998; Pérez, 1998; Audemard,  
 1219 1999a) or a group of earthquakes in given regions  
 1220 (Marín, 1982; Lozano, 1984; Mendoza, 1989; Bach,  
 1221 1991; Bach et al., 1992; Malavé, 1992; Russo et al.,  
 1222 1992; CEE-INTEVEP, 1993; Romero, 1993; Malavé and  
 1223 Suárez, 1995; Valera, 1995) or composite focal  
 1224 mechanisms of rather small magnitude clustered  
 1225 earthquakes (Laffaille, 1981; Pérez and Aggarwal,  
 1226 1981; Ramos and Mendoza, 1991; Audemard and  
 1227 Romero, 1993; Pérez et al., 1997a,b; Jaimes et al.,  
 1228 1998). Cisternas and Gaulon (1984) have made the  
 1229 first compilation of the entire southern Caribbean  
 1230 region. However, the most thorough focal mechanism  
 1231 compilations for Venezuela prior to the present one  
 1232 are those of Tovar (1989) and Romero (1994); both in  
 1233 unpublished Funvisis reports. The latter compilation  
 1234 forms the core of that we are presenting herein.

### 1235 5.1. Methods

1236 The present compilation gathers 125 focal mech-  
 1237 anism solutions proposed for 114 (single or compo-  
 1238 site) events (Table 3 and Fig. 6). This difference in  
 1239 number resides in that some earthquakes have  
 1240 occasionally been interpreted as multi-focal events  
 1241 (Caracas 1967—label 09 through 12 in Table 3 and  
 1242 Fig. 6—and Boca de Tocuyo 1989—label 71  
 1243 through 75 in Table 3 and Fig. 6). On the contrary,  
 1244 two alternate solutions have rarely been proposed for  
 1245 single events (Curarigua August–September 1991—  
 1246 pairs labelled 82–83, 85–86 and 88–89 in Table 3  
 1247 and Fig. 6—and Los Arangues December 29,  
 1248 1995—labels 93 and 94 in Table 3 and Fig. 6—  
 1249 earthquakes), which are both compatible with known  
 1250 neighbouring fault kinematics and stress tensor

1251 derived from geologic data. For several events, it is  
 1252 worth mentioning that a choice of one solution  
 1253 among many proposed by different authors had to be  
 1254 made, taking into account which would fit best both  
 1255 attitude (strike and dip) and slip of the potentially  
 1256 causative fault. Due to space limitations, we ask the  
 1257 reader to refer to appendix in Audemard et al. (1999;  
 1258 available from the author) for more details on this  
 1259 selection.

1260 This compilation also includes 27 new solutions  
 1261 for earthquakes of small magnitude (<5 mb),  
 1262 recorded by the new Venezuelan seismological net-  
 1263 work in the last couple of years (solutions labelled  
 1264 99 through 125 in Table 3), added to the first  
 1265 Audemard et al.'s (1999) compilation. This has been  
 1266 possible because the array has been upgraded  
 1267 (enlarged and modernized) and has 28 new three-  
 1268 component broadband stations installed throughout  
 1269 the country as of April 2003. On the contrary, the  
 1270 present compilation shown in Fig. 6a through c does  
 1271 not incorporate 20 published focal mechanism  
 1272 solutions of small earthquakes, recorded during two  
 1273 microseismicity surveys carried out in western  
 1274 Venezuela (Bach, 1991; Bach et al., 1992; CEE-  
 1275 INTEVEP, 1993), and also in eastern Venezuela in  
 1276 1990 (CEE-INTEVEP, 1993), by a Comunidad  
 1277 Económica Europea-INTEVEP multidisciplinary task  
 1278 group. Neither the  $P$  arrivals nor the tension ( $T$ ) and  
 1279 pressure ( $P$ ) axis orientations nor the nodal plane  
 1280 attitudes of those solutions were available. All these  
 1281 data would have allowed the exact reconstruction of  
 1282 the focal mechanisms. Moreover, this information is  
 1283 essential to any reliability assessment or quality  
 1284 control. Some slight picking was performed among  
 1285 the proposed focal solutions by the CEE-INTEVEP  
 1286 group (Fig. 7). The discarded focal mechanisms were  
 1287 originally built as composite solutions and the event  
 1288 gathering for their construction did not follow either  
 1289 any tectonic criteria or time and space clustering.  
 1290 Nevertheless,  $P$  and  $T$  axes from focal mechanisms  
 1291 proposed for small earthquakes recorded during that  
 1292 northwestern Venezuela campaign (labelled as 2 in  
 1293 Fig. 7) coincide well with those of Fig. 6.

### 1294 5.2. Focal mechanism results

1295 Similarly to the stress tensors derived from geologic  
 1296 data, these focal mechanism solutions exhibit good

t3.1 Table 3

t3.2 Focal mechanism solutions for Venezuelan earthquakes spanning from 1957 through 2003 (updated and modified from Audemard et al., 1999)

t3.3	Date (yy/mm/dd)	Latitude (deg)	Longitude (deg)	Focal depth (km)	Magnitude (mb)	Nodal plane A			Nodal plane B			T axis		P axis		Fig. 5 label no.	Reference
						AZI	DIP	RAKE	AZI	DIP	RAKE	AZI	DIP	AZI	DIP		
t3.5	57/10/02	10.94	−62.80	60		261	90	180	351	90	0	36	0	126	0	1	Molnar and Sykes, 1969
t3.6	57/10/02	10.88	−62.90	10	5.5	47	86	135	313	45.14	174.4	171	26.7	280.3	33.2	2	Russo et al., 1992
t3.7	57/10/04	10.86	−62.77	6	6.7	75	45	41	196	62.4	127	59.8	60.6	316.4	7.4	3	Russo et al., 1992
t3.8	57/10/06	10.88	−62.68	10		132	44	−90	312	46	−90	42	1	222	89	4	Russo et al., 1992
t3.9	57/12/25	10.46	−62.55	22	5.8	215	87	100.3	321	10.8	16.3	135.7	47	305	41.1	5	Russo et al., 1992
t3.10	63/07/14	10.44	−62.74	20		90	63	−123.6	214	42.1	−42.6	216.7	0.9	307.5	41.1	6	Molnar and Sykes, 1969
	65/07/19	9.25	−70.44	20.0	5.2	55	90	180	145	90	0.0	190	0.0	280	0.0	7	Dewey, 1972 (in Pennington, 1981)
t3.11																	
t3.12	66/05/14	10.38	−63.05	37		274	71	−173.9	182	84.2	−19.1	229.4	−19.1	136.5	17.5	8	Molnar and Sykes, 1969
t3.13	67/01/04	10.70	−62.05	74		89	52	−136.8	329	57.4	−47	38.1	3.1	295.7	54.7	9	Molnar and Sykes, 1969
t3.14	67/07/30	10.60	−67.30	14.0	6.5	261	85	180	351	90	5.0	216.1	3.5	125.9	3.5	10	Suárez and Nabelek, 1990 <sup>a</sup>
t3.15	67/07/30	10.70	−66.95	14.1	6.5	265	69	−177.2	174	87.4	−21	221.4	12.8	127.5	16.6	11	Suárez and Nabelek, 1990 <sup>a</sup>
t3.16	67/07/30	10.18	−66.76	7.7	6.5	50	81	173.6	141	83.7	9.1	5.7	10.8	275.3	1.9	12	Suárez and Nabelek, 1990 <sup>a</sup>
t3.17	67/07/30	10.95	−66.88	21.0	6.5	276	59	128.4	39	47.8	44	239.9	57	339.8	6.4	13	Suárez and Nabelek, 1990 <sup>a</sup>
	67/12/21	7.00	−72.00	29.0	4.0	138	76	0.0	48	90	166	2.1	9.8	93.9	9.8	14	Dewey, 1972 (in Pennington, 1981)
t3.18																	
t3.19	68/03/12	13.15	−72.30	58	5.3	64	28	90	244	62	90	154	73	334	17	15	Pérez et al., 1997a <sup>a</sup>
	68/05/13	9.06	−71.10	29.0	4.9	228	60	130.9	348	49.1	41.4	191.3	54.7	290.2	6.3	16	Dewey, 1972 (in Pennington, 1981)
t3.20																	
t3.21	68/09/20	10.76	−62.70	103.0	6.2	226	15	66.7	70	76.2	96	348.2	58.3	155	31	17	Pérez and Aggarwal, 1981 <sup>a</sup>
t3.22	68/11/17	9.60	−72.60	150.0	5.8	149	8	179	240	89.9	82	142.1	44.6	337.9	44.3	18	Malavé and Suárez, 1995
t3.23	69/10/20	10.90	−72.40	36.0	5.7	47	50	−52.4	170	65	−136.6	270	9	23	49.0	19	Pennington, 1981
t3.24	69/10/20	10.87	−72.49	36.0	5.7	2.9	72.3	0.0	92.9	90	−162.3	226.5	12.4	319.3	12.4	20	Malavé, 1992
t3.25	70/01/27	7.49	−72.09	31	5.6	240	60	−143.9	130	59.4	−35.5	4.9	0.4	95.3	45.6	21	Kafka and Weidner, 1981
	70/05/19	10.90	−68.90	15.0	5.1	5	70	−38.1	110	54.6	−155.2	60.6	9.7	322.2	40.7	22	Dewey, 1972 (in Audemard and Romero, 1993) <sup>b</sup>
t3.26																	
t3.27	70/12/14	9.90	−72.68	158.0	5.1	159	14	−122.2	12.0	78.2	−82.4	95.6	32.8	291.6	56.2	23	Malavé, 1997
t3.28	73/07/08	6.80	−73.00	156.0	5.4	44	64	154.1	146	66.9	28.5	5.8	36	274.5	1.9	24	Pennington, 1981
	74/06/12	10.61	−63.47	0.0	5.7	213	70	−31.9	315	60.3	−156.8	265.8	6.3	171.2	36.3	25	Rial, 1978 (in Perez and Aggarwal, 1981) <sup>a</sup>
t3.29																	
	75/03/05	9.13	−69.87	25	5.6	210	50	56.4	76	50	123.4	52.6	64.9	143.1	0.2	26	Laffaille, 1981 (in Giraldo, 1985b) <sup>a</sup>
t3.30																	
	75/04/05	10.10	−69.60	36.0	5.5	112	80	168.6	204	78.8	10.2	67.9	15.1	158.1	0.8	27	Molnar and Sykes, 1969 (in Pennington, 1981)
t3.31																	
t3.32	75/04/05	9.56	−69.52	2.0	5.5	294	68	0.0	204	90.0	158	156.8	15.4	251.2	15.4	28	Marín, 1982
t3.33	77/10/04	10.16	−61.99	21	5.1	273	52	−161	171	75.1	−39.6	226.7	14.7	124.8	38.1	29	CMT

(continued on next page)

t3.34 Table 3 (continued)

t3.35	Date (yy/mm/dd)	Latitude (deg)	Longitude (deg)	Focal depth (km)	Magnitude (mb)	Nodal plane A			Nodal plane B			<i>T</i> axis		<i>P</i> axis		Fig. 5 label no.	Reference
						AZI	DIP	RAKE	AZI	DIP	RAKE	AZI	DIP	AZI	DIP		
t3.36																	
t3.37	77/12/11	9.56	−69.52	2.0	5.5	70	65	139.3	180	53.7	31.6	30.2	45.8	127.3	6.9	30	Marín, 1982 <sup>b</sup>
t3.38	79/05/05	9.09	−71.56	22	5.6	119	53	5	26	86	142.9	335.8	28.3	78.5	22.1	31	CMT
t3.39	79/06/C <sup>c</sup>	10.45	−63.60	1.5		177	85	−11.3	268	78.7	−174.9	222.9	4	132	11.5	32	Pérez and Aggarwal, 1981 <sup>b</sup>
t3.40	79/06/C <sup>c</sup>	10.40	−63.60	1.5		337	75	−161.3	242	72	−15.8	109.1	2	200	23.7	33	Pérez and Aggarwal, 1981 <sup>a</sup>
t3.41	79/07/C <sup>c</sup>	10.50	−63.25	1.5		250	85	−141.3	156	51.4	−6.4	16.6	22.3	120.4	30.2	34	Pérez and Aggarwal, 1981 <sup>a</sup>
t3.42	79/07/C <sup>c</sup>	10.45	−63.17	1.0		58	10	180	148	90	80	48.1	44.1	247.9	44.1	35	Pérez and Aggarwal, 1981 <sup>a</sup>
t3.43	80/01/02/C <sup>c</sup>	8.71	−71.08			29	65	103.2	180	28.1	63.9	323.7	67.3	109.2	19	36	Laffaille, 1981 <sup>b</sup>
t3.44	80/01/02/C <sup>c</sup>	8.66	−71.03			221	30	−106.6	60	61.4	−80.6	143.1	15.9	351.9	72	37	Laffaille, 1981 <sup>b</sup>
t3.45	80/11/26	7.96	−72.62	40	5.2	57	64	170.9	151	81.9	26.3	17	24.2	281.4	12.1	38	CMT
t3.46	82/05/10	10.50	−62.56	79.8	5.3	204	9	−4	298	89.4	−99	36.8	43.7	199	44.9	39	CMT
t3.47	82/07/04	7.65	−72.19	53.5	5.5	136	66	4.9	44	85.5	155.9	357.4	20.1	92.4	13.4	40	ISC
t3.48	83/03/08	10.89	−62.03	85.0	5.9	260	7	119.8	50.0	83.9	86.5	316.1	51.0	143.2	38.8	41	ISC
t3.49	83/04/11	10.08	−62.61	19.2	6	3	43	−57.6	142	54.9	−116.6	250.6	6.3	356.1	61.5	42	CMT
t3.50	84/C <sup>c</sup>	8.40	−70.90	20	4	45	44	77.6	242	47.3	101.7	222.9	81.3	323.7	1.7	43	Pérez et al., 1997a
t3.51	84/02/11	12.08	−60.00	39.1	5.3	348	53	−142.2	233	61	−43.6	292	4	195.5	50.5	44	ISC
t3.52	84/06/14	10.05	−69.78	18	5.2	340	65	−11.7	75	79.4	−154.5	205.4	9.7	300	25.4	45	CMT
t3.53	84/08/20	10.62	−62.53	21.8	5.1	80	71	165	175	75	19.6	38.3	23.8	306.8	3.3	46	CMT
t3.54	84/10/05	11.34	−60.25	41.2	4.4	172	57	−150.7	65	65.8	−36.7	120	5.0	25	43	47	ISC
t3.55	85/87/90C <sup>c</sup>	9.90	−68.70	15	3–3.9	168	84	0	78	90	174	32	4.2	123.2	4.2	48	Pérez et al., 1997b
t3.56	85/87/94C <sup>c</sup>	10.7	−67.00	15	3–3.9	355	60	0	85	90	−150	215.9	20.7	314.1	20.7	49	Pérez et al., 1997b
t3.57	85/11/28	11.76	−61.36	49.0	5.2	201	27	123.9	344	68	74.1	227	64	86	21	50	ISC
t3.58	86/C <sup>c</sup>	10.2	−67.00	15	3.0–5.8	48	65	−7.1	141	83.6	−25.2	272	12.7	7.3	22.2	51	Pérez et al., 1997b
t3.59	86/C <sup>c</sup>	9.5	−69.20	20	3.0–4.0	315	60	0	225	90	150	175.9	20.7	274.1	20.7	52	Pérez et al., 1997b
t3.60	86/C <sup>c</sup>	9.2	−69.90	20	4.0	190	40	52.5	55	59.3	117	13.3	64.5	125.9	10.4	53	Pérez et al., 1997a
t3.61	88/89/90C <sup>c</sup>	10.3	−67.00	15	3.0–4.0	39	75	−31.5	138	59.7	−162.6	91.2	10	351.8	32.7	54	Pérez et al., 1997b
t3.62	86/06/11	10.7	−62.93	20	6.0	97	52	−159.4	354	73.9	−39.8	50	13.9	308.4	39.1	55	CMT
t3.63	86/07/18	10.80	−69.35	15.0	5.6	64	41	106.2	223	51	76.4	78	78	323	5	56	ISC
t3.64	86/07/18C <sup>c</sup>	10.80	−69.36	44.9	5.6	204	85	21.8	112	678.3	174.6	70.1	78.9	336.1	11.6	57	Audemard and Romero, 1993
t3.65	86/09/12C <sup>c</sup>	11.04	−69.44	8.2	4.4	65	53	144.8	178	62.6	42.7	36.1	48.7	299.5	5.7	58	Audemard and Romero, 1993
t3.66	87/06/01	12.24	−61.54	156	4.0	62	36	177.5	154	89	54	33	36	274	34	59	ISC
t3.67	88/C <sup>c</sup>	10.30	−69.80	20	4.0	325	55	180	55	90	145	184	24	286	24	60	Pérez et al., 1997a
t3.68	88/03/10	10.16	−60.13	54	7.0	256	38	−67.3	48	56	−106.8	150	9.0	274	73	61	ISC
t3.69	88/03/11	10.06	−60.32	47	4.5	213	38	−131.2	81	63	−62.8	152	14	35	62	62	ISC
t3.70	88/03/12	10.19	−60.20	33	5.3	42	31	−132.6	269	68	−67.9	343	20	213	61	63	ISC

t3.71	88/03/16	9.72	-60.47	55	5.2	40	45	-118.1	257	51	-64.8	330	3	230	70	64	ISC
t3.72	88/03/25	10.04	-60.26	56	4.9	16	63	-173.4	283	85	-27.2	333	15	236	23	65	ISC
t3.73	88/04/12	10.35	-63.00	53.9	5.5	66	45	136.4	190	60.8	54.1	49.2	57.7	301.8	8.9	66	CMT
t3.74	88/06/24	10.28	-60.25	53	4.9	238	44	-89.3	59	46	-90.7	148.0	1.0	328.9	89.0	67	ISC
t3.75	88/07/12	11.04	-62.96	15	5.1	104	50	-166.2	5	79.4	-40	60.5	19	316.2	35.7	68	CMT
t3.76	89/01/30	7.80	-72.17	11.2	4.4	46	50	58.2	270	49.4	122.2	157.9	0.3	248.6	66.2	69	Mendoza, 1989
t3.77	89/04/15	8.50	-60.32	18.5	5.8	194	29	-153	80	77.3	-63.7	149.3	27.6	19.6	50.7	70	CMT
t3.78	89/04/30	11.10	-68.18	11.1	5.7	167.9	62.7	-177.3	259.2	87.6	-27.3	126.3	18.9	29.5	18.9	71	Malavé, 1992
t3.79	89/04/30	11.10	-68.18	11.1	5.7	178.1	52.9	-170.6	273.8	82.5	-37.5	139.5	25.2	36.7	25.2	72	Malavé, 1992
t3.80	89/04/30	11.10	-68.18	11.1	5.7	167.2	67.8	-158.0	265.9	69.7	-23.8	123.8	13.7	29.5	17.3	73	Malavé, 1992
t3.81	89/05/04	11.14	-68.21	13.6	5.0	137.2	74.2	-168.7	230.3	79.1	-16.1	93.3	11.1	1.1	11.1	74	Malavé, 1992
t3.82	89/05/04	11.14	-68.21	13.6	5.0	163.5	54.8	-86	336.5	35.4	-95.7	250.6	9.7	89.8	79.7	75	Malavé, 1992
t3.83	90/C <sup>c</sup>	10.8	-65.50	15	3-5.8	81	70	180	171	90	20	37.8	14	304.2	14	76	Pérez et al., 1997b
t3.84	90/03/21	10.72	-65.36	32.4	5.2	109	62	-36.3	218	58.5	-146.6	72.1	44	164.2	21	77	Ramos and Mendoza, 1993
t3.85	91/08/07	9.99	-69.992	18.2	5	45	70	-141.9	300	54.6	-24.8	169.4	9.7	267.8	40.7	78	Valera, 1995
t3.86	91/08/17	10.003	-70.032	16.2	5.3	310	45	-35.8	67	65.6	-129.1	184.1	12	290.1	52.4	79	Valera, 1995 <sup>b</sup>
t3.87	91/08/17	9.74	-69.83	15	5.5	344	86	0	74	90	-176	200.9	2.8	299.1	2.8	80	CMT
t3.88	91/08/17	10.54	-62.20	45.2	5.3	124	14	-48.9	262	79.5	-99.3	359.9	33.9	160.6	51.6	81	CMT
t3.89	91/08/20	10.05	-70.10	1.8	4.5	19	68	174.7	111	85.1	22.1	337.1	19	243	11.8	82	Romero, 1993
t3.90	91/08/20	10.054	-70.105	1.8	4.5	331	42	-18.5	75	77.7	-130.5	194.7	22	306.5	42.5	83	Valera, 1995 <sup>b</sup>
t3.91	91/08/20	9.988	-70.014	18	4.2	345	40	-10.4	83	83.3	-129.5	203.5	27.4	317.8	38.6	84	Valera, 1995 <sup>b</sup>
t3.92	91/08/21	10.038	-70.032	15.1	4.5	75	75	-126.9	326	39.5	-24	192.1	21.3	306.6	46.8	85	Valera, 1995 <sup>b</sup>
t3.93	91/08/21	10.03	-70.03	15.1	4.5	30	55	-20.3	132	73.5	-143.2	256.4	11.8	356.5	37.4	86	Romero, 1993
t3.94	91/09/02	10.063	-70.032	7.9	4.7	0	45	12.6	261	81.1	134.3	209.5	37.5	318.6	23	87	Valera, 1995 <sup>b</sup>
t3.95	91/09/14	10.021	-70.041	9.3	4.1	280	65	123.1	43	40.6	40.5	234.7	56.7	346.6	13.8	88	Valera, 1995 <sup>b</sup>
t3.96	91/09/14	10.02	-70.41	41	4.1	37	66	-6.0	130	84.8	-149	259.7	16.8	357.7	24.7	89	Romero, 1993
t3.97	94/05/31	7.423	-72.001	13.5	6.1	63	75	-128.5	315	40.9	-23.3	181.1	20.6	293.8	45.8	90	Rodríguez, 1995 <sup>b</sup>
t3.98	94/11/09	7.53	-71.73	21.3	5.2	178	42	112.4	329	51.8	71.1	100.7	74.4	72.3	5	91	CMT
t3.99	95/C <sup>c</sup>	10.2	-67.90	15	3-4.0	0	80	16	267	73.5	169.6	224.3	18.9	132.8	4.5	92	Pérez et al., 1997 <sup>c</sup>
t3.100	95/12/29	9.99	-70.08	16.2	5.1	47	65	103.7	197	28.3	63.1	342.6	67.1	126.8	18.9	93	Acosta et al., 1996
t3.101	95/12/29	9.99	-70.08	16.2	5.1	47	65	155.3	148	67.7	27.2	8.2	34.5	277	1.8	94	Audemard et al., 1999
t3.102	95/12/31	9.86	-69.91	15	5.1	257	74	-176.4	166	86.5	-16	212.6	8.7	120.4	13.8	95	CMT
t3.103	97/04/15	10.69	-69.63	15	5.2	109	65	163.8	206	75.4	25.9	69.6	28.5	335.8	6.9	96	CMT

(continued on next page)

t3.104 Table 3 (continued)

t3.105	Date (yy/mm/dd)	Latitude (deg)	Longitude (deg)	Focal depth (km)	Magnitude (mb)	Nodal plane A			Nodal plane B			T axis		P axis		Fig. 5 label no.	Reference
						AZI	DIP	RAKE	AZI	DIP	RAKE	AZI	DIP	AZI	DIP		
t3.106	97/07/09	10.545	−63.515	9.41	6.9	270	75	−136.1	166	47.9	−20.4	32.2	16.9	137.5	41.1	97	Audemard et al., 1999
t3.108	00/10/04	11.016	−62.30	119	6.0	90.0	58	78.5	291	33.8	107.7	328.8	74.2	188.3	12.3	98	Sobiesiak et al., 2002
t3.109	01/10/31	10.729	−67.016	6.6	3.8	55.0	45	20.8	311	76.6	131.1	261	42.6	9.3	18.8	99	this paper
t3.110	02/04/01	10.095	−69.07	0.0	3.4	3.0	49	9.1	267	83.1	138.6	216.4	33.3	322	22.3	100	this paper
t3.111	02/04/12	9.609	−69.996	18.5	4.4	60	70	0.0	330	90	−20	16.8	14	283.2	14	101	this paper
t3.112	02/04/14	10.158	−67.919	5.5	3.5	262	71	−146.9	160	58.9	−22.4	28.7	7.8	124.5	36.6	102	this paper
t3.113	02/04/18	12.033	−69.459	30.2	4.2	28	47	0.0	298	90	137	244.2	28.8	351.8	28.8	103	this paper
t3.114	02/04/18	10.199	−64.91	0.0	4.0	30	40	35.9	271	67.9	124.2	223.4	53.9	336.6	16	104	this paper
t3.115	02/04/27	10.49	−63.762	2.9	3.7	82	75	−125.4	332	38.1	−24.8	198.2	21.9	314.5	47.7	105	this paper
t3.116	02/05/27	10.698	−67.995	12	3.5	122	49	−69.3	272	45	−112.2	197.5	2	100.3	74.4	106	this paper
t3.117	02/05/28	10.638	−66.813	9	3.4	90	40	176.1	183	87.5	50.1	59.4	34.9	304.9	30.7	107	this paper
t3.118	02/05/28	12.201	−70.065	18.7	4.3	320	74	−49.7	68	42.9	−156.1	21.1	18.9	270.7	45.5	108	this paper
t3.119	02/06/02	10.383	−67.116	1.4	4.0	72	63	100.9	229	29	69.6	5	70	153.9	17.3	109	this paper
t3.120	02/06/02	10.358	−67.094	3.9	3.4	206	58	7.5	112	83.6	147.8	64.1	26.9	163.2	17.2	110	this paper
t3.121	02/06/03	10.402	−67.106	4.7	3.6	38	85	0.0	128	90	−175	262.9	3.5	353.1	3.5	111	this paper
t3.122	02/06/10	10.189	−67.677	1.2	4.1	260	66	−144.8	154	58.2	−28.6	25.5	4.9	119.7	41.3	112	this paper
t3.123	02/06/21	9.756	−69.264	4.8	4.0	60	71	159.3	157	70.5	20.2	18.4	27.8	108.6	0.3	113	this paper
t3.124	02/06/21	9.656	−69.303	0.0	4.1	4	47	64.5	219	48.7	114.8	199.1	71.6	291.7	0.9	114	this paper
t3.125	02/10/04	10.404	−62.425	8	4.0	195	47	8.8	99	83.6	136.7	47.4	34.1	154.8	23.8	115	this paper
t3.126	02/10/10	9.899	−69.950	0.3	3.4	52	48	152.8	161	70.1	45.4	25.8	45.5	281.7	13.5	116	this paper
t3.127	02/10/15	10.531	−63.691	1.6	4.7	190	48	8.9	94	83.4	137.7	42.9	33.7	149.4	23.1	117	this paper
t3.128	02/11/28	10.878	−62.233	60.7	4.0	308	22	0.0	218	90	−68	287.5	41	148.5	41	118	this paper
t3.129	02/12/04	10.814	−62.573	77.5	4.2	86	42	−82.5	256	48.4	−96.7	305.7	3.2	113.5	84.1	119	this paper
t3.130	03/01/07	9.83	−69.987	0.2	4.0	313	45	0.0	223	90	135	168.3	30	277.7	30	120	this paper
t3.131	03/01/15	8.876	−70.223	12.6	4.2	260	50	128.4	29	53.1	53.5	237.1	61.5	143.9	1.7	121	this paper
t3.132	03/02/11	10.213	−67.204	00	3.1	73	84	118.3	174	28.8	12.5	10.7	43.9	139.4	33.1	122	this paper
t3.133	03/02/18	8.975	−70.609	0.1	3.7	44	67	180	134	90	23	1.4	16	266.6	16	123	this paper
t3.134	03/04/01	9.838	−70.819	0.1	3.2	39	67	131.3	153	46.2	32.8	355.5	50	100.5	12.3	124	this paper
t3.135	03/04/01C	9.817	−70.804			34	63	131.7	151	48.3	37.4	354.3	52.3	95.6	8.6	125	this paper

t3.136 ISC=International Seismological Center; CMT=Centroid Moment Tensor.

t3.137 <sup>a</sup> Reassessed by G. Romero.<sup>b</sup> Modified by Audemard et al. (1999b).<sup>c</sup> 88/09/12C, Composite Focal Mechanism.

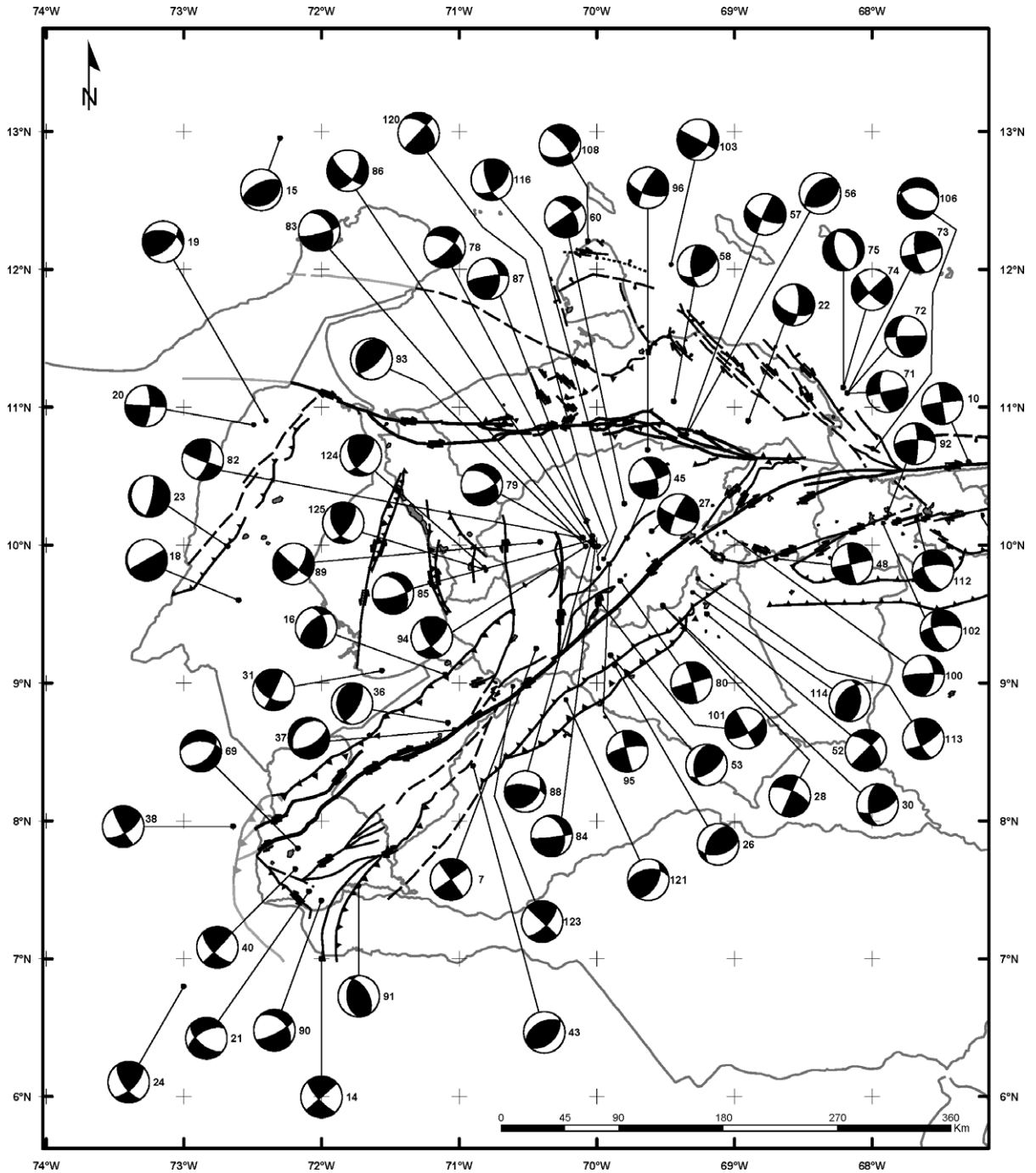


Fig. 6. Compilation map of focal mechanism solutions for Venezuela. Except for the southern end of the Lesser Antilles subduction and few scattered Netherlands Antilles slab-related earthquakes in northwestern Venezuela, all solutions correspond to crustal earthquakes (updated and modified from Audemard et al., 1999). Tensor labelling corresponds to the numbers in Table 3. This map is fractioned regionally in three (a through c): western, central and eastern Venezuela. The tectonic base map corresponds to the one displayed in Figs. 2 and 3 (for toponyms, refer to those figures).

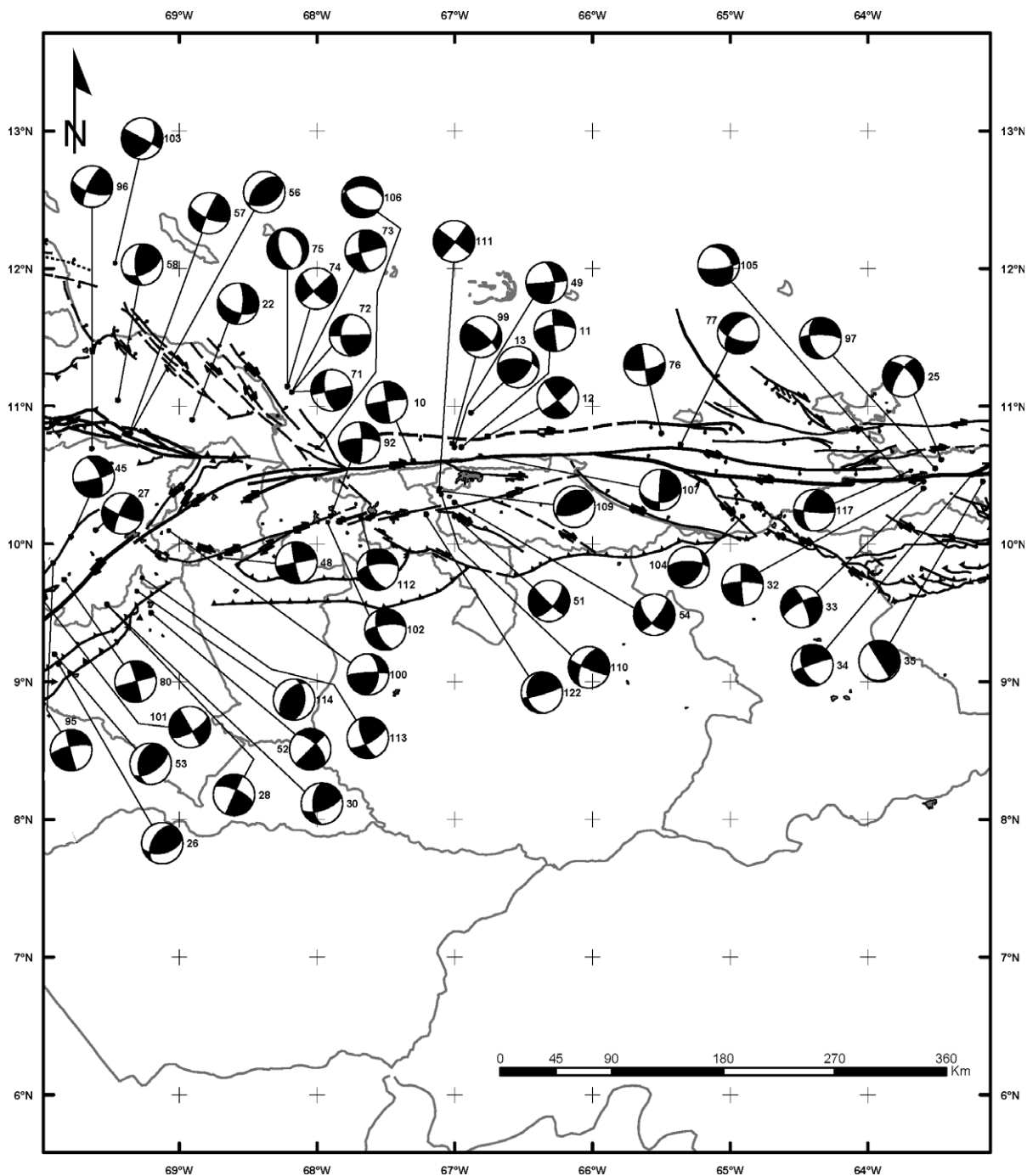


Fig. 6 (continued).

1345 consistency and persistency in  $P$  and  $T$  axis orienta-  
 1346 tions throughout northern Venezuela (Fig. 6). The  $P$   
 1347 and  $T$  axes respectively trend NW–SE to NNW–SSE

( $N145^\circ$  to  $170^\circ$ ) and NE–SW to ENE–WSW. No focal  
 1348 mechanism inversion has been performed for this  
 1349 paper, by applying a method such as the [Angelier and](#)  
 1350

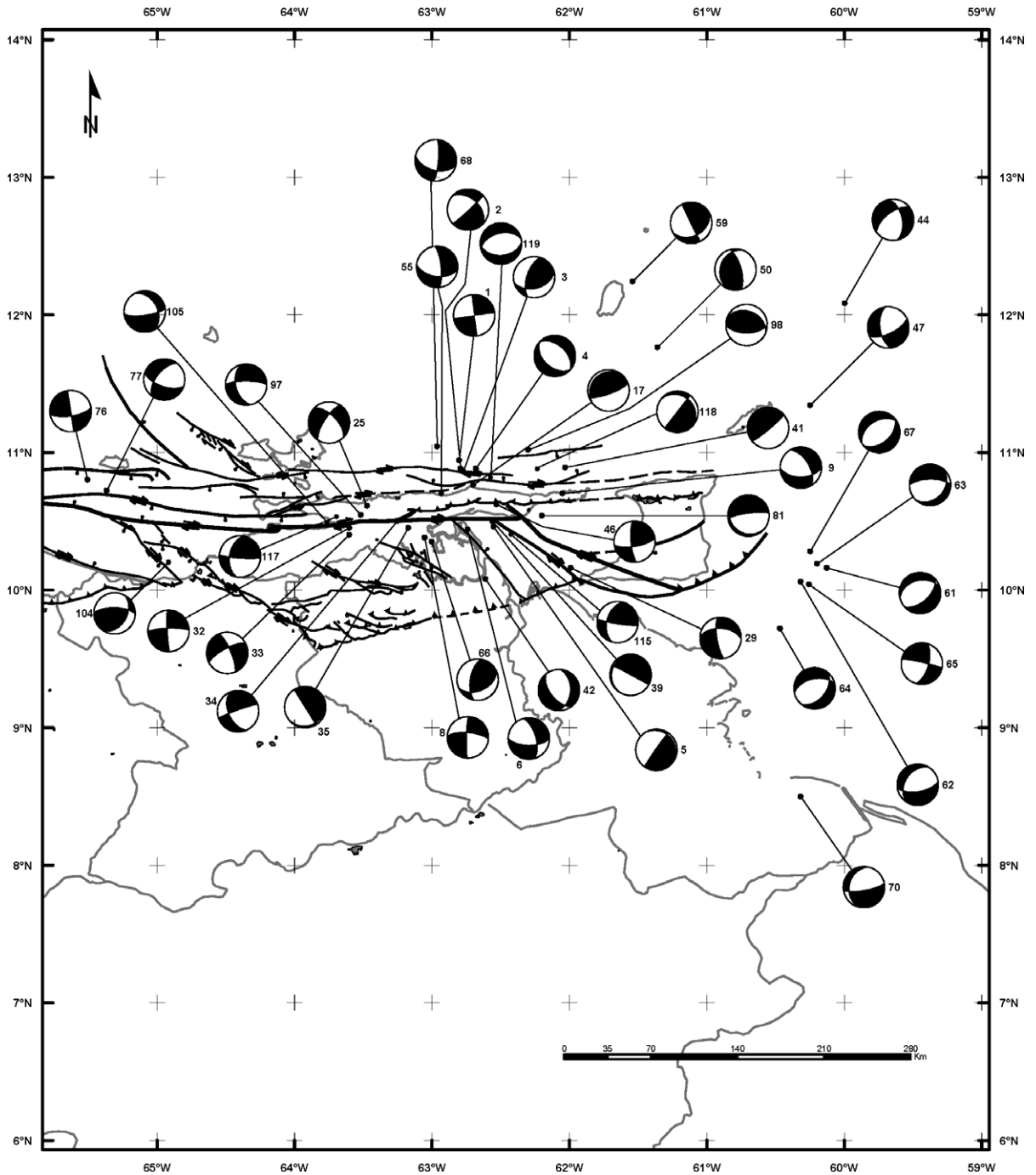


Fig. 6 (continued).

1351 Mechler's (1977) dihedral method. We plan this as  
 1352 future work, which would allow a direct comparison  
 1353 between the two sets of tensors. Nonetheless, the two

sets of independent data, the geologically derived  
 stress tensors and the  $P$  and  $T$  axes from fault-plane  
 solutions, seem to reflect the same fault kinematics

1354  
 1355  
 1356

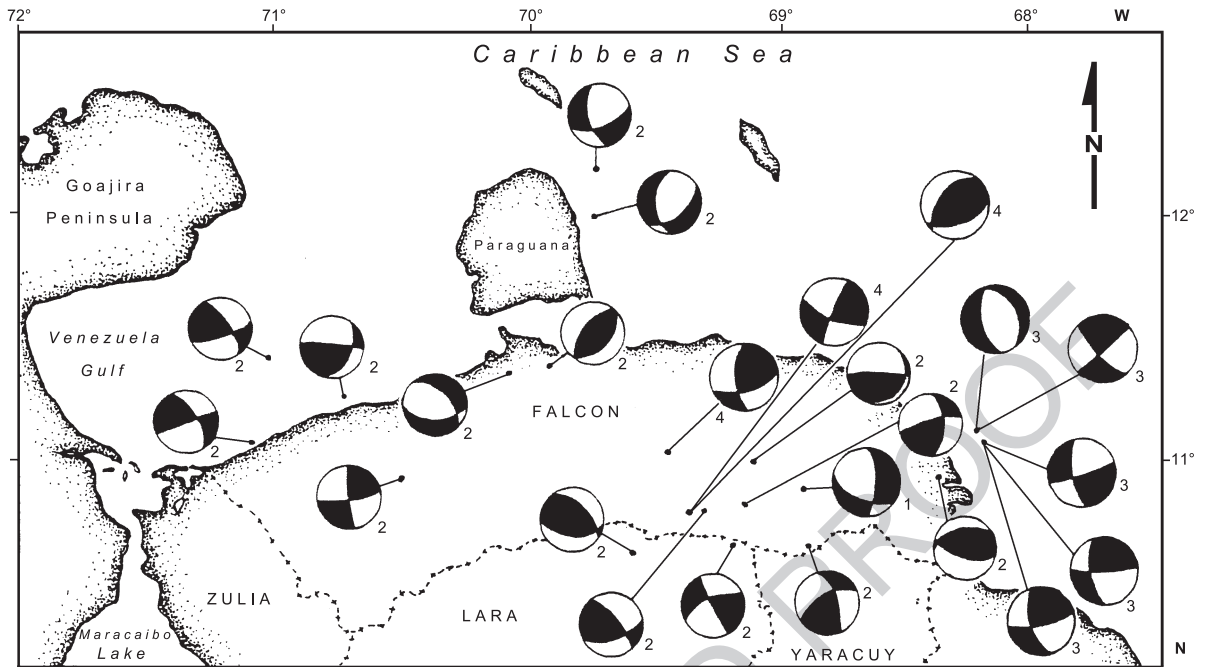


Fig. 7. Focal mechanism solutions for the Falcón region (modified from Audemard et al., 1999). Solutions labelled: (1) is from Dewey (1972) (modified by Audemard and Romero, 1993); (2) were obtained from a microseismicity survey made in 1990 in an Intevep-CEE project (modified from Bach, 1991); (3) are from Malavé (1992); and (4) are from Audemard and Romero (1993).

1357 along this complex plate boundary zone. The focal  
 1358 mechanism  $P$  and  $T$  axes match well with the axis  
 1359 orientations of the geologically derived (from both  
 1360 microtectonic and borehole data) stress tensors  
 1361 throughout the region (compare Figs. 5 and 6).  
 1362 Additionally, this comparison is also valid for the  
 1363 Mérida Andes chain at very shallow crustal levels (<40  
 1364 km deep): the  $P$  axis trends east–west when nearing  
 1365 the Boconó fault, similar to the maximum horizontal  
 1366 stress derived from microtectonic data (compare Figs.  
 1367 5a and 6a). Consequently, the focal mechanism  
 1368 solutions give additional supporting evidence to the  
 1369 present activity and kinematics of the seven fault  
 1370 families present along northern Venezuela described in  
 1371 Section 2, as well as to those active faults charac-  
 1372 terized in the Mérida Andes.

1373 Beyond the crustal deformation described previ-  
 1374 ously by means of their causative stress tensors or  
 1375 their kinematics derived from the rupture nucleation,  
 1376 few intermediate earthquakes, up to 200 km deep,  
 1377 have been detected under lake Maracaibo basin in  
 1378 northwestern Venezuela (Fig. 4B). They have been  
 1379 attributed, using focal solutions (e.g., Dewey, 1972;

Kellogg and Bonini, 1982; Malavé and Suárez, 1995;  
 Pérez et al., 1997a) and seismic tomography (Van der  
 Hilst, 1990), either to the SSE-directed oceanic slab of  
 the Leeward Antilles subduction (LAS in Fig. 1) or to  
 its western extension. This prolongation bends around  
 northwestern South America until it strikes north–  
 south and gently dips east under Colombia. Since our  
 prime aim in this paper is to determine the present-day  
 tectonic regime at crustal level, only three focal  
 mechanism solutions related to the LAS are included  
 in this compilation (focal solutions labelled 15, 18 and  
 23 in Table 3 and Fig. 6a). The solution labelled 15 (at  
 58 km deep) images the compressive regime at the  
 coupled zone between both plates, whereas the two  
 other solutions depict the moment-bending normal  
 faulting occurring at around 150 km in depth.

When addressing present southern Caribbean seis-  
 motectonics, it is impossible to skip the intermediate-  
 depth seismicity under Trinidad, the Paria peninsula  
 and the gulf of Paria. Both shallow and intermediate  
 depth earthquake focal mechanisms in the latter region  
 are herein presented to define where the main  
 wrenching within the plate boundary zone should be

1380  
 1381  
 1382  
 1383  
 1384  
 1385  
 1386  
 1387  
 1388  
 1389  
 1390  
 1391  
 1392  
 1393  
 1394  
 1395  
 1396  
 1397  
 1398  
 1399  
 1400  
 1401  
 1402

1403 (Los Bajos–El Soldado normal–dextral fault system),  
 1404 splitting apart crustal earthquakes on the southwest  
 1405 (Fig. 4A) from the slab-related earthquakes of the  
 1406 southern tip of the type-B Lesser Antilles subduction  
 1407 (Fig. 4B). This boundary is more precisely revealed by  
 1408 comparing the seismicity distribution in eastern  
 1409 Venezuela and Trinidad, shown in Fig. 4A and B.

1410 In the same way that Malavé and Suárez (1995)  
 1411 have proposed the occurrence of slab pull effect based  
 1412 on the intermediate-depth earthquakes under the Perijá  
 1413 range (in western Venezuela) and northern Colombia,  
 1414 Choy et al. (1998) has imaged it at the southern tip of  
 1415 the Lesser Antilles subduction, under the volcanic arc  
 1416 (similar to mechanisms 41 and 81 of Fig. 6c and Table  
 1417 3). Moreover, in the same region but at shallower  
 1418 depth (between 30 and 70 km deep), a set of focal  
 1419 mechanisms (44, 47, 61 through 64 of Fig. 6c and  
 1420 Table 3, among others; also in Fig. 3 of Choy et al.,  
 1421 1998) attest to moment bending normal faulting of the  
 1422 outer upper edge of the subducting slab at such depth.

1423 At more local scale, some tectonic processes or  
 1424 stress perturbations can also be derived from the  
 1425 evaluation of certain focal solutions, in the same way  
 1426 that the evaluation of the microtectonically derived  
 1427 stress tensors can (as discussed in Section 4):

1428

1429 (a) Laffaille (1981) generates two closely located  
 1430 but very different focal mechanisms: one for  
 1431 each of the valleys of the Mucujún and Chama  
 1432 rivers, respectively (locations given by focal  
 1433 solutions 36 and 37 in Fig. 6a). The first of the  
 1434 two (solution 36) corresponds to north–south  
 1435 reverse faulting paralleling the Mucujún valley,  
 1436 whereas the second to NE–SW-trending normal  
 1437 faulting paralleling the Chama valley and the  
 1438 Boconó fault. The first tensor fits the regional  
 1439 stress field (east–west trending  $\sigma_H$ ), whereas the  
 1440 second images local transtension, as should be  
 1441 expected along this portion of the Boconó fault,  
 1442 where the fault steps across the Las González  
 1443 pull apart-basin (“B” in Fig. 2).

1444 (b) When evaluating the Churuguara 1986 seismic  
 1445 swarm, Audemard and Romero (1993) deter-  
 1446 mined the occurrence of dextral reverse slip on a  
 1447 secondary fault to the Oca–Ancón during an  
 1448 aftershock (focal mechanism 58 in Fig. 6a) after  
 1449 dextral slip on the Oca–Ancón fault system  
 1450 during a larger event (mechanism 57 in Fig. 6a).

(c) The low frequency of moderate-to-large earth-  
 1451 quakes in Venezuela, and the consequent little  
 1452 generation of focal mechanisms solutions before  
 1453 the very recent seismological network modern-  
 1454 ization, has been partly overcome by making  
 1455 composite focal mechanism solutions from earth-  
 1456 quake sets tightly gathered in space and time.  
 1457 They have mostly confirmed the fault kinematics  
 1458 established via geologic criteria (Laffaille, 1981;  
 1459 Pérez and Aggarwal, 1981; Ramos and Mendoza,  
 1460 1991; Audemard and Romero, 1993; Pérez et al.,  
 1461 1997a,b; Jaimes et al., 1998).

(d) Ramos and Mendoza (1993) proposed a focal  
 1463 solution for the march 21, 1990 earthquake,  
 1464 located south of the Tortuga island. This solution  
 1465 images (solution 77 in Fig. 6b and Table 3) east–  
 1466 west-trending normal faulting, which supports  
 1467 the kinematics of the San Sebastián/El Pilar fault  
 1468 relay where the Cariaco trough pull-apart basin  
 1469 is forming. Then, the northern border normal  
 1470 fault of the basin slipped.

## 1473 6. Discussion

1474 Active fault kinematics derived from focal mecha-  
 1475 nisms solutions of crustal (<30 km deep) earthquakes  
 1476 along the plate boundary zone, in northern and western  
 1477 Venezuela, is in good agreement with geologic fault-  
 1478 plane kinematic-indicators. This fact could also be  
 1479 inferred by simply comparing  $P$  and  $T$  axis orientations  
 1480 from focal solutions with the principal horizontal stress  
 1481 orientations derived from geologic (microtectonic and  
 1482 borehole) data. Although this comparison should be  
 1483 avoided because both dataset are not equivalent, this  
 1484 implies that  $P$  axis orientations from focal mechanism  
 1485 solutions coincide pretty well with the maximum  
 1486 horizontal stress trajectories derived from microtec-  
 1487 tonically derived stress tensors (compare Figs. 5 and 6).  
 1488 This affirmation will only be firmly confirmed after  
 1489 focal mechanism inversions are made. However, the  
 1490 common intersection resulting from mentally adding  
 1491 the  $P$  area(s) of closely gathered focal mechanism  
 1492 solutions, as well as the  $T$  area(s), which defines  
 1493 respectively the most likely common maximum and  
 1494 minimum horizontal stress orientations of those sol-  
 1495 utions, foresees that matching between stress tensors  
 1496 derived from both datasets should be very close.

1497 Throughout northern Venezuela, the comparison of  
1498 both datasets (kinematics from focal mechanism  
1499 solutions and stress tensors from microtectonic data)  
1500 allows to gather active faults in seven main fault  
1501 trends: (a) east–west right-lateral faults; (b) NW–SE  
1502 right-lateral faults, synthetic to the east–west faults;  
1503 (c) NNW–SSE normal faults; (d) NW–SE to NNW–  
1504 SSE normal–dextral to dextral–normal faults; (e)  
1505 North–South to NNE–SSW left-lateral faults, anti-  
1506 thetic to the east–west faults, with the rare exception  
1507 of the ENE–WSW-trending Punta Charagato and  
1508 Laguna Grande faults; (f) ENE–WSW to east–west  
1509 right-lateral faults—P shears; and (g) ENE–WSW  
1510 reverse faults, parallel to folding axis. In the Mérida  
1511 Andes of western Venezuela, our conclusion is that  
1512 active partitioning is taking place: NE–SW trending  
1513 dextral wrenching along the Boconó and minor  
1514 parallel faults simultaneous with normal-to-chain  
1515 shortening (vertical growth through folding and  
1516 thrusting). The new focal mechanism solutions  
1517 presented herein bring additional supporting evidence  
1518 to the ongoing partitioning hypothesis originally  
1519 proposed from geologic data (Audemard and Aude-  
1520 mard, 2002). These focal solutions show mainly pure  
1521 strike or reverse slip in this region (Fig. 6a). A recent  
1522 compilation of focal solutions for the northern Mérida  
1523 Andes made by Palme et al. (2001) also reached the  
1524 same conclusion. Though the number of focal  
1525 mechanism solutions for the entire Mérida Andes is  
1526 not large (Fig. 6a), it distinctly shows that wrenching  
1527 essentially occurs along the chain axis, whereas three  
1528 mechanisms (solutions 26, 30 and 53 in Fig. 6a and  
1529 Table 3) on the eastern side of the Andes (among  
1530 them: the Guanare 1975 and the Ospino 1977 earth-  
1531 quakes) show dominant reverse slip.

1532 From the geologic data inversion, northern Ven-  
1533 ezuela is undergoing a compressive-transcurrent  
1534 (transpressional s.l.) regime characterized by maxi-  
1535 mum and/or minimum horizontal stresses trending  
1536 NNW–SSE to NW–SE and ENE–WSW to NE–SW,  
1537 respectively. This is further supported by slip vectors  
1538 in eastern Venezuela derived by Pérez et al. (2001).  
1539 Furthermore, the magnitude and orientation of those  
1540 vectors, besides confirming the active transpression,  
1541 are in pretty good agreement with the slip rates of the  
1542 major active faults in that region proposed from  
1543 geologic criteria (compare with slip rates in Audemard  
1544 et al., 2000). As well as in central Venezuela,

wrenching is the dominant process in eastern Ven-  
ezuela, with a slip rate concentrated on the El Pilar  
fault in the order of 8–10 mm/year, but other minor  
faults with various orientations, including subparallel  
faults and even slightly oblique thrust faults to the  
main dextral system, slip an order of magnitude less  
faster (<1–2 mm/year). Slip of such a magnitude  
cannot be yet resolved by GPS data, because the fault  
slip rates is within the average GPS velocity errors  
( $\rho$ 1–2 mm/year) indicated for the South American  
sites by Weber et al. (2001a,b). Longer GPS records,  
over one to two decades long, are in need to be able of  
determining accurately so slow slip rates.

The Mérida Andes is also subject to a similar  
stress tensor of the compressive-transcurrent type but  
 $\sigma_H$  is rotated to an east–west orientation. Meanwhile,  
 $\sigma_H$  shows an intermediate orientation between the  
Andes and northern Venezuela regions. This suggests  
that the stress field turns counter-clockwise, as  
originally proposed by Giraldo and Beltrán (1988;  
Fig. 8). The bending of the trajectories proposed  
herein is however more pronounced than those of  
Giraldo and Beltrán (1988) when crossing the  
Mérida Andes axis. This has also been determined  
by Palme et al. (2001) for the northern Mérida  
Andes, between the Valera and Boconó faults. As  
well, the maximum horizontal stress trajectories in  
this paper along northern Venezuela trend almost  
normal to the east–west-trending wrenching system,  
supporting ongoing transpression. Although wrench-  
ing in the Andes is also the prevailing active  
deformational mechanism, shortening across the  
chain seems much more important here than along  
northern Venezuela. This argument is supported,  
besides the present relief of the chain reaching  
almost 5000 m in elevation, by the geologically  
derived slip rates of both foothills thrust fault  
systems, which slip at about 0.5 mm/year.

## 7. Conclusions

An integrated compilation of microtectonic (fault-  
plane kinematic indicators) analyses, borehole data and  
focal mechanism solutions, complemented by regional  
neotectonic assessments, show that strain along north-  
ern and western Venezuela at present is being  
partitioned along the entire active plate boundary zone.

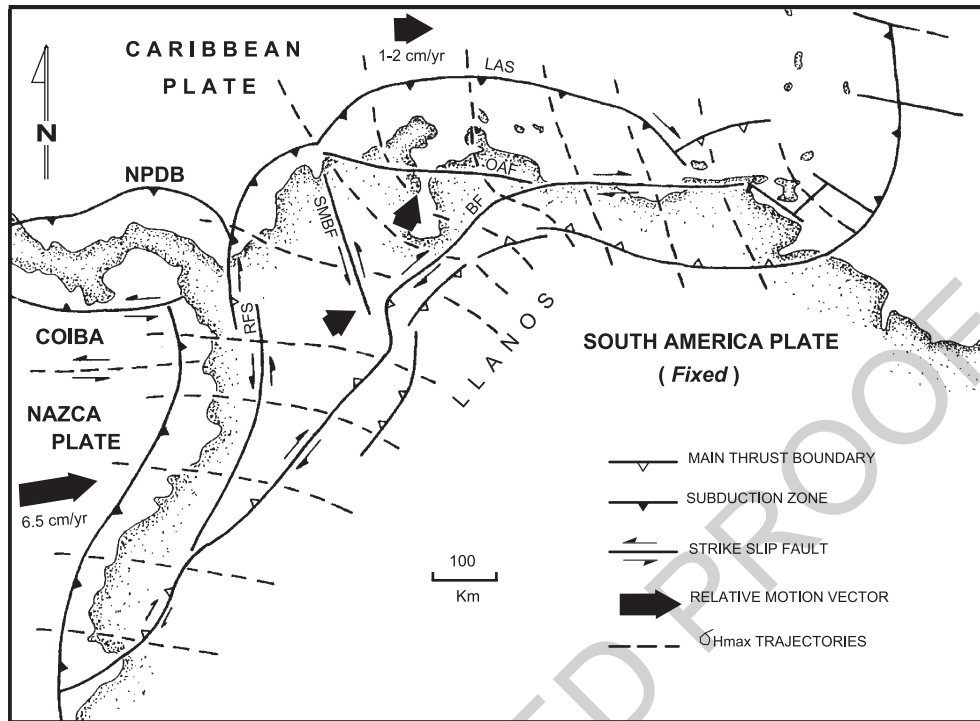


Fig. 8. Maximum horizontal stress trajectories for northern South America, based on neotectonic data, fault-plane kinematic indicators and focal mechanism solutions. Legend: BF: Boconó fault, LAS: Leeward Antilles subduction, OAF: Oca–Ancón fault, RFS: Romeral fault system, SMBF: Santa Marta–Bucaramanga fault (modified from Audemard and Audemard, 2002).

1590 On one hand, deformation along the southern Car-  
 1591ibbean coast results from a compressive strike-slip  
 1592 (transpressional s.l.) regime characterized by a NNW–  
 1593 SSE maximum horizontal stress ( $\zeta_H = \zeta_1$ ) and/or an  
 1594 ENE–WSW minimum ( $\zeta_h = \zeta_3$  or  $\zeta_2$ ) horizontal stress,  
 1595 which is responsible for present activity and kinematics  
 1596 of seven sets of structural—both brittle and ductile—  
 1597 features: east–west right-lateral faults (Oca–Ancón,  
 1598 San Sebastián, El Pilar, Northern Coast), NW–SE  
 1599 right-lateral faults—synthetic Riedel shears (Urumaco,  
 1600 Río Seco, La Soledad, Costa Oriental de Falcón, Río  
 1601 Guarico, Táchata, Araguaita, Píritu, Urica, San Francisco,  
 1602 Los Bajos–El Soldado), ENE–WSW to east–west  
 1603 dextral faults—P shears (La Victoria fault), NNW–  
 1604 SSE normal faults (Costa Occidental de Paraguaná, Los  
 1605 Médanos, Río San Juan Graben, Bohordal), almost  
 1606 north–south left-lateral faults—antithetic Riedel shears  
 1607 (Carrizal, Quebrada Chacaito), ENE–WSW reverse  
 1608 faults—sub-parallel to fold axes and mostly in the  
 1609 subsurface (Matapalo, Taima-Taima, Cantagallo, Tala,  
 1610 Interior range frontal thrusts, Tunapuy) and associated

1611 ENE–WSW trending folding (well-developed in the  
 1612 Falcón basin—northwestern Venezuela—and the Inter-  
 1613 interior range in the east). The main exceptions to this  
 1614 general configuration are found in eastern Venezuela:  
 1615 the Punta Charagato and Laguna Grande faults, at  
 1616 Punta Charagato (northern Cubagua island) and Araya  
 1617 Peninsula, respectively, that display left-lateral slip  
 1618 along the ENE–WSW direction. In most of northern  
 1619 Venezuela, brittle deformation obeys the simple shear  
 1620 model.

1621 On the other hand, the stress field on the  
 1622 Maracaibo block and south of the Oca–Ancón fault  
 1623 progressively turns counter-clockwise to become  
 1624 more east–west oriented, allowing left- and right-  
 1625 lateral slip along the north–south striking (e.g., Valera  
 1626 and Burbusay) and NE–SW striking (e.g., Boconó,  
 1627 Caparo, Queniquéa, San Simón) faults, respectively.  
 1628 This regional stress field in western Venezuela results  
 1629 from the superposition of the two major neighbouring  
 1630 interplate maximum horizontal stresses ( $\zeta_H$ ): east–  
 1631 west trending stress across the Nazca–South America

1632 type-B subduction along the Pacific coast of Colombia  
1633 and NNW–SSE oriented one across the Caribbean  
1634 southern boundary. Therefore, the Maracaibo block is  
1635 simultaneously being shortened on the NW–SE  
1636 direction (expressed by the vertical growth of the  
1637 Santa Marta block and Perijá and Mérida ranges) and  
1638 extruded roughly towards NNE.

1639 The stress tensors derived from geologic (micro-  
1640 tectonic and borehole) data compiled herein, as well  
1641 as the *P* and *T* axis orientations from focal mechanism  
1642 solutions, seem in good agreement with recent slip  
1643 vectors derived from several GPS studies performed  
1644 both in western and eastern Venezuela, essentially  
1645 during the 1990s. Wrenching is the dominant geo-  
1646 dynamic process, but it is always accompanied by  
1647 compression of variable magnitude along strike of the  
1648 major strike-slip fault system comprising the Boconó,  
1649 San Sebastián and El Pilar faults. Only locally,  
1650 transtension becomes significantly important, such  
1651 as in the Cariaco trough and gulf of Paria in  
1652 association with the El Pilar fault. Furthermore, the  
1653 GPS slip vectors do not only support the hypothesis of  
1654 ongoing transpression along most of this complex  
1655 plate boundary zone, but also tend to confirm most of  
1656 the active fault slip rates derived from geologic and  
1657 neotectonic studies carried out in Venezuela for  
1658 almost 25 years by Funvisis staff.

#### 1659 8. Uncited references

- 1660 Audemard, 1984
- 1661 Audemard, 1985
- 1662 Audemard, 2000a
- 1663 Audemard et al., 1988
- 1664 Audemard et al., 1995
- 1665 Beck, 1979
- 1666 Beck, 1986
- 1667 Blin, 1989
- 1668 Fanti et al., 1980
- 1669 Funvisis, 1984
- 1670 Gallardo, 1985
- 1671 Loyo, 1986
- 1672 Malavé, 1997
- 1673 Mathieu, 1989
- 1674 Mocquet, 1984
- 1675 Soulas et al., 1987
- 1676 Wozniak and Wozniak, 1979

#### Acknowledgements

Comments from John Weber (Grand Valley State  
University, Allendale, USA) to an earlier version of  
this manuscript improved this contribution, for which  
we are very thankful. Our thanks also go to the  
Managing Editor, Dr. Giuliano F. Panza, for providing  
helpful recommendations. This publication results  
from a project financed by PDVSA-CVP, under the  
leadership of Jairo Lugo. We much appreciate the  
continuous funding from Funvisis to this fundamental  
research line of the Earth Sciences Department that  
allowed most of the dataset collection and generation.  
Our appreciation also goes to Raymi Castilla (formerly  
at Funvisis, Caracas, Venezuela) and Guillaume Backe  
(graduate student at Université de Pau et des Pays de  
l'Adour, Pau, France) who helped to depurate some  
typing errors in the focal mechanism dataset. Marina  
Peña is thanked for her drawings. This paper is a  
contribution to FONACIT projects G-2002000478 and  
PI-2003000090, as well as to IGCP-433.

#### References<sup>1</sup>

- Acosta, L., 1995. Estudio geológico en la quebrada de Tacagua.  
Parte alta. Distrito Federal. Undergraduate thesis, Universidad  
Central de Venezuela, 213 pp + appendices. 1699  
1700
- Acosta, L., 1997. Estudio de la traza activa de la falla de Tacagua–  
El Avila para fines de microzonificación del corredor estratégico  
Caracas–Litoral Norte–central de Venezuela. Proceedings VIII  
Congreso Geológico Venezolano, Porlamar, vol. 1, pp. 21–27. 1701  
1702  
1703  
1704  
1705
- Acosta, L., Arzola, A., Hernández, A., Grimán, C., 1996. El sismo  
de Los Arangues del 29 de Diciembre de 1995. Unpublished  
FUNVISIS' report, 54 pp. 1706  
1707  
1708
- Aggarwal, Y., 1983. Neotectonics of the Southern Caribbean: recent  
data, new ideas. Acta Científica Venezolana 34 (1), 17. 1709  
1710  
1711
- Angelier, J., 1994. Fault slip analysis and paleostress reconstruction.  
In: Hancock, P. (Ed.), Continental Deformation. Pergamon,  
Oxford, pp. 53–100. 1712  
1713  
1714
- Angelier, J., Mechler, P., 1977. Sur une méthode graphique  
de recherche des contraintes principales également utilis-  
able en tectonique et séismologie: la méthode des diedres  
droits. Bulletin de la Société Géologique de France 19 (6),  
1301–1318. 1715  
1716  
1717  
1718  
1719
- Audemard, F.A., 1984. Evaluación geológica de la Cuenca del Tuy  
para fines de investigaciones neotectónicas. Undergraduate  
thesis, Universidad Central de Venezuela. 226 pp + appendices.  
2 Vol. 1720  
1721  
1722  
1723

<sup>1</sup> Labelling of references is needed for Tables 1 through 3.

- 1726 Audemard, F.A., 1985. Neotectónica de la Cuenca del Tuy.  
1727 Proceedings VI Congreso Geológico Venezolano, Caracas, vol.  
1728 4, pp. 2339–2377.
- 1729 Audemard, F.E., 1991a. Tectonics of Western Venezuela. PhD  
1730 thesis. Rice University, 245 pp + appendices.
- 1731 Audemard, F.A., 1991b. Proyecto suministro Falcón–Zulia  
1732 (SUF AZ): Actividad cuaternaria y caracterización sismogénica  
1733 de las fallas de Lagarto y Río Seco. Afinamiento de las  
1734 características sismogénicas del sistema de fallas de Oca–Ancón  
1735 y de Urumaco. Unpublished Funvisis' report for Maraven; 91 pp  
1736 + appendices.
- 1737 Audemard, F.A., 1993. Néotectonique, Sismotectonique et Aléa  
1738 Sismique du Nord-ouest du Vénézuéla (Système de failles  
1739 d'Oca–Ancón). PhD thesis, Université Montpellier II, France,  
1740 369 pp + appendix.
- 1741 Audemard, F.A., 1996. Paleoseismicity studies on the Oca–Ancon  
1742 fault system, northwestern Venezuela. *Tectonophysics* 259,  
1743 67–80.
- 1744 Audemard, F.A., 1997a. Holocene and Historical Earthquakes on  
1745 the Boconó Fault System, Southern Venezuelan Andes: trench  
1746 confirmation. *Journal of Geodynamics* 24 (1–4), 155–167.
- 1747 Audemard, F.A., 1997b. Tectónica activa de la región septentrional  
1748 de la cuenca invertida de Falcón, Venezuela occidental.  
1749 Proceedings VIII Congreso Geológico Venezolano, Porlamar,  
1750 vol. 1, pp. 93–100.
- 1751 Audemard, F.A., 1998. Evolution Géodynamique de la Façade Nord  
1752 Sud-américaine: Nouveaux apports de l'Histoire Géologique du  
1753 Bassin de Falcón, Vénézuéla. Proceedings XIV Caribbean  
1754 Geological Conference, Trinidad, 1995, vol. 2, pp. 327–340.
- 1755 Audemard, F.A., 1999a. El sismo de Cariaco del 09 de julio de  
1756 1997, edo. Sucre, Venezuela: nucleación y progresión de la  
1757 ruptura a partir de observaciones geológicas. Proceedings VI  
1758 Congreso Venezolano de Sismología e Ingeniería Sísmica,  
1759 Mérida, in CD-Rom.
- 1760 Audemard, F.A., 1999b. Morpho-structural expression of active  
1761 thrust fault systems in the humid tropical foothills of Colombia  
1762 and Venezuela. *Zeitschrift für Geomorphologie* 118, 1–18.
- 1763 Audemard, F.A., 1999c. Nueva percepción de la sismicidad  
1764 histórica del segmento en tierra de la falla de El Pilar, Venezuela  
1765 nororiental, a partir de primeros resultados paleosísmicos.  
1766 Proceedings VI Congreso Venezolano de Sismología e Ingeniería  
1767 Sísmica, Mérida, in CD-Rom.
- 1768 Audemard, F.A., 2000a. Neotectónica de la Cuenca del Tuy:  
1769 Observaciones complementarias. Memorias de las Jornadas  
1770 Científicas 55 Aniversario Escuela de Geología, Minas y  
1771 Geofísica, 1938–1993, Caracas, Boletín GEOS 32 (Diciembre  
1772 1997), 39–42.
- 1773 Audemard, F.A., 2000b. Major Active Faults of Venezuela.  
1774 Proceedings 31st International Geological Congress, Rio de  
1775 Janeiro, Brasil, 4pp. (extended abstract; in CD-Rom).
- 1776 Audemard, F.A., 2001. Quaternary tectonics and present stress  
1777 tensor of the inverted northern Falcón Basin, Northwestern  
1778 Venezuela. *Journal of Structural Geology* 23, 431–453.
- 1779 Audemard, F.A., 2002. Ruptura de los grandes sismos históricos  
1780 venezolanos de los siglos XIX y XX revelados por la sismicidad  
1781 instrumental contemporánea. Proceedings XI Congreso Vene-  
1782 zolano de Geofísica, 8 pp. (CD-Rom format).
- Audemard, F.A., Arzola, A., 1995. Evaluación de la actividad 1783  
tectónica de las fallas de sitio para el proyecto “Terminal de 1784  
Almacenamiento y Embarque de Crudo por Jose—TAECJ, Fase 1785  
II (Jose, Edo. Anzoátegui). Unpublished Funvisis' report for 1786  
CORPOVEN, 32 pp + appendices. 1787
- Audemard, F.E., Audemard, F.A., 2002. Structure of the Mérida 1788  
Andes, Venezuela: relations with the South America–Caribbean 1789  
geodynamic interaction. *Tectonophysics* 345, 299–327. 1790
- Audemard, F.E., De Mena, J., 1985. Falcón oriental, nueva 1791  
interpretación estructural. Proceedings VI Congreso Geológico 1792  
Venezolano, pp. 2317–2329. 1793
- Audemard, F.A., Romero, G., 1993. The Churuguara area— 1794  
Seismic evidence of contemporary activity of the Oca–Ancón 1795  
system. Proceedings, Caribbean Conference on Natural Haz- 1796  
ards: Volcanoes, Earthquakes, Windstorms, Floods. St. August- 1797  
tine, pp. 21–32. 1798
- Audemard, F.A., Singer, A., 1996. Active fault recognition in 1799  
northwestern Venezuela and its seismogenic characterization: 1800  
neotectonic and paleoseismic approach. *Geofísica Internacional* 1801  
35, 245–255. 1802
- Audemard, F.A., Singer, A., 1997. La Ingeniería de Fallas 1803  
Activas en Venezuela: historia y estado del arte. Seminario 1804  
Internacional de Ingeniería Sísmica: Aniversario del Terremoto 1805  
de Caracas de 1967. Universidad Católica Andrés Bello, 1806  
Caracas, pp. 11–27. 1807
- Audemard, F.A., De Santis, F., Lugo, M., Singer, A., Costa, C., 1808  
1988. Sismotectónica y Sismicidad Histórica, In Singer, A. 1809  
(coord.): Estudio de Amenaza Sísmica para las Urbanizaciones 1810  
La Punta y Mata Redonda, al Sur de Maracay. Unpublished 1811  
Funvisis' report for MINDUR. 2 Vol. 1812
- Audemard, F.A., Singer, A., Beltrán, C., Rodríguez, J.A., Lugo, M., 1813  
Chacín, C., Adrianza, A., Mendoza, J., Ramos, C., 1992. 1814  
Actividad tectónica cuaternaria y características sismogénicas de 1815  
los sistemas de falla de Oca–Ancón (tramo oriental), de la 1816  
Península de Paraguaná y región de Coro y de la costa 1817  
nororiental de Falcón. Unpublished Funvisis' report for INTE- 1818  
VEP, Los Teques, 2 Vol., 245 pp. 1819
- Audemard, F.A., Beltrán, C., Singer, A., 1993. Evaluación Neo- 1820  
tectónica Preliminar de la Galería Superior del Estribo Caracas 1821  
del Viaducto N° 1 de la Autopista Caracas-La Guaira. 1822  
Unpublished Funvisis' report for RDS y WS Asesoramientos 1823  
Técnicos, 19 pp + 3 appendices. 1824
- Audemard, F.A., De Santis, F., Singer, A., Ramos, C., 1995. El 1825  
Sistema de Fallas de La Victoria, Venezuela Norcentral: Trazas 1826  
Activas, Complejidades Estructurales, Cinemática y Sismicidad 1827  
Asociada. Proceedings IX Congreso Latinoamericano de 1828  
Geología, Diskette. 1829
- Audemard, F.A., Romero, G., Rendón, H., 1999. Sismicidad, 1830  
Neotectónica y Campo de Esfuerzos del Norte de Venezuela. 1831  
Unpublished Funvisis' report for PDVSA-CVP, 221 pp. 1832
- Audemard, F.A., Machette, M., Cox, J., Dart, R., Haller, K., 2000. 1833  
Map and Database of Quaternary Faults and Folds in 1834  
Venezuela and its Offshore Regions. USGS Open-File report 1835  
00-0018 (accessible from USGS webpage; open file reports 1836  
ofr-00-0018). 1837
- Audemard, F.A., Castilla, R. and Malavé, G. 2003. Eventuales 1838  
deformaciones permanentes de origen cosísmico en un área 1839

- 1840 costera ubicada al SW de Güiría, estado Sucre: evaluación  
1841 preliminar. VII Congreso Venezolano de Sismología e Ingen-  
1842 dería Sísmica (CD-Rom format).
- 1843 Bach, B., 1991. Interpretation und Analyse tektonischer Prozesse  
1844 anhand mikroseismischer Messungen im Estado Falcon, nordve-  
1845 nezuela. Master thesis, Universitat Hamburg, 95 pp.
- 1846 Bach, B., Muñoz, M., Franke, M., Villaseñor, A., Gajardo, E.,  
1847 1992. Estudios de microsismicidad en el norte de  
1848 Venezuela: 2. zona noroccidental. Proceedings VI Congreso  
1849 Venezolano de Geofísica, Sociedad Venezolana de Ingenieros  
1850 Geofísicos, pp. 522–528.
- 1851 Badell, C., 1981. El terremoto de San Pablo del 05 de Abril de  
1852 1975. Proceedings III Congreso Venezolano de Sismología e  
1853 Ingeniería Sísmica, Caracas, pp. 257–273.
- 1854 Beck, C., 1979. New data about recent tectonics in the central part  
1855 of the Caribbean chain: the Santa Lucía–Ocumare del Tuy  
1856 graben, Miranda State, Venezuela. Proceedings IV Latin  
1857 American Geological, pp. 59–68.
- 1858 Beck, C., 1986. Géologie de la Chaîne Caraïbe au méridien de  
1859 Caracas (Venezuela). Publication-Société Géologique du Nord  
1860 14 (462 pp.).
- 1861 Bell, J., 1972. Geotectonic evolution of the southern Caribbean area.  
1862 Memoir-Geological Society of America 132, 369–386.
- 1863 Beltrán, C. (comp.), 1993. Mapa Neotectónico de Venezuela. Escala  
1864 1: 2,000,000. Funvisis.
- 1865 Beltrán, C., 1994. Trazas activas y síntesis neotectónica de  
1866 Venezuela a escala 1:2.000.000. Proceedings VII Congreso  
1867 Venezolano de Geofísica, Caracas. 541–547.
- 1868 Beltrán, C., 1998. Preliminary observations on Quaternary reverse  
1869 faulting along the southern foothills of the Northern Range of  
1870 Trinidad. Proceedings XIV Caribbean Geological Conference,  
1871 Trinidad, 1995, vol. 1, pp. 233–239.
- 1872 Beltrán, C., Giraldo, C., 1989. Aspectos neotectónicos de la región  
1873 nororiental de Venezuela. Proceedings VII Congreso Geológico  
1874 Venezolano, Barquisimeto, vol. 3, pp. 1000–1021.
- 1875 Blanco, B., Giraldo, C., 1992. Síntesis tectono-estratigráfica  
1876 de la cuenca Tuy-Cariaco y plataforma externa. Proceed-  
1877 ings VI Congreso Venezolano de Geofísica, Caracas, vol. 1,  
1878 pp. 47–54.
- 1879 Blin, B., 1989. Le front de la Chaîne Caraïbe Vénézuélienne entre la  
1880 Serranía de Portuguesa et la région de Tiznados (surface et  
1881 subsurface): Apport des données paléomagnétiques. Interpréta-  
1882 tion géodynamique. PhD thesis, Université de Bretagne  
1883 Occidentale, Brest, France, 389 pp+ appendices.
- 1884 Boinet, T., 1985. La Frontière Méridionale de la Plaque Caraïbe  
1885 aux confins Colombo–Venezueliens (Norte de Santander,  
1886 Colombie): Données Géologiques. PhD thesis, Université  
1887 Paris VI., 204 pp + appendices.
- 1888 Bott, M., 1959. The mechanics of oblique slip faulting. *Geology*  
1889 *Magnetics* 96, 109–117.
- 1890 Carey, E., 1976. Analyse numérique d'un modèle mécanique  
1891 élémentaire appliqué à l'étude d'une population de failles.  
1892 Calcul d'un tenseur moyen des contraintes à partir de stries de  
1893 glissement. PhD Thesis, Université Paris Sud, 138 pp.
- 1894 CEE-INTEVEP, 1993. Seismotectonic of northern Venezuela (The  
1895 contact between the Caribbean and South American Plates).  
1896 Final report., 48 pp + appendices.
- Choy, J., 1998. Profundidad y mecanismo focal del terremoto de El  
Tocuyo, 1950. *Revista de Geofísica (Venezolana)* 39 (1–2),  
203–217.
- Choy, J., Morandi, M.T., Palme De Osechas, C., 1998. Determi-  
nación de patrones de esfuerzos tectónicos para el Oriente de  
Venezuela-Sureste del Caribe a partir de mecanismos focales.  
Proceedings IX Congreso Venezolano de Geofísica, Caracas,  
CD-Rom; paper no. 17.
- Cisternas, A., Gaulon, A., 1984. Síntesis Sismotectónica del  
noroeste de Venezuela. *Revista de Geofísica* 40, 3–10.
- Cluff, L., Hansen, W., 1969. Seismicity and Seismic-Geology of  
northwestern Venezuela. Unpublished Woodward-Clyde's report  
for Shell. 2 volumes.
- Colletta, B., Roure, F., De Toni, B., Loureiro, D., Passalacqua, H.,  
Gou, Y., 1996. Tectonic inheritance and structural styles in the  
Merida Andes (western Venezuela). III International Sympo-  
sium on Andean Geodynamics (3 ISAG), Saint-Malo, France,  
pp. 323–326.
- Colletta, B., Roure, F., De Toni, B., Loureiro, D., Passalacqua, H.,  
Gou, Y., 1997. Tectonic inheritance, crustal architecture, and  
contrasting structural styles in the Venezuelan Andes. *Tectonics*  
16 (5), 777–794.
- De Toni, B., Kellogg, J., 1993. Seismic evidence for blind thrusting  
of the northwestern flank of the Venezuelan Andes. *Tectonics* 12  
(6), 1393–1409.
- Dewey, J., 1972. Seismicity and tectonics of western Ven-  
ezuela. *Bulletin of the Seismological Society of America* 62 (6),  
1711–1751.
- Espínola, E., Ollarves, R., 2002. Estudio tectono-estratigráfico del  
borde septentrional de la cuenca de Barlovento, estado Miranda.  
Implicaciones neotectónicas. Unpublished undergraduate thesis,  
Universidad Central de Venezuela, 241 pp.
- Etchecopar, A., Vasseur, G., Daignieres, M., 1981. An inverse  
problem in microtectonics for the determination of stress tensors  
from fault striation analysis. *Journal of Structural Geology* 3,  
51–65.
- Fanti, O., Frontado, L., Vecchio, A., 1980. Tectónica y sismicidad  
del área de Caracas y sus alrededores. Undergraduate thesis.  
Universidad Central de Venezuela, 132 pp.
- Fleischmann, K., Nemcok, M., 1991. Paleostress inversion of fault-  
slip data using the shear stress solution of Means (1989).  
*Tectonophysics* 196, 195–202.
- Frey Mueller, J.T., Kellogg, J.N., Vega, V., 1993. Plate motions in  
the north Andean region. *Journal of Geophysical Research* 98,  
21853–21863.
- Funvisis, 1984. Estudios de Riesgo Sísmico, Ferrocarril Caracas-La  
Guaira. Unpublished Funvisis' report for Ferrocarril. 2 Vol. + 3  
appendices.
- Funvisis et al., 1997. Evaluación preliminar del sismo de Cariaco  
del 09 de Julio de 1997, Estado Sucre, Venezuela (versión  
revisada). Funvisis. 123 pp + 5 appendices.
- Gallardo, C., 1985. Esquisse sismotectonique de la region centro-  
occidentale du Venezuela et sa relation avec la geodynamique  
des Caraïbes. PhD thesis, Université de Montpellier II  
(U.S.T.L.). 276 pp.
- Giraldo, C., 1985a. Neotectónica y sismotectónica de la región de  
El Tocuyo-San Felipe (Venezuela centro-occidental). Proceed-

- 1954 ings VI Congreso Geológico Venezolano, Caracas, vol. 4,  
1955 pp. 2415–2451.
- 1956 Giraldo, C., 1985b. Néotectonique et sismotectonique de la région  
1957 d'El Tocuyo-San Felipe (Vénézuéla centro-occidental). PhD  
1958 thesis, Université de Montpellier II. 130 pp.
- 1959 Giraldo, C., Beltrán, C., 1988. Evaluación del campo de esfuerzos  
1960 durante el Cuaternario en la región nororiental de Venezuela  
1961 (Proyecto CONICIT S1-1161). Unpublished Funvisis' report for  
1962 CONICIT. 68 pp.
- 1963 Hancock, P., Barka, A., 1987. Kinematic indicators on active  
1964 normal faults in western Turkey. *Journal of Structural Geology*  
1965 9, 573–584.
- 1966 Hernández, J., Rojas, E., 2002. Estudio tectono-estratigráfico del  
1967 borde meridional de la cuenca de Barlovento, estado Miranda.  
1968 Implicaciones neotectónicas. Unpublished undergraduate thesis,  
1969 Universidad Central de Venezuela.
- 1970 Hess, H., Maxwell, J., 1953. Caribbean research project. *Bulletin of*  
1971 *the Geological Society of America* 64 (1), 1–6.
- 1972 Jácome, M.I., 1994. Interpretación geológica, sísmica y gravimé-  
1973 trica de un perfil transandino. Undergraduate thesis, Universidad  
1974 Simón Bolívar, Caracas, Venezuela, 68 pp.
- 1975 Jaimes, M., Pérez, O., Garciacaro, E., 1998. Subducción de la Placa  
1976 del Caribe bajo la Sudamericana en el Noroeste de Venezuela:  
1977 evidencias sísmológicas. *Proceedings IX Congreso Venezolano*  
1978 *de Geofísica*, CD-Rom; paper no. 39.
- 1979 Jordan, T., 1975. The present-day motions of the Caribbean plate.  
1980 *Journal of Geophysical Research* 80, 4433–4439.
- 1981 Kafka, A., Weidner, D., 1981. Earthquake focal mechanisms and  
1982 tectonic processes along the Southern boundary of the  
1983 Caribbean Plate. *Journal of Geophysical Research*; 86 (B4),  
1984 2877–2888.
- 1985 Kaniuth, K., Drewes, H., Stuber, K., Temel, H., Hernández, J.N.,  
1986 Hoyer, M., Wildermann, E., Kahle, H.G., Geiger, 1999. Position  
1987 changes due to recent crustal deformations along the Caribbean–  
1988 South American plate boundary derived from CASA GPS  
1989 project. General Assembly of the International Union of  
1990 Geodesy and Geophysics (IUGG), Birmingham, U.K. Poster  
1991 at Symposium G1 of International Association of Geodesy.
- 1992 Kellogg, J., Bonini, N., 1982. Subduction of the Caribbean Plate  
1993 and Basement Uplifts in the overriding South-American Plate.  
1994 *Tectonics* 1 (3), 251–276.
- 1995 Kellogg, J., Vega, V., 1995. Tectonic development of Panama, Costa  
1996 Rica, and the Colombian Andes: Constraints from Global  
1997 Positioning System geodetic studies and gravity. *Special*  
1998 *Paper-Geological Society of America* 295, 75–90.
- 1999 Kozuch, M., 1995. Earthquake Hazard Analysis of Venezuela using  
2000 site-specific attenuation. PhD thesis, University of Colorado,  
2001 154 pp.
- 2002 Laffaille, J., 1981. Mecanismos focales de algunos eventos sísmicos  
2003 ocurridos en el Occidente de Venezuela. Undergraduate thesis,  
2004 Universidad de Los Andes, Mérida, 142 pp.
- 2005 Loyo, B., 1986. Estudio Tecto-estratigráfico de la Cuenca del Tuy,  
2006 Edo. Miranda, Venezuela. Undergraduate thesis, Universidad  
2007 Central de Venezuela. 179 pp.
- 2008 Lozano, I., 1984. Microsismicidad en los alrededores de Gavidia,  
2009 Edo. Mérida. Undergraduate thesis in Physics, Universidad de  
2010 Los Andes, Mérida, 137 pp.
- Malavé, G., 1997. Inversión de ondas de volumen de algunos 2011  
sismos importantes del noroccidente de Venezuela: relación con 2012  
la tectónica regional. Master thesis, Instituto de Geofísica, 2013  
UNAM, México, 93 pp. 2014
- Malavé, G., 1972. Sismotectónica del Occidente de Venezuela. PhD 2015  
thesis, Instituto de Geofísica, UNAM, México, 224 pp. 2016
- Malavé, G., Suárez, G., 1995. Intermediate-depth seismicity in 2017  
northern Colombia and western Venezuela and its relationship to 2018  
Caribbean plate subduction. *Tectonics* 14 (3), 617–628. 2019
- Malfait, B., Dinkelman, M., 1972. Circum-Caribbean tectonic and 2020  
igneous activity and the evolution of the Caribbean plate. 2021  
*Geological Society of America Bulletin* 83 (2), 251–272. 2022
- Marín, L., 1982. Mecanismo focal de algunos eventos sísmicos 2023  
ocurridos en Venezuela. Undergraduate thesis, Facultad de 2024  
Ingeniería, Escuela de Ingeniería Geodésica, Universidad del 2025  
Zulia, Maracaibo. 2026
- Mathieu, X., 1989. La Serranía de Trujillo-Ziruma aux confins du 2027  
Bassin de Maracaibo, de la Sierra de Falcon et de la Chaîne 2028  
Caraïbe. PhD thesis, Université de Brest. 266 pp + appendices. 2029
- Mattauer, M., 1973. Les déformations des matériaux de l'écorce 2030  
terrestre. Hermann, Paris. 2031
- Mendoza, J., 1989. Reporte especial sobre los sismos del 2032  
Táchira ocurridos en Enero-Febrero de 1989. Unpublished 2033  
Funvisis' report. 2034
- Minster, J., Jordan, T., 1978. Present-day plate motions. *Journal of* 2035  
*Geophysical Research* 83, 5331–5354. 2036
- Mocquet, A., 1984. Phases de déformation plio-cuaternaire liées au 2037  
fonctionnement d'une faille transformante émergée: La faille 2038  
d'El Pilar (Vénézuéla). *Memoir D.E.A.*, Université de Rennes, 2039  
35 pp. 2040
- Molnar, P., Sykes, L., 1969. Tectonics of the Caribbean and Middle 2041  
America Regions from focal mechanisms and Seismicity. 2042  
*Geological Society of America Bulletin* 80, 1639–1684. 2043
- Muñoz, M., 2002. Evaluación geomecánica para la estimación de 2044  
los esfuerzos (dirección-magnitud) in-situ del Domo de Santa 2045  
Rosa, en las formaciones San Juan y San Antonio (Cretácico), 2046  
Merecure (Oligoceno) y Oficina (Mioceno), area Mayor de 2047  
Anaco (AMA), edo. Anzoátegui, en el desarrollo de la 2048  
perforación. Undergraduate thesis, Universidad Central de 2049  
Venezuela. 134 p. 2050
- Palme, C., Choy, J., Morandi, M., 2001. Mecanismos focales 2051  
sísmicos y esfuerzos tectónicos en la región norte de los Andes 2052  
merideños, Venezuela. *Interciencia* 26 (5), 201–209. 2053
- Pennington, W., 1981. Subduction of the Eastern Panama Basin and 2054  
Sismotectonics of Northwestern South America. *Journal of* 2055  
*Geophysical Research* 86 (B11), 10.753–10.770. 2056
- Pérez, O., 1998. Seismological Report on the Mw 6.8 Strong 2057  
Shock of 9 July 1997 in Cariaco, northeastern Venezuela. 2058  
Short Notes, *Bulletin of the Seismological Society of America* 2059  
88 (3), 874–879. 2060
- Pérez, O., Aggarwal, Y., 1981. Present-day tectonics of southeastern 2061  
Caribbean and northeastern Venezuela. *Journal of Geophysical* 2062  
*Research* 86, 10791–10805. 2063
- Pérez, O., Jaimes, M., Garciacaro, E., 1997a. Microseismicity 2064  
evidence for subduction of the Caribbean plate beneath the 2065  
South American plate in northwestern Venezuela. *Journal of* 2066  
*Geophysical Research* 102 (B8), 17.875–17.882. 2067

- 2068 Pérez, O., Sanz, C., Lagos, G., 1997b. Microseismicity, tectonics  
2069 and seismic potential in southern Caribbean and northern  
2070 Venezuela. *Journal of Seismology* 1, 15–28.
- 2071 Pérez, O., Bilham, R., Bendick, R., Hernández, N., Hoyer, M.,  
2072 Velandia, J., Moncayo, C., Kozuch, M., 2001. Velocidad  
2073 relativa entre las placas del Caribe y Sudamérica a partir  
2074 de observaciones dentro del sistema de posicionamiento  
2075 global (GPS) en el norte de Venezuela. *Interciencia* 26 (2),  
2076 69–74.
- 2077 Petit, J.-P., Proust, F., Tapponnier, P., 1983. Critères de sens  
2078 de mouvement sur les miroirs de failles en roches non  
2079 calcaires. *Bulletin de la Société Géologique de France* XXV,  
2080 589–608.
- 2081 Phan-Trong, T., 1993. An inverse problem for the determination of  
2082 the stress tensor from polyphased fault sets and earthquake focal  
2083 mechanisms. *Tectonophysics* 224, 393–411.
- 2084 Pindell, J., Dewey, J., 1982. Permo-Triassic reconstruction of  
2085 western Pangea and the evolution of the Gulf of Mexico/  
2086 Caribbean region. *Tectonics* 1 (2), 179–211.
- 2087 Proust, F., Petit, J.-P., Tapponnier, P., 1977. L'accident du Tizi n'Test  
2088 et le rôle des décrochements dans la tectonique du Haut Atlas  
2089 occidental (Maroc). *Bulletin de la Société Géologique de France*  
2090 XIX, 541–551.
- 2091 Ramos, C., Mendoza, J., 1991. Actividad Sísmica en la costa  
2092 nororiental del estado Falcón entre los días 26-04-89 y 02-06-  
2093 89. Unpublished Funvisis' report, 28 pp.
- 2094 Ramos, C., Mendoza, J., 1993. Actividad Sísmica al sur de la isla La  
2095 Tortuga entre los días 18 de marzo y 13 de Abril de 1990.  
2096 Boletín-Instituto de Materiales y Modelos Estructurales, IMME-  
2097 UCV 80, 69–86.
- 2098 Rial, J., 1978. The Caracas, Venezuela, earthquake of July 1967; a  
2099 multiple-source event. *Journal of Geophysical Research* 83  
2100 (B11), 5.405–5.414.
- 2101 Ritz, J.-F., 1991. Évolution du champ de contraintes dans Les Alpes  
2102 du sud depuis la fin de l'Oligocène. Implications sismotectoni-  
2103 ques. PhD thesis, Université de Montpellier II.
- 2104 Rod, E., 1956a. Earthquakes of Venezuela related to strike slip  
2105 faults? *Bulletin of the American Association of Petroleum*  
2106 *Geologists* 40, 2509–2512.
- 2107 Rod, E., 1956b. Strike-slip faults of northern Venezuela. *Bulletin*  
2108 *of the American Association of Petroleum Geologists* 40 (3),  
2109 457–476.
- 2110 Rodríguez, M., 1995. Estudio del enjambre sísmico ocurrido en  
2111 el estado Táchira en el año 1994. Undergraduate thesis,  
2112 Escuela de Ciencias, Departamento de Física, Universidad de  
2113 Oriente. 57 pp.
- 2114 Romero, G., 1993. Estudio y Determinación de Características de  
2115 Fuentes Sísmicas en Venezuela por Medio del Análisis Espectral  
2116 de Ondas Corpóreas. Master thesis, Universidad Central de  
2117 Venezuela. Caracas.
- 2118 Romero, G., 1994. Recopilación y base de datos de mecanismos  
2119 focales en Venezuela y zonas adyacentes. Unpublished Funvisis'  
2120 report. 29 pp.
- 2121 Russo, R., 1999. Dynamics and deep structure of the southeastern  
2122 Caribbean–South America Plate Boundary Zone: relationship  
2123 to shallow seismicity. AGU Spring Meeting, Boston, U.S.A.,  
2124 pp. S228. abstract.
- Russo, R., Speed, R., 1992. Oblique collision and tectonic wedging  
of the South American continent and Caribbean terranes.  
*Geology* 20, 447–450.
- Russo, R., Okal, E., Rowley, K., 1992. Historical seismicity of the  
Southeastern Caribbean and tectonic implications. *PAGEOPH*  
139 (1), 87–120.
- Saleh, J., Weber, J., Balkaransingh, S., Dixon, T., Ambeh, W.,  
Leong, T., Charles, F., Wdowinski, S., Webb, F., under review.  
Neotectonics and seismic risk in Trinidad, West Indies, from  
historic triangulation (1901–1903) and GPS (1994–1999)  
Geodesy. *Journal of Geophysical Research*.  
Sánchez, M., Vásquez, A., Van Alstine, D., Butterworth, J., García,  
J., Carmona, R., Poquioma, W., Ramones, M., 1999. Application  
of geomechanics in the development of the naturally fractured  
carbonates of the Mara Oeste field, Venezuela. 1999 SPE Latin  
American and Caribbean Petroleum Engineering Conference,  
Caracas, Venezuela, SPE 54008.
- Schubert, C., 1979. El Pilar fault zone, northeastern Venezuela: brief  
review. *Tectonophysics* 52, 447–455.
- Schubert, C., 1980a. Morfología neotectónica de una falla rumbo-  
deslizante e informe preliminar sobre la falla de Boconó, Andes  
merideños. *Acta Científica Venezolana* 31, 98–111.
- Schubert, C., 1980b. Late Cenozoic pull-apart basins, Boconó fault  
zone, Venezuelan Andes. *Journal of Structural Geology* 2 (4),  
463–468.
- Schubert, C., 1982. Neotectonics of the Boconó fault, western  
Venezuela. *Tectonophysics* 85, 205–220.
- Schubert, C., 1984. Basin formation along Boconó–Morón–El Pilar  
fault system, Venezuela. *Journal of Geophysical Research* 89,  
5711–5718.
- Singer, A., Audemard, F.A., 1997. Aportes de Funvisis al desarrollo  
de la geología de fallas activas y de la paleosismología para los  
estudios de amenaza y riesgo sísmico. *Publicación Especial*  
*Academia de las Ciencias Naturales, Matemáticas y Físicas*  
vol. 33, pp. 25–38.
- Slemmons, D., 1977. Faults and earthquake magnitudes. Miscella-  
neous paper S-73-1, U.S. Army Engineer Waterways Experi-  
ment Station, Vicksburg.
- Sobiesiak, M., Alvarado, L., Vásquez, R., 2002. Sisimicidad  
reciente del Oriente de Venezuela. XI Congreso Venezolano  
de Geofísica, 4pp. (CD-Rom format).
- Soulas, J.-P., 1986. Neotectónica y tectónica activa en Venezuela y  
regiones vecinas. *Proceedings VI Congreso Geológico Venezo-  
lano*, Caracas, 1985 vol. 10, pp. 6639–6656.
- Soulas, J.-P., Giraldo, C., Bonnot, D., Lugo, M., 1987. Actividad  
cuaternaria y características sismogénicas del sistema de fallas  
Oca–Ancón y de las fallas de Lagarto, Urumaco, Río Seco y  
Pedregal. Afinamiento de las características sismogénicas de las  
fallas de Mene Grande y Valera. (Proyecto COLM). Unpub-  
lished Funvisis' report for Intevep, 69 pp.
- Stephan, J.-F., 1982. Evolution géodynamique du domaine Caraïbe,  
Andes et chaîne Caraïbe sur la transversale de Barquisimeto  
(Vénézuéla). PhD thesis, Paris, 512 pp.
- Suárez, G., Nabelek, J., 1990. The 1967 Caracas Earthquake: fault  
geometry, direction of rupture propagation and sismotectonic  
implications. *Journal of Geophysical Research* 95 (B11),  
17459–17474.

- 2182 Sykes, L., McCann, W., Kafka, A., 1982. Motion of Caribbean Plate  
2183 during last 7 million years and implications for earlier Cenozoic  
2184 movements. *Journal of Geophysical Research* 87 (B13),  
2185 10656–10676.
- 2186 Tjia, H., 1971. Fault movement, reoriented stress field and  
2187 subsidiary structures. *Pacific Geology* 5, 49–70.
- 2188 Tovar, E., 1989. Recopilación y obtención de mecanismos focales  
2189 en Venezuela, Unpublished Funvisis' report.
- 2190 Trenkamp, R., Kellogg, J., Freymueller, J., Mora, H., 2002. Wide  
2191 plate margin deformation, southern Central America and north-  
2192 western South America, CASA GPS observations. *Journal of*  
2193 *South American Earth Sciences* 15, 157–171.
- 2194 Valera, M., 1995. Estudio de la tormenta sísmica ocurrida en el  
2195 estado Lara en los meses Agosto–Septiembre de 1991. Under-  
2196 graduate thesis, Escuela de Ciencias, Departamento de Física,  
2197 Universidad de Oriente. 66 pp.
- 2198 Van der Hilst, R., 1990. Tomography with P, PP, and pP delay-time  
2199 data and the three-dimensional mantle structure below the  
2200 Caribbean region. PhD thesis, University of Utrecht, Nether-  
2201 lands, *Geologica Ultraiectina* 67, 250 pp.
- 2202 Vedder, J., Wallace, R., 1970. Map showing recently active breaks  
2203 along the San Andreas and related faults between Cholame  
2204 Valley and Tejon Pass, California. U. S. Geological Survey  
2205 Miscellaneous Geologic Investigations Map I-574, scale  
2206 1:24,000.
- 2207 Wadge, G., Burke, K., 1983. Neogene Caribbean plate rotation and  
2208 associated Central American tectonic evolution. *Tectonics* 2 (6),  
2209 633–643.
- 2237
- Weber, J., Dixon, T., DeMets, C., Ambeh, W., Jansma, P., Mattioli,  
2210 G., Saleh, J., Sella, G., Bilham, R., Pérez, O., 2001a. GPS  
2211 estimate of relative motion between the Caribbean and South  
2212 American plates, and geologic implications for Trinidad and  
2213 Venezuela. *Geology* 29 (1), 75–78.
- 2214  
2215 Weber, J., Ferrill, D., Roden-Tice, M., 2001b. Calcite and quartz  
2216 microstructural geothermometry of low-grade metasedimentary  
2217 rocks, Northern Range, Trinidad. *Journal of Structural Geology*  
2218 23, 93–112.
- 2219 Wesson, R., Helley, E., Lajoie, K., Wentworth, C., 1975. Faults and  
2220 future earthquakes U.S. Geological Survey Professional Paper  
2221 P941A.
- 2222 Wilcox, R., Harding, T., Seely, D., 1973. Basic wrench tectonics.  
2223 *Bulletin of the American Association of Petroleum Geologists*  
2224 57, 74–96.
- 2225 Willson, S.M., Last, N.C., Zoback, M.D., Moos, D., 1999.  
2226 Drilling in South America: a wellbore stability approach for  
2227 complex geologic conditions. 1999 SPE Latin American and  
2228 Caribbean Petroleum Engineering Conference, Caracas,  
2229 Venezuela, SPE 53940.
- 2230 Wozniak, J., Wozniak, M., 1979. Geología de la región de Cabure  
2231 Estado Falcón. Unpublished Ministerio de Energía y Minas'  
2232 report. 64 pp + appendices.
- 2233 Ysaccis, R., Cabrera, E., Del Castillo, H., 2000. El sistema  
2234 petrolífero de la Blanquilla, costa afuera Venezuela. Proceedings  
2235 VII Congreso Bolivariano Exploración Petrolera en las Cuencas  
2236 Subandinas, Caracas, pp. 411–425.